DOCTOR OF PHILOSOPHY

Investigating the Feasibility of Using Focussed Airborne Ultrasound as Tactile Feedback in Medical Simulators

Hung, Gary

Award date:
2014

Awarding institution:
Bangor University

Investigating the Feasibility of Using Focussed Airborne Ultrasound as Tactile Feedback in Medical Simulators

PRIFYSGOL
BANGOR
UNIVERSITY

Gary M.Y. Hung
School of Computer Science
Bangor University, Wales

Thesis submitted in candidature for the degree of
Doctor of Philosophy

September 2013

Acknowledgements

Gratitude is expressed towards Bangor University's 125th Anniversary PhD Scholarship for providing an opportunity for me to obtain an honourable qualification that would open many doors in my future.

I would like to express particular thanks to my supervisor, Professor Nigel W. John who had placed his trust in my ability to overcome the difficulties in successfully completing this study in the last three years. His infinite patience, devotion and thoughtful guidance had been a tremendous aid in my professional attitude, interpersonal skills and personal development. Thank you Nigel, I would not have made it to this day without you.

I would like to thank several people for providing technical advice through the course of my study, in particular Professor Chris Hancock, Bangor University and Takayuki Hoshi, Nagoya Institute of Technology Japan.

Special thanks to Honorary Professor Derek A. Gould of Royal Liverpool University Hospital, for providing clinical guidance on the development of the project.

I would also like to extend my thanks and appreciation to my family as they have been with me through every step of this battle.

Abstract

Novice medical practitioners commonly practice on live patients in real medical procedures. However, due to the inexperience of the practitioner, mistakes are likely which exposes the patient to undue risk. To improve the training of novices, medical simulators create a virtual patient providing a safe environment for the user to practice within. An important clinical skill is palpation, a physical examination technique. The practitioners use their hands to feel the body of the patient to make diagnosis. A virtual patient has a visual representation but as it is virtual, the patient is not physically present. Haptics technology provide additional benefits to the training session by stimulating the physical sense of touch. A novel technique has recently emerged for stimulating tactile sensation called acoustic radiation pressure from focussed airborne ultrasound.

Acoustic radiation creates a focal point of concentrated acoustic pressure in a three-dimensional field producing a force in mid-air. Airborne ultrasound has several advantages over conventional technologies. It was also initially theorised that using airborne ultrasound to simulate palpation compared to a previous system called PalpSim which consists of a rubber tube filled with water permanently embedded in a block of silicone, will offer better controllability over the displayed sensation to simulate various tactile sensations.

The thesis has investigated the feasibility of using focussed airborne ultrasound as tactile feedback in medical simulators. A tactile device called UltraSendo was completely custom built to simulate an arterial pulse and a thrill sensation. UltraSendo was integrated with an augmented reality simulator displaying a virtual patient for user interaction. The simulator was brought to Ysbyty Glan Clwyd hospital for user feedback. A wide range of user responses were gathered. The majority of responses felt the arterial pulse was not sufficiently realistic whilst there were higher ratings for the thrill sensation which is acceptably realistic. Positive feedback suggests that airborne ultrasound can indeed provide tactile feedback in a medical context and is better at simulating a thrill sensation compared to a pulse sensation.

Contents

Chapter 1

Introduction

In medicine, it is common practice for a trainee to operate on live patients under the supervision of an experienced senior clinician. This allows the trainee to gain experience and the skill set required to perform the procedure however, this exposes the patient to unnecessary risks.

Virtual medical simulators have been introduced to mitigate risk and improve patient safety by allowing the trainee to obtain competency in performing the procedure before operating on patients. These virtually created patients have a visual representation but have no physical presence. As medical procedures involve the clinician physically interacting with the patient, it is important to simulate and stimulate the sense of touch to make the training session beneficial. Palpation procedures in particular rely heavily on tactile cues as the clinician uses their hands to conduct diagnosis and treatment.

Haptic feedback has two distinct components: force and tactile. The former aims to simulate the large forces felt from interacting with a virtual object whilst the latter simulate small-scale forces and other cutaneous attributes such as texture, temperature, surface friction and softness. There already exists many force feedback devices but combination of tactile and force feedback in medical simulators is still in its infancy [1, 2]. There are several enabling technologies that allow tactile feedback to be generated. The most common and prevalent are shape-memory alloys, pneumatics, electromagnetism and electrodes.

A more novel technology is beginning to be adopted in recent applications. A physical phenomenon known as acoustic radiation pressure is generated by focussing multiple ultrasonic transducers to create a force field. The force can be concentrated at a particular point in three-dimensional space and the width of the focal point can be as small as 5mm in the transmission medium of air.

This thesis aimed to investigate the feasibility of using acoustic radiation pressure from focussed airborne ultrasound to simulate two common tactile sensations found on the body.

1.1 Thesis Structure

Chapter 1 will served as an introduction to this thesis and its objectives with essential background information. Chapter 2 will discuss the characteristics of skin on the hand and how existing technology are able to provide tactile stimuli. The chapter will also briefly discuss general applications that contains tactile cues and tactile interfaces. Chapter 3 will describe the physical phenomenon known as Acoustic Radiation Pressure that allows focussed airborne ultrasound to achieve tactile feedback. Chapter 4 will detail the design, development and implementation of UltraSendo from its initial prototypes through to its finalized version. The integration of UltraSendo with an augmented reality simulator used to display a virtual patient will also be discussed. Chapter 5 will present the user feedback gathered from medical practitioners testing UltraSendo at Ysbyty Glan Clwyd. Chapter 6 will conclude the thesis and discuss future work.

1.2 Publications

At the time of this thesis submission, another paper detailing this feasibility study regarding the results of the user feedback is being written and pending submission to the IEEE Transactions on Biomedical Engineering.

- Hung G.M.Y and John N.W., "Airborne Ultrasound Pulse Force Device for Palpation Simulation" in Theory and Practice of Computer Graphics, Warwick University, UK, 2011, pp. 61-62.
- Hung G.M.Y., John N.W., Hancock C., Gould D.A., Hoshi T. "UltraPulse Simulating a Human Arterial Pulse with Focussed Airborne Ultrasound" in the 35th Annual International Conference of the IEEE Engineering in Medicine and Biology Society, 2013, Osaka, Japan, pp. 2511-2514.

1.3 Hypothesis

Currently various mechanical technologies have been used to simulate tactile effects. Tactile feedback from focussed airborne ultrasound is a new technology that has only been utilized in a few exemplar applications. One key area this thesis explores is the feasibility of using focussed airborne ultrasound to generate tactile feedback for medical training simulation, such as the palpation technique. To the best of our knowledge, we are the first institution to explore the usage of airborne ultrasound in such a manner. The hypothesis is outlined as the following question:

- Can acoustic radiation pressure from focussed airborne ultrasound deliver a realistical tactile sensation in a medical simulator?

To investigate this hypothesis we explore the simulation of two tactile sensations suggested by our clinical collaborators: a pulse and a thrill. Detection of a pulse and/or thrill are commonly carried out to aid diagnosis for a variety of illnesses, and is a skill that every clinician needs to learn. A custom airborne ultrasound tactile device was built to investigate this hypothesis. This device was initially called UltraPulse but was later renamed UltraSendo (Sendo meaning ”vibrations” in Japanese) to avoid confusion with a laser device with the same name. From this point forward, the device will be referred to as UltraSendo. User feedback was gathered in order to confirm whether UltraSendo is able to display a feasible tactile sensation in a medical context and to determine the realism of the simulated pulse sensation and thrill sensation. UltraSendo was brought to Ysbyty Glan Clwyd where medical practitioners were asked to test the device and to complete a questionnaire rating the tactile sensation presented.

1.4 Palpation Technique

Palpation is a physical examination technique. A clinician will use his hands to touch and explore the patient's body. A good example of this is breast cancer diagnosis. The clinician touches and analyse the breast to detect anomalies such as stiff lumps and regions in the tissue which could indicate the patient has cancer. Opposed to open surgery where access to the internal organs of the body is obtained with large incisions, endovascular procedures is a form of minimally invasive surgery which uses palpation to locate an access site to the body's major blood vessels allowing small tools to enter the body. It is a type of percutaneous procedure where the initial access is facilitated by a needle puncture guiding the second entry of a catheter tube, called the Seldinger technique [3]. Since physical trauma to the patient is significantly lower in comparison to the open surgery approach, recovery time is much quicker and leaves less cosmetic scars, however, due to the complexity of manoeuvring in such a small amout of space the duration of the procedure is substantially longer.

This thesis focusses on the palpation of the arterial pulse sensation and the thrill sensation as suggested by our clinical collaborators. Detection of a pulse and thrill are commonly carried out to aid diagnosis for a variety of illnesses, and is a skill that every clinician needs to learn.

1.4.1 Pulse Sensation

An arterial pulse sensation is the expansion motion of the artery wall which "pulses" when the heart beats to circulate blood around the body. In order to feel the pulse, the palpation site must allow the artery to be compressed against a bone or denser part of the body to exert pressure on the wall. The clinician normally uses their fingertips to carry out this technique.

Palpable arteries can be found in different anatomical locations. Different arteries also have different functions. The carotid artery for example delivers oxygen to the head and is located at the neck. Depending on which artery is being palpated the clinician will touch different parts of the body (Fig.1.1). In endovascular procedures, the femoral artery near the groin is typically used to gain access to other arteries such as the carotid. The clinician can feel the structural difference in anatomy between a wrist, neck and thigh as the underlying bone structure, the surrounding bones and how much flesh is at that particular body area will differ.

(a) Radial artery

(b) Carotid artery [4]

(c) Femoral artery [5]

Figure 1.1: Some of the different parts of the body with palpable arterial pulses

The physiology of the arterial sensation could vary in terms of strength and rhythm. The strength of the pulse can indicate the adequacy of the patient's blood flow. A weak pulse could indicate a health problem with the patient, however, an elderly person or someone with a high body fat percentage will also exhibit a more difficult pulse to palpate. An irregular pulse rhythm condition called Arrythmia could indicate a potential health problem compared to a healthy patient with a strong regular pulse. Training for Arrthymia is difficult as accessibility to real patients with this condition is limited. A novice needs to spend quality training time to learn the physical feeling of this irregular rhythm. A medical simulator can provide 24/7 access with the ability to simulate any patient profile for training.

1.4.2 Thrill Sensation

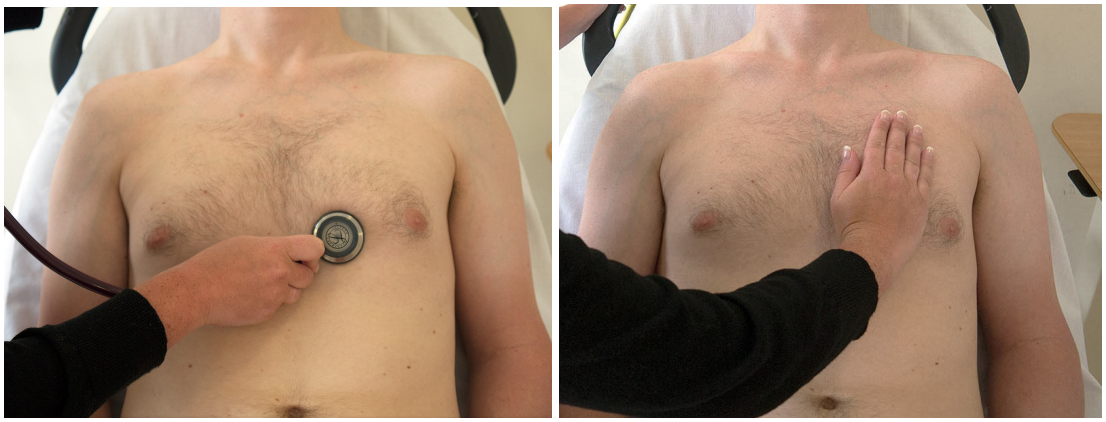

(a) Auscultation with a stethoscope (b) Palpable thrill with the palm of the hand

Figure 1.2: Part of the cardiovascular examination procedure [6]

A heart mumur is a condition where the valves of the heart show abnormal pulsations. Auscultation is one technique for diagnosing a murmur. The clinician listens to the sound of the heart using a stethoscope placed on the chest (Fig.1.2a). In contrast to auscultation, a thrill sensation however, is palpable and can be felt with the palm of the hand without the use of an external tool (Fig.1.2b). This sensation is similar to a vibration but has a larger region of effect in comparison to an arterial pulse felt with the fingertips.

1.5 Medical Training for Novices

For any learning process, training consistency and frequency are important factors when attempting to improve skill proficiency. It is not unheard of for in-training clinicians to operate on live patients whilst supervised by an expert. A study was carried out recently to evaluate patients consenting to have a trainee performing the surgical procedure [7]. From this study, it was shown that patients are more reluctant to allow a trainee to perform the operation in comparison to a senior clinician. This makes gaining consistent, frequent access to a significant number of patients for training purposes difficult.

Medical simulators are an alternative platform for which the trainee can practice indefinitely for longer periods of time without the worry of making fatal mistakes which would otherwise harm a real patient. They are allowed to explore and "learn" the technique through trial and error which would not be an acceptable practice on real patients.

1.5.1 Mannequins

Figure 1.3: A full scale Human Patient Simulator mannequin by Canadian Aviation Electronics (CAE) Healthcare [8]

Human Patient Simulators (HPS) are life-sized mannequins with various physiological functions implemented. Trainee clinicians gain practical experience by performing on such mannequins. A HPS by CAE Healthcare (Fig.1.3) is one example of these life-sized mannequins providing a high fidelity for simulating a real clinical scenario when the HPS is blended into the scene (Fig.1.4). Most of the CAE Healthcare mannequin products feature automatic palpable pulses in several different parts of the body that change depending on the condition of the HPS.

Despite the mannequin's ability to produce palpable pulses, only recently did Takeuchi claim that they could not find any HPS scenarios available which solely focussed on training arterial and arrhythmia palpation [10]. In their study, they created several different pulse conditions for the HPS and asked participants to deliver a diagnosis. The study showed improvements in the participants' percentage in giving the correct diagnosis after learning

Figure 1.4: HPS blends into a clinical environment to provide high fidelity simulation of a medical scenario [8]

Figure 1.5: The Cardiology Patient Simulator K by Limbs and Things [9]

with the HPS, however, this work only investigates the palpation of the radial artery at the wrist whilst there are other areas of the body which are potential sites for arterial palpation.

An auscultation simulator [11] uses a mannequin with embedded speakers to replicate the audible sounds of the heart. However, it is mainly designed to be used with a stethoscope and does not present a palpable thrill.

There are several issues with such mannequins. Currently the cost of these smart mannequins can be substantial. A cardiology patient simulator by Limbs and Things (Fig.1.5) is a torso mannequin with eight palpable sites and can also simulate auscultation and a palpable thrill sensation, cost around £42,000. The complexity of the mannequin warrants the high cost but it also means there is a higher potential for malfunction as many parts need to work together. The mannequins occupy a significant amount of space and does not provide much variety in its outer appearance; the mannequin will always look like the same ”person“ i.e. if the mould of the mannequin is male, it cannot possibly imitate patient-specific data of a female or a child and so would require another appropriate unit to be purchased, and if needles were to be inserted, it would need replacement.

1.5.2 Virtual Simulators

Most virtual patients are presented on a monitor screen. This limits the amount of viewing perspective available due to the size of the monitor and does not give the full sense of presence of the patient. Lab for Educational Technology created an online training tool called vpSim [12]. This webpage simulates the patient in a textual format on screen without any form of physical interaction. The webpage presents a list of multiple choices answered by selecting with a mouse cursor. This type of tool, however, is used mainly to develop reasoning of the diagnosis and is insufficient for training a practical skill such as palpation.

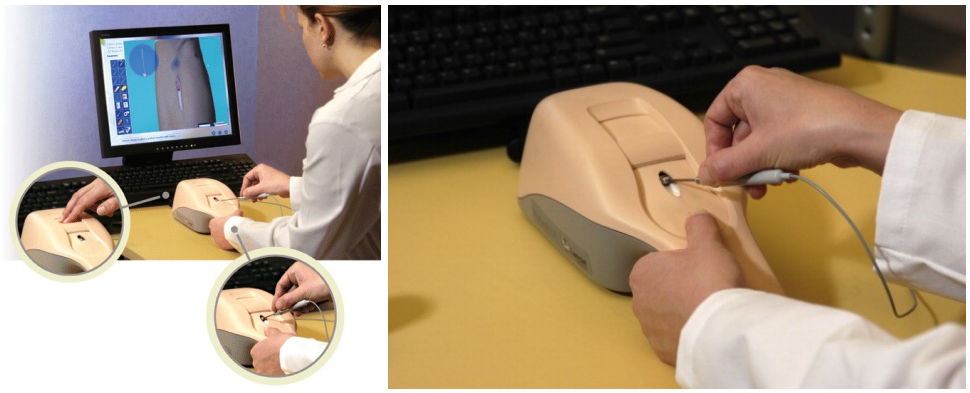

Figure 1.6: Virtual I.V. Simulator with an external palpable interface [13]

Touch feedback can be implemented with virtual simulators. A virtual simulator that uses haptic feedback for intravenous (IV) therapy, which is the introduction of a substance directly into a vein, for example morphine to relieve pain, consists of a palpable interface for the radial artery (Fig.1.6) and displays only the arm of the virtual patient on screen. The user then interacts with an external device positioned in front of the screen to locate the pulsation before manipulating an attached tethered needle to position the tip on screen. A palpation simulator for the femoral artery with percutaneous procedure displays a virtual patient on screen and consists of mechanical devices which delivers touch feedback via joysticks (Fig.1.7). For this simulator, the fingers of the user is attached to the joystick and so may not feel as natural as the real procedure where the hands are not attached with any peripherals.

The main issue with these simulators is the user is looking away from their hands where the manipulation task is taking place, and looking at the screen instead. A novel approach by Coles [15] uses augmented reality to merge the user's own hands into the virtual environment so the user is looking directly and interacting with the workspace. This mechanism does not require any wearable pheripherals, the only real requirement for the

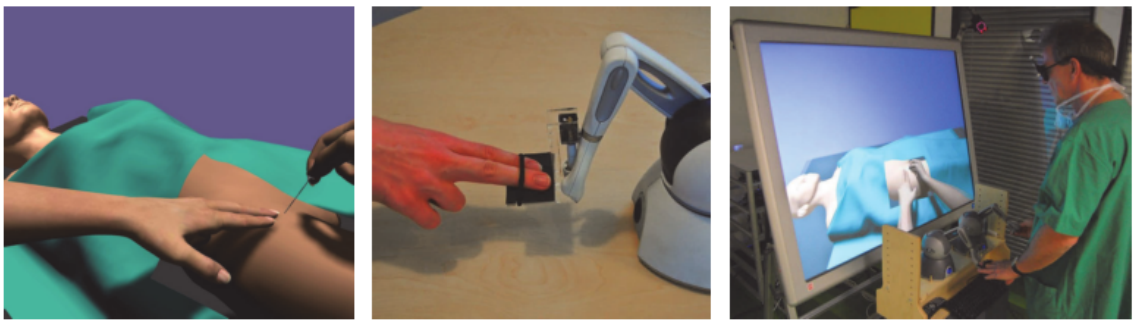

Figure 1.7: A femoral palpation simulator using an external mechanical joystick with force feedback. Virtual patient is displayed on screen [14]

augmented reality function to work correctly is for the user to wear the disposable surgical gloves, which would also be worn in a true surgical procedure, as the program analyses the colours in the environment to decide what pixels to convert to transparent. In Coles' femoral artery simulator, the arterial pulse sensation is created by a hydraulic pump which inflates a rubber tube inside a tray of silicone. The issue with this approach is the fixed location of the pulse. The amount of maintenance to ensure the rubber tube is completely filled with water is also not trivial as air pockets in the tube would prevent the pressure building up to inflate the tube. Water also evaporates over time.

1.6 Summary

The pulse and thrill are common tactile sensations that all clinicians should learn to diagnosis which are mainly palpated using the hand. Practical medical training for trainee clinicians involve obtaining the consent of a patient and being supervised by a senior clinician. Gaining access to these willing patients is difficult and thus medical simulators provide an alternative platform to gain experience. Human Patient Simulator are full-sized mannequins featuring various physiological functions. A mannequin can be blended into an environment for high fidelity simulation. The main issue is the size and cost and the fact that it will always look like the same "person". Virtual patients displayed on computer monitors offer the flexibility of changing the clinical scenario without the need to replace physical counterparts but the level of immersion can be limited due to the practical screen size in which to display the patient. Since the patient is virtual they have no physical presence and thus requires external devices to simulate the sense of touch. The next chapter discuss the current technologies used to achieve tactile feedback.

Chapter 2

Tactile Sensation and Enabling Technologies

Haptics consists of two components: force feedback and tactile feedback. The technology used to achieve each component is considerably different. Force feedback will mainly use torque from motors to achieve resistance against motion whilst tactile feedback will involve complex mechanisms relying on technologies such as piezoelectric, pneumatics, electrodes, shape-memory alloys and so on. Most force feedback applications will use a joystick whilst tactile cues will mainly require a contact surface or interface for the user to "touch" and thus the device through which the force or tactile feedback is provided will also need consideration depending on the application.

This chapter will briefly discuss the cutaneous properties of the skin mainly on the human hand since, generally, the user will use their hands to interact with most tactile devices, and how different stimuli could be applied to create tactile feedback will be discussed. The chapter will then discuss how tactile feedback can be provided through various existing technologies. Finally, the use of tactile feedback in general applications will be discussed.

2.1 Tactile Sensation

Generally tactile devices are designed to stimulate the skin of the user. We first discuss some characteristics of the skin and then discuss the different types of stimulation that can be applied to create tactile feedback.

2.1.1 Mechanoreceptors

Vallbo in 1984 studied the cutaneous properties of the human hand [16]. It is estimated that there are 17,000 receptors on the hand. There are four types of receptors broadly categorized by how quickly they adapt to a static physical stimulus e.g. an indentation on the skin, and the size of its receptive area: fast adapting (FA) type I and II, and slow adapting (SA) type I and II. The type I receptors are characterized by their smaller receptive area in comparison to type II however, there are more type I receptors (FA and SA type I constitutes 68% of the total number of receptors in the human hand) in comparison to type II. The number of type I receptors in the skin suggests that type I is more likely to be related to detecting spatial resolution. The receptors are situated at different depths from the surface of the skin as shown in Fig.2.1. We pay particular attention to Merkel cell receptors and Meissners corpuscle as they are closest to the surface of the skin. Merkel cells respond to pressure on the skin and Meissners corpuscle responds to low frequency vibrations i.e. they are sensitive to the lightest touch.

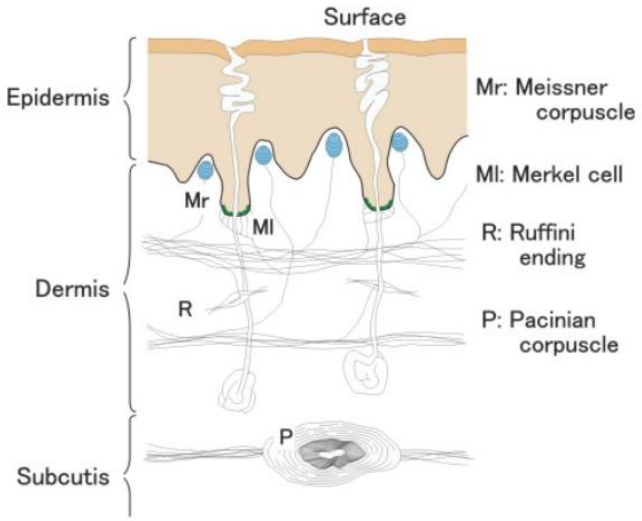

Figure 2.1: Location of mechanoreceptors cited from [17]

2.1.2 Tactile Stimuli

The mechanoreceptors can be artificially stimulated by replicating the skin deformation on the fingertip incurred by physical contact with natural objects. Mechanical deformation of the skin, however, is not the only method of stimulating receptors. Vibro stimuli or directly exciting the nerve endings also generate tactile sensations.

2.1.2.1 Mechanical Deformation

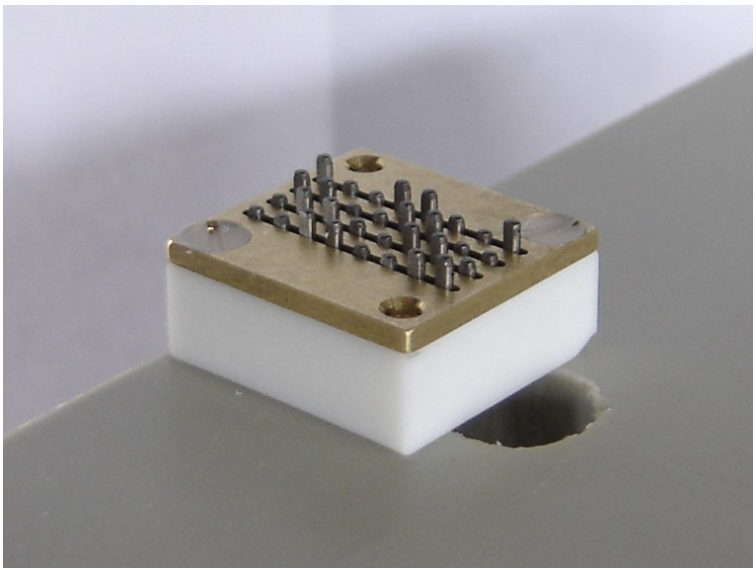

Figure 2.2: An array of metal pins push against the fingertip when raised [18].

Mechanical deformation can be achieved by displaying a grid of points with metal pins or pneumatic balloons (see section 2.2). Configuring the height of these pins (Fig.2.2) different patterns can be created which indents the fingertip touching the array. A study on human detecting capabilities, namingly their ability to identify features on an otherwise smooth surface with their fingertips was carried out to determine the parameters of such activity by Johansson and LaMotte [19]. They found the height difference to discern that there is a point present on a smooth surface must be at least 0.85 micrometres (Micron). They also state the detection of two distinct points on our fingertip needs a minimum separation of 1mm.

2.1.2.2 Vibro Stimulant

Kontarinis in 1995 discussed the use of vibro-tactile feedback in teleoperations and virtual environments [20]. Kontarinis suggested there were three categories of uses: directly interpreting the vibration information; using vibration to relay other types of information;

vibration that are not directly useful in determining the success of the task but is necessary to faithfully replicate the physical sense of touch for the task at hand.

Figure 2.3: A ball bearing component designed to turn gears [21]. There are two rings each with a narrow track that makes very small contact with the metal balls sitting in between. The inner ring may remain static. When the outer ring rotates, so does the metal balls which assists the rotatory motion by reducing the friction between the two rings. The mechanical nature of this device subjects the component to wear and tear limiting its lifespan [22]

The first use is to directly interpret the meaning of the vibration information itself. A simple example would be detecting the smoothness when a ball bearing is turned (Fig.2.3). If the metal balls are not adequately smooth then abnormal vibrations from the component can be detected. Kontarinis conducted an experiment to confirm that users were able to better identify this abnormality with vibration feedback rather than force and no feedback at all. However, in their experiment, only three subjects participated in the trials. The second category use vibration to relay other types of information. [23] investigated the relationship between vibration feedback and the perceived weight of a load, [24] also investigated a similar relationship but for handheld mobile phones so manufacturers can choose an appropriate and most effective frequency for providing vibration feedback for mobile alerts. The third catergory is considered ambient vibration which enhances the realism of a virtual environment but is not actually useful in improving the performance of the task itself. For example, if a vehicle simulator lacked the vibration on a steering wheel of a vehicle, it will differ from the real driving experience giving the user a reason to not believe it is the real thing. The vibration on the steering wheel will do little to assist in steering more accurately but is required to fully simulate the actual environment.

2.1.2.3 Nerve Endings

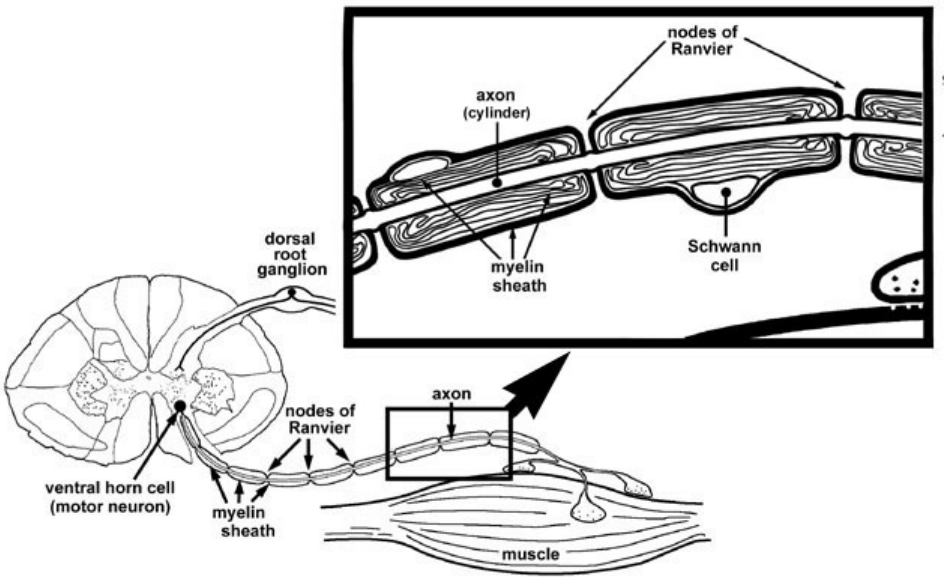

Figure 2.4: Diagram of a myelinated axon, the myelin sheath and ranvier nodes [25]

The mechanoreceptors nerve fibre can be directly stimulated by electrotactile feedback, also known as electrocutaneous as electricity is applied to the skin. Fig.2.4 shows a nerve fibre, also known as an axon. It is responsible for passing information around the nervous system by transmitting electric impulses. A myelinated axon is a nerve fibre that has myelin sheaths surrounding it and the gaps between these sheaths is the ranvier nodes. In comparison to an unmyelinated nerve, the former can transmit electric impulses quicker. The nerve fibres can be activated by external electric pulses when the nerve cells membrane voltage potential threshold is exceeded.

Electrocutaneous stimulations have been haunted by unpredictable pain sensations since their first usage. There is difficulty in regulating the amplitude of the electrical pulse as even the smallest change to the stimuli parameters e.g. skin resistance can cause pain to the user [26]. The feeling can range from being imperceptible to pain in the form of a sharp prick or burning sensation. The pain arises from thermal damage to the corneal layer in the skin when the electric current is applied.

The type of sensation does not vary as typical electro-tactile devices are limited to on and off signals. Kajimoto's Tactile Colors theory [27] suggests a possible approach to overcome this limitation. Analogous to how the human eye can perceive different optical information by selectively stimulating red, green and blue retina cones, by selectively

stimulating different nerve fibres it is possible to give different vibration and pressure sensations to the fingertip. Kajimoto claims that one possible way to do such is by switching the central electrode of an array of electrodes to either be a cathode or an anode, changing the current pathway and electric field, can selectively penetrate the different depths and thus, activate only certain nerve fibres.

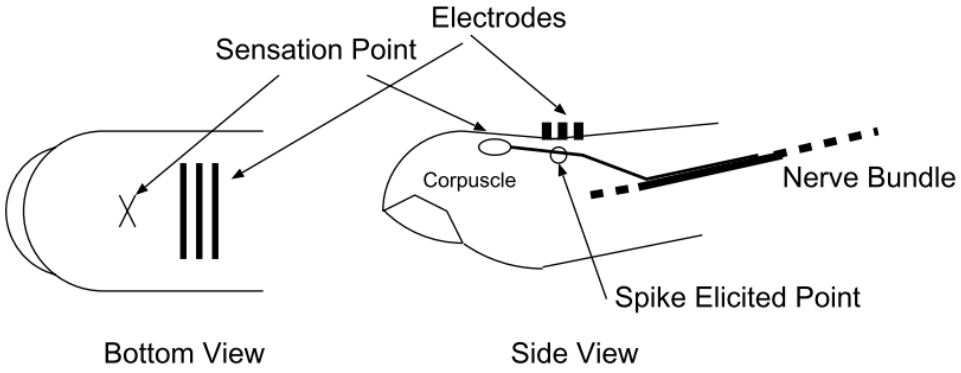

Figure 2.5: Despite stimulating the fingertip at a particular point, the sensation is felt further away from this site by 1-3mm [27]

A potential problem that Kajimoto has identified is known as the Sensation Shift (Fig.2.5). A nerve axon maybe activated by an electrode at a known location but the sensation may occur at a distant arbitrary location. For a myelinated nerve, it is only possible to pass the electric current into the nerve via the Ranvier nodes which means the point of stimulation is not the site of sensation. Currently it is not yet sufficiently accurate as it is unknown which fibre directly corresponds to a particular mechanoreceptor at a specific location out of the thousands that reside in the skin. This nonlinear behaviour will affect the spatial targeting difficult.

Kuroki et al [28] believed that devices exaggerated claims of having a high temporal resolution. The Pacinian corpuscles are more difficult to stimulate because it lies at a much deeper region of the skin. This statement, however, was later rectified by one of authors, Kajimoto [27] stating the Pacinian corpuscle can be neglected as its population is sparse compared to the other three mechanoreceptors.

A stimulus need not necessarily be applied to glabrous skin exclusively. Stimulating hair follicles with vibration [29] were investigated to determine whether emotive sensations could be conveyed and applying electrotactile stimulation to the tongue [30] has also been considered as alternative areas in which stimuli could be applied.

2.2 Tactile Technologies

Tactile feedback has been applied to various applications driven by different underlying technologies. There are advantages and shortcomings to each type of driver. In this chapter, a summary of each technology will be given.

2.2.1 Shape Memory Alloys

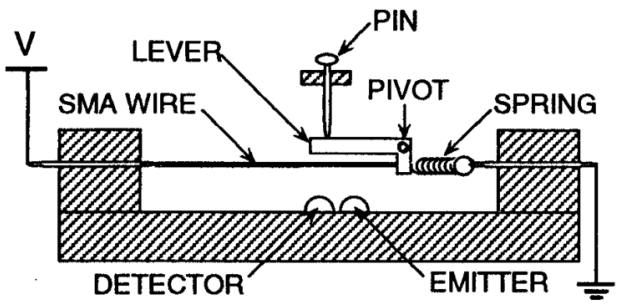

Figure 2.6: The actuator of a pin using shape memory alloy wires [31]

Kontarinis [32] describes the use of Shape Memory Alloy (SMA) in the form of wires. The length of the wire contracts when heat is applied and returns to their original shape when the heat is removed. Applying and removing an electric current through the SMA wire will achieve said effect as heat is generated when a current is met with substantial electrical resistance since the wire is thin. When the wire connected to a lever contracts, the lever will rise which in turn pushes up a pin (Fig.2.6). An array of these pins can be actuated by this type of mechanism. Using a wire actuator offers the advantage of tightly configuring an array of pins to give a relatively high spatial resolution since the mechanism is not bulky.

Matsunaga [33] incorporates the working principle of this system by adding magnetic latches to the top of the pin. The idea is to reduce the amount of electrical consumption and heat being passed from one pin to another. Once a pin is raised, the magnetic latch holds it in place removing the need to keep supplying an electrical current. Besides actuating pins, very thin SMA wires can be made to vibrate for vibrotactile feedback [34] as they rapidly contract and return to its original state. Another novel way of using SMA wires was shown by [35]. The SMA wire is coiled around a thimble worn on the finger. When SMA contracts around the thimble, the feedback is felt by the fingers.

SMA however, suffers from hysteresis giving rise to nonlinear behaviour making it difficult to control the lowering and raising of pins in a timely manner. Slow rate of heat

dissipation causes a delay in response time. Attempts have been made to facilitate the heat dissipation with pneumatic cooling [31] for faster response times.

SMA is attractive as the entire mechanism can be compacted into one fingertip sized casing. Rather than rely on heat to cause the retraction, a motor could be used instead [36]. It will eliminate hysteresis at the cost of increasing the size of the entire system. The motor has also been used to actuate a small cylindrical brush to simulate rough and abrasive textures [37] instead of driving a pin array.

2.2.2 Pneumatics

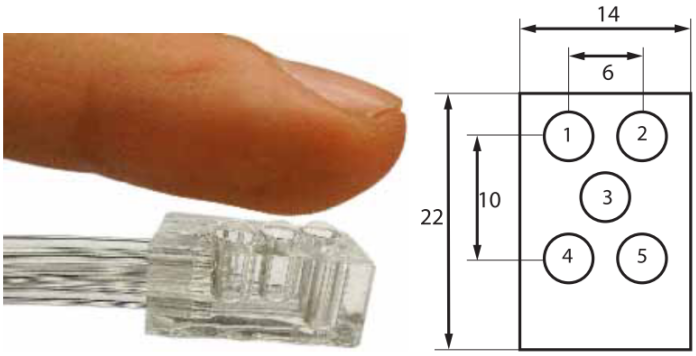

Figure 2.7: An array of balloon pockets [38].

Pneumatics involve the use of air which is considered a clean source. An array of small balloons can be inflated with air to deliver mechanical deformation stimuli (Fig.2.7). The diameter of the balloon and spacing between each pocket determines the spatial resolution of the array. In comparison to metal pin arrays, the spatial resolution is lower as the head size of a metal pin can be much smaller than an air pocket. Although balloons do not suffer the same degree of hysteresis as typical SMA actuation, balloons provide less indentation.

A much larger balloon, called a bladder, can provide a bigger force output whilst withstanding higher pressure. One example of using a pneumatic bladder is seen in a colonoscopy simulator [39] where the patient is intubated with a colonoscope via the colon. Occassionally the camera may be obstructed by the internals of the patient and one method to remedy this situation is to apply an external force to abdomen. This haptic output, however, is not capable of conveying tactile feedback as the force is felt as resistance on the joints of the limb rather than on the skin of the hands as touch contact information.

Alternatively tactile feedback can be delivered directly through air tubes [40]. A finger is placed on top of a flat array of valves. When air is vented through the tubes a pressure is induced where the finger blocks a valve. This, however, requires the contact between the finger and the valve to be sealed so pressure can build up. Moy [41] demonstrated that this condition can be fulfilled much more readily with a flexible silicone mould that wraps around the finger. In this case, the finger is strapped to the mould to ensure the finger is fully pressed against the valves. The disadvantage of this approach is the feedback device is attached to the wearer which may hinder movement.

A pneumatic cylinder has two chambers separated by a movable plate (Fig.2.8). By pressurizing one of the chambers in the cylinder the plate can be displaced which in turn

Figure 2.8: A pneumatic cylinder with a plate separating two chambers that can be filled and pressurized with air [42].

pushes a rod out of the cylinder [43]. Rod retraction could either be done by attaching a spring coil to the plate (single acting) or pressurizing the opposite chamber to push back the plate (double acting). This can be used to drive pistons facilitating force/tactile feedback as seen in a breast cancer palpation simulator [44]. The pistons are limited in the sense that it can only move in a linear motion, however, rotary actuators do exist but there is a trade-off between deliverable power and the cost and size of the device. This type of technology will also suffer from mechanical wear and tear.

2.2.3 Electromagnetism

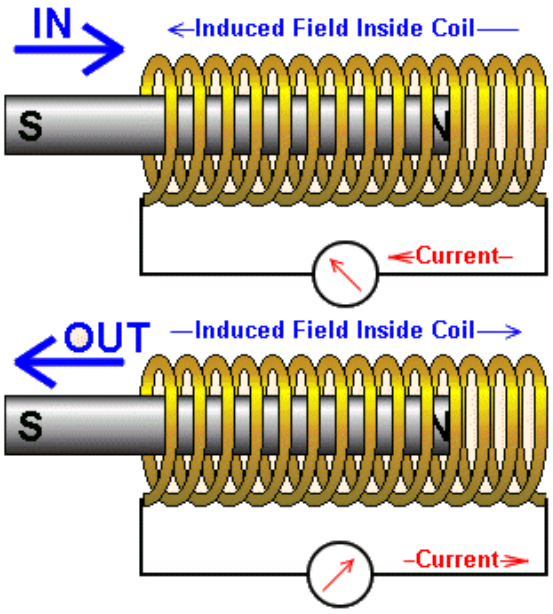

Figure 2.9: A metal plunger moves linearly into and out of a coil of wire [45].

Solenoids are helical coils of wire that generate an electromagnetic field when an electric current is applied. The polarity of the electromagnetic field is controlled by which direction the current is passing through and thus, linear actuation can be achieved when the coil surrounds a metal plunger and the polarity is switched (Fig.2.9). As this mechanism is controlled by an electric circuit, the fast response time is considered to be this technology's advantage and was attempted to be used to generate vibration by switching the polarity at a higher frequencies. Hwang [46] investigated the use of solenoid vibration instead of a conventional motor to provide vibration feedback in mobile phone devices. Hwang states that motors deteriorate quickly with use and by replacing this with a simpler electromagnetic actuation reduces the number of parts that can be subjected to wear and tear improving its lifespan, but the relative strength of the vibration is lower due to the size of the metal component responsible for generating the vibration in the housing.

Solenoids can also be used to drive an array of metal pins similar to that of SMA. In comparison to SMA wires, solenoids are larger in size therefore arranging them to give a high spatial resolution can be a challenge. Frisken-Gibson [47] has attempted to increase the resolution by a double layer of solenoids (Fig.2.10). Linear solenoids are difficult to control precisely i.e. the plunger either gets pulled to the left or right hand side with no middle ground. Frisken-Gibson's device only manage to deliver four height levels at most instead of the other possible variants between the minimum and maximum height.

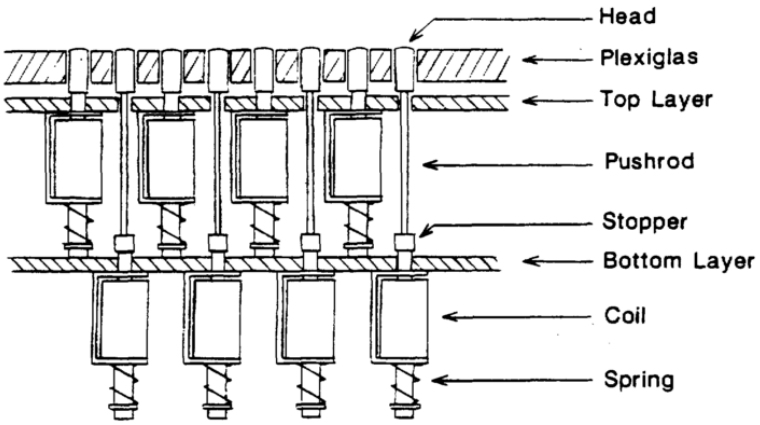

Figure 2.10: A double layer of solenoid coils where the pushrod from the bottom layer sits between each solenoid in the top layer to increase resolution [47].

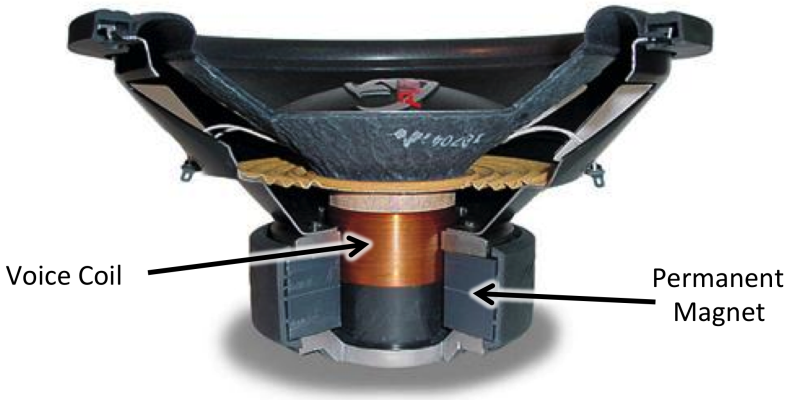

Figure 2.11: Voice coil used in a loud speaker for linear actuation of the loudspeaker diaphragm [48].

Voice coils are very similar to solenoids, however, one major difference is the use of a permanent magnet and a movable coil. A loudspeaker is one common example of using voice coils (Fig.2.11). The coil is attached to the apex of a speaker cone and is either attracted towards or repelled away from the permanent magnet at the base depending on the direction of the current running through the coil. By allowing the lighter weight component to move, higher acceleration and speed can be achieved to provide vibrotactile feedback.

2.2.4 Electrodes

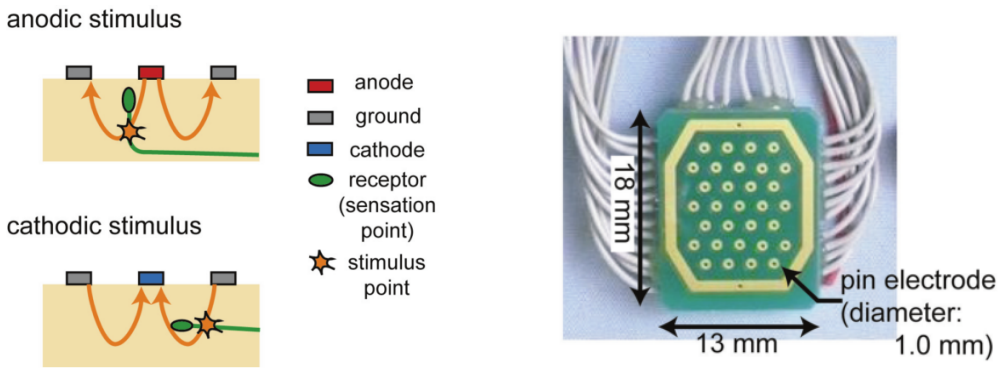

(a) Coaxial electrodes and which axons the type of stimulus can activate

(b) Pin sized electrodes

Figure 2.12: An array of electrodes where the user may place their fingertip for electrocutaneous stimulation [49]

Surface electrodes are used to achieve electrocutaneous stimulation by applying a small electric current to the skin in an attempt to active the underlying axon giving the impression of vibration or pressure. (Fig.2.12a) shows how axon activation could be achieved depending on the charge of the electrode which determines the flow of the electric current. An anode is a positively charged electrode where electrons travel away from it, towards ground and a cathode is a negatively charged electrode where electrons travel towards it. Kajimoto [50] explains that when the central electrode is an anode, an anodic stimulus will stimulate axons that are more vertically aligned inducing pressure sensations. When the central electrode is a cathode, a cathodic stimulus will activate axons which are parallel to the skin more readily to induce vibration sensations.

The pin sized electrodes can potentially be arranged in an array (Fig.2.12b). The pin sized electrodes allows such devices to be small in size requiring less power than moving mechanical components which also suffer from mechanical wear and tear. Electrodes are also quiet during operation.

As mentioned earlier in subsection 2.1.2.3: Nerve Endings, painful sensations can occur. Conductive electrode paste has been used to reduce pain occurrences but unfortunately the paste must be reapplied frequently, is messy to apply and can eventually ruin the electrodes. Additional current must also be supplied if the current is to be successful in penetrating the paste and passing through to the skin which can inadvertently increase pain. This is the contributing factor to the reluctant use of electrocutaneous stimulation.

2.3 Applications

Tactile feedback has been utilized in a variety of application areas which will be briefly discussed.

2.3.1 Cross-Modality and Tacton Perception

There is research into how vibrotactile and pin arrays can be used as another modality for representing information besides our visual sensory system. Tactile icon (Tacton) is a symbolic representation of information. Tactons can be represented by modulating the frequency and pulse of the vibration signal or pictorially with pin arrays (Fig. 2.13).

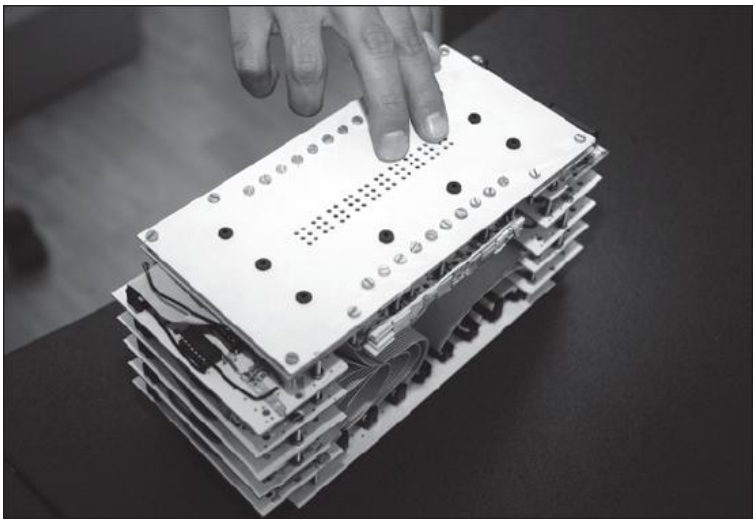

Figure 2.13: Braille; a series of patterns that convey information to the person via their tactile sense [51]

Han [52] investigated the use of vibrotactile feedback for in-vehicle information delivery, as more functions are being added to a vehicle the navigation menu becomes increasingly difficult to use whilst operating a vehicle. In an attempt to come up with an improved interface, the vibration modality is explored. The challenges lies in designing a feedback that is distinguishable from the ambient vibrations already present in the vehicle and also how easy it is for the user to learn the pattern. Ambient vibrations are different depending on the status of the vehicle such as when the engine is on but parked, the vehicle is clutched, driving on a paved road or highway at different speeds and also depending on the age of the car the amount of vibration could increase from mechanical wear and tear so designing a robust vibration pattern that can be universal will be difficult.

Karam [53] attempts to make a sensory substitution system to try and transmit emotional information to the deaf or hard of hearing by transmitting vibrations to the back via a chair with voice coils. The authors state that movies and music contain important emotions stimulated by sound and if absent, the user may not be able to fully enjoy the entertainment. This sensory substitution system aims to provide this missing part to the deaf or hard of hearing by converting the sound to vibrotactile feedback. By using a chair to deliver the feedback, the user is free to use their arms for other activities although the back is considered a less sensitive area of the body in comparison to the fingertips.

Okada [54] explains that deaf people fear walking in the street as they cannot hear signs of danger e.g. a passing vehicle for instance. They attempt to build a system which detects sounds and translate that into an electrocutaneous signal for the user to interpret. Tang [55] also tackles the same problem but instead uses a mouthpiece to deliver electrocutaneous feedback. A tethered mouthpiece would be impractical and so a remote signalling system was also developed to facilitate the use of the device (Fig.2.14). It is unreported how wearing the mouthpiece affects the user's ability to make speech but nonetheless, is an improvement over Ikeya's system [56] as the device consisted of a camera to process the video of the captured environment to detect for collisions in the user's path and is worn around the neck, the feedback device is also held in one hand leaving only the other for other activities like opening doors.

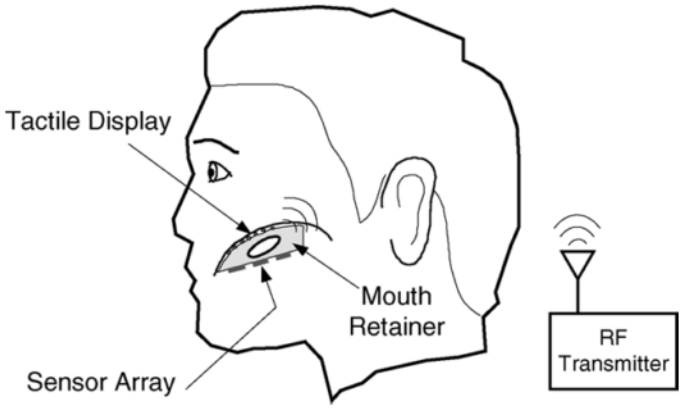

Figure 2.14: A mouthpiece that can deliver electro stimulus to the roof of the mouth for blind navigation [55]

Supriya [57] used solenoids to create a braille pad consisting of an array of metal pins for blind users to be able to use personal computers for tasks such as reading documents, knowing the location of the cursor etc. The braille pad is integrated into a keyboard. Rantala [58] in contrast worked on making mobile handheld devices usable by the blind

with smaller piezoelectric actuators. Velazquez [59] makes a system to convert existing ebooks to a braille version as they claim that audio-books is no substitute for a book that is to be read. The converted version can then be displayed in a portable braille interface (Fig.2.13)

There has been research in using tactile feedback to enhance security such as biometrics. Finger biometric can be compromised by a fake or dead finger. By presenting a tacton to the user, they have to select which pattern was displayed to them before gaining security clearance [60].

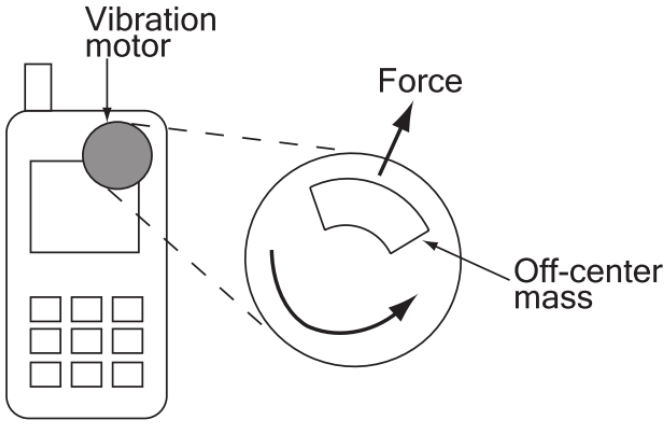

Figure 2.15: Vibration from a mobile device can be achieved with a rotary motor and an offset mass [61]

Vibrations from a mobile phone alert the user of incoming calls and other services and is commonly provided by a rotary motor with an offset mass (Fig.2.15). Shafiq ur-Rehmamn [61] attempted to convey the interaction of a football in a live game to a mobile phone held by a user. When the football is kicked, feedback is provided on the mobile phone. Yang [62] states that vibration alone on a mobile device is insufficient to convey more detailed information such as texture. They have miniaturized a pin array with springs and solenoids to create a module small enough to be mounted inside a mobile phone sized device. However, such a small pin array actuated by solenoids will not provide a very strong force output from the pins and is also limited to outputting an upward vertical force. Gamepad controllers for the current generation of video gaming consoles also have vibration feedback to reflect what the game character is experiencing in the virtual environment but these are commonly offset mass motors that cannot represent the direction of the force.

2.3.2 Therapy and Learning

The aim for this type of application is to deliver feedback to the user so they can use this information to adjust their movements or positioning of their limbs accordingly. This aids rehabilitation of limbs that may not be moving in the correct manner or learning new skills. Vuillerme [63] investigated the use of a tongue stimulating device to provide information about the position of the user's ankle. Danilov [64] also used a tongue stimulating device to help correct balance disorder. The problem foreseen with such devices is, how willing the user is to using a mouth piece. Attaching the device to one's tongue impairs the ability to communicate verbally. Wu [65] also tackled balance disorder but instead used a wearable vest with pneumatic actuators to provide feedback felt on the shoulders and torso. These areas are considered to be less sensitive as it contains less mechanoreceptors.

Figure 2.16: A wearable vest with hidden vibration motors embedded at selected joint positions. The white markers aid in optical tracking of the limb [66]

Seps [67] investigated the placement of electrocutaneous feedback on the lowerback to provide the missing sensations from prosthetic limbs. Placing the sensation on the lowerback with a lower density of mechanoreceptors than other areas of the body is not ideal but other parts of the body that are more sensitive such as the hands are already overloaded with other tasks such as manipulating everyday objects to continue a normal life. They determined the effect of using different electrode sizes and found it was easier to avoid

the pain threshold with larger electrodes but decreased the ability to distinguish between inter-electrodes.

In skill building, Lieberman [66] created a wearable vest with markers attached at selected joint positions (Fig.2.16). They claim that wearing a feedback vest is more efficient than a teacher as the vest can stimulate several different points on the body simultaneously. The markers on the vest is used in optical tracking to input the positions of the real limb for comparison against the ideal position. Vibration motors are then used to indicate to the user whether they need to move the limb to correct their posture. Alahakone [68] placed sensors on their wearable device but in doing so increased the complexity of the device itself and increased the size of the wearable device.

2.3.3 Robot-assisted Surgery

Teleoperation such as minimally invasive surgery involves the manipulation of delicate human tissue and is carried out with robotic graspers through a small incision on the patients body [69]. The absence of touch sensory information means the surgeon has difficulty in gauging how much force they should apply. Inappropriate amount of force from the grasper could damage the tissue during manipulation. Attempts have been made to tackle this area. Bethea [70] used a visual representation in the form of a colour bar scale ranging from yellow to green to red indicating the tension in the robotic graspers. The participants were asked to keep the colour bar in the green zone which was calibrated to be a mean tension pre-recorded for the task of tying a knot to seal a wound. Although this method indicates the amount of tension used, it does not indicate whether contact has been made with the tissue.

Figure 2.17: A robotic grasper with a thin piece of piezoelectric material overlaid on the bottom to sense contact with tissue [71]

Wottawa [71] integrated a thin piezoelectric sensor on the robotic grasper to sense when contact is made with human tissue (Fig.2.17). This is not completely ideal as the overlaying piezoelectric covers the tiny teeths on the grasper used in the gripping of the tissue. The tactile feedback is displayed in the form of a balloon array attached to the handle of the grasper. McMahan [72] also used a similar sensor in their device but displayed contact information in the form of vibration. King [73] confirmed that the addition of tactile information induced less force used in manipulating tissue and hence avoids undue damage.

2.4 Simulating a pulse and thrill sensation

We now consider using the technologies mentioned previously to simulate an arterial pulse and thrill sensation. We use our own radial artery as a benchmark for this discussion. We determined that the arterial pulse sensation on our own wrist when felt with the fingertip has an area of effect roughly 15mm in diameter on the wrist. One possible way of mimicking the pulsation is by using a potentially 10mm wide piston to actuate a piece of fake sillicone skin vertical up and down (Fig.2.18). A piston approach is mechanically the simplest in simulating an arterial pulsation as it mimics the act of pushing against the layer of skin.

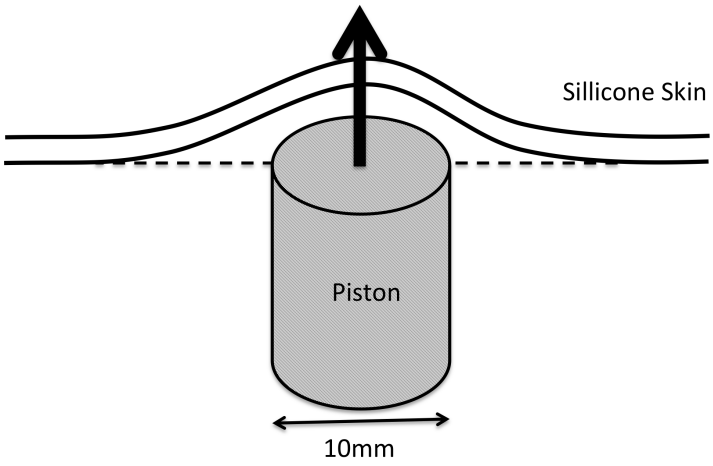

Figure 2.18: A piston roughly 10mm wide pushes against a layer of fake sillicone skin to mimic the motion of an arterial pulsation

SMA wires are commonly used to actuate smaller metal pins. If the collection of pins all push upwards on a fake silicone piece of skin, the user may feel the individual metal heads of each pin through the fake skin. Also, due to latency in SMA (hysterysis) the return time for the pins to lower may not be sufficiently quick enough to mimic the same frequency of an arterial pulsation. Solenoids have much faster response times but the components are much bigger in size in comparison. Pneumatic actuation could actuate a piston which pushes against a fake skin to mimic the arterial motion but the location of this sensation is fixed in one spot. Creating an array of these pistons allows the sensation to be placed in different regions of the workspace but due to the size of the piston itself and the technolgy used to actuate these pistons, the achievable spatial resolution would be quite limited. This piston approach, however, is not ideal as the edge of the piston itself could

possibly be felt through the fake skin. The fake skin could be made to be thicker to hide the piston further but in doing so, would make the sensation seem to come from a deeper region of the body.

A thrill is an even larger region of effect in comparison to an arterial pulsation and could be felt as vibration. Voice coils can provide vibrations which could be used to simulate a thrill sensation but may not be sufficient to actuate a piston. Pneumatic balloon arrays could simulate an arterial pulse to some degree as the air pocket can be inflated and deflated quickly, however, its ability to simulate a thrill sensation is limited as pneumatics are not commonly used to generate vibration. Air jets has a very limited spatial resolution and so would be difficult to control the area size of the sensation. Electrocutaneous stimulation could also provide some form of vibration sensation but this approach suffers from unpredictable pain sensations and the sensation shift where the location of the stimulation is different to where the sensation is perceived.

All of the mentioned technologies has shortcomings that make it inadequate to simulate an arterial pulse and thrill sensation. This information is displayed as a table of comparison (Table.2.1). A new approach is required to improve this type of simulation.

	Advantages	*Disadvantages*	*Controllability: can it display an arterial pulse or thrill sensation?*	*Spatial resolution of tactile region*
SMA	- Small footprint - Compact - Low power	- Hysteresis - Limited vibrotactile stimulation.	Very difficult due to heat hysteresis. Will not be fast enough to simulate a pulse rhythm.	Restricted by size of metal pins.
Servo Motor	- Small footprint - Compact - Low power	- Only vibrotactile	Only vibrotactile feedback which is not similar to the actual movement of the arterial wall in the artery.	Restricted by size of motor.
Pneumatic	- Clean source - No mechanical resonance - Flexible tubing	- Height displacement of balloon in a 'pin array' is very limited -Length of tube can introduce hysteresis.	Difficult to control the strength of the arterial pulse or thrill.	If balloon is too small, height displacement extremely limited
Electro-magnet	- No hysteresis	- Difficult to finely control height displacement in pin array. - Size of device	Difficult to control the strength of the arterial pulse or thrill.	Restricted by the size of the solenoids which tend to be chunky.
Electro-cutaneous	- Solid state - Stimulate texture - No hysteresis	- Pain sensation - Energy projected into the body. - Requires absolute precision to stimulate the right nerve.	Does not mimic the same movement as an arterial pulse.	Restricted by the size of the electrode.
Air jets	- Clean source - Simulate windy environment effect	- Limited spatial resolution	Not possible to simulate due to large area of effect.	Large due to the blasting of air.

Table 2.1: Table comparing the technologies to simulate a pulse or thrill sensation.

2.5 Summary

In this chapter, a brief discussion of tactile stimuli was given. Tactile feedback can be achieved in three approachs; mechanical deformation, vibration and stimulating the nerve endings. Several different existing tactile technologies such as SMA, pneumatics, solenoids and electrodes were used to provide these type of stimulus in a range of applications such as cross-modality and teleoperation but they all have shortcomings which may not be suitable in simulating an arterial pulse and thrill sensation. A new approach is required and airborne ultrasound is a relatively new and novel technology which has yet to be implemented as tactile feedback in the context of a medical simulator. The next chapter will discuss the characteristics properties of acoustic radiation pressure which can be used to generate tactile feedback.

Chapter 3

Acoustic Radiation Pressure

Tactile feedback can be generated from a physical phenomenon called Acoustic Radiation Pressure. It is essentially a force field with a point of concentrated pressure emitted from multiple ultrasonic transducers in three-dimensional space. Interestingly, ultrasound can provide any three of the mentioned stimuli in section 2.1; exert pressure on skin, generate vibrations and directly stimulate nerve endings depending on the frequency and power [17]. Iwamoto's earlier work suggests that radiation pressure is much better suited to surface deformation as stimulating nerve endings provided very limited sensations as it was difficult to selectively excite the nerves.

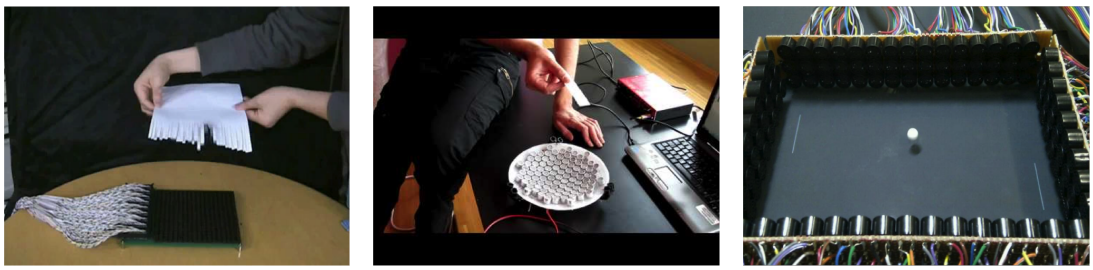

(a) Hoshi [74] (b) Ciglar [75] (c) Marshall [76]

Figure 3.1: Examples of existing airborne ultrasound tactile devices from other researchers

There are only a few exemplar applications using airborne ultrasound for tactile feedback (Fig.3.1). The first key application used acoustic radiation pressure to make holograms touchable by Hoshi [74]. This device consisted of around 400 ultrasound transducers arranged in a square array, each controlled individually to focus 40KHz ultrasonic beams at a focal point and thus a complex system needed to be fabricated to operate it. A few years later other authors had attempted to make use of acoustic radiation pressure in other areas. Ciglar [75] adapted the technology to create a musical instrument. Ciglar arranged the ultrasonic transducers in a hemispherical arrangement which physically aligned the transducers to a single focal point. This approach allowed the device to be operated with just

one control signal but in doing so disabled the ability to re-position the sensation at any other position. Marshall [76] attempted to establish a link between digital content and the physical world via an interactive table and a polystrene ball. For their device, they created four mini panels of ultrasound transducers to form a box. The previous device emitted ultrasound vertically upwards in the y-axis. Although this device cannot emit ultrasound in the y-axis, it is able to emit in both the x-axis and z-axis. Because there are less than eighty ultrasound transducers, the force output from this device is considerably weaker and thus is only able to fully manipulate a polystrene ball no bigger than the size of a garden pea.

Ultrasound could also be used for other applications other than tactile feedback. High intensity focussed ultrasound (HIFU) is used as a medical treatment for cancer and its workings and properties are well explained in an article by [77]. The guide for HIFU explains that ultrasound at megahertz frequencies is transmitted into the body to cause heat that ablates tumours. This differs from airborne ultrasound tactile devices as the frequency used for such is in the kilohertz range. Ultrasound is also used for acquiring images of the patient's inner body. The echoes of the ultrasound reflected from the different material in the body such as bones and fat deposits are detected and used to create a grayscale image. In the case of HIFU and ultrasound imaging, for ultrasound to penetrate the skin, a special gel is applied to the surface of the skin before the ultrasound emitter is used. These applications also only use a very small number of transducers.

The number of exemplary applications that use airborne ultrasound as tactile feedback has been very small and as of yet, this technology has not been used in a medical simulation context. In this chapter, a discussion on the theory behind acoustic radiation pressure will be given along with equations for calculating the Coefficient of Reflection and Acoustic Attenuation. The characteristics and advantages of using ultrasound will then be discussed. How to achieve a force-field from ultrasonic transducers will be explained.

3.1 Theoretical Framework

Acoustic Radiation Pressure is the acoustic pressure from a sound wave and can be understood in relation to momentum. Sound propagates through air as longitudinal waves, the air particles oscillate and transfers its momentum by hitting the adjacent particle which in turn also oscillate horizontally. When a particle hits a surface, it transfers the momentum to that surface (Fig.3.2). If this surface was the palm of a hand then a significant amount of energy would create a force that can be felt. This means that the user need not physically be in contact with the tactile device itself and the sensation can be remotely transmitted

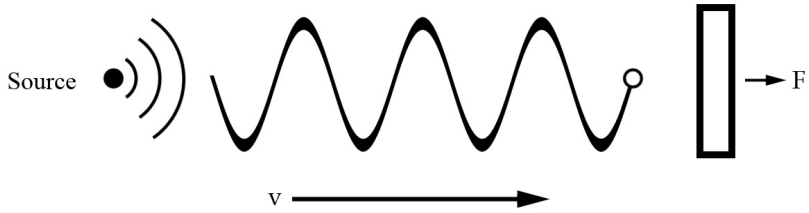

Figure 3.2: The oscillation of air particles hit against surface and transfer their momentum to it inducing an amount of force that could be felt if the surface was the palm of a hand.

The equation for radiation pressure on a surface is given as:

$$P = \alpha \frac{p^2}{\rho c^2} \tag{3.1}$$

Where the symbols:

p = total sound pressure from all ultrasonic transducers [Pa]

α = constant of reflection coefficient [unitless]

ρ = density of the transmission medium [kg/m^3]

c = speed of sound in the transmission medium [m/s]

As the equation suggests, it is possible to control the radiation pressure (P), in units of Pascals, as it is exponentially proportional to the total sound pressure of the ultrasonic transducers (p), therefore, to create an acoustic pressure that is sufficient enough to be felt is principally depends on how many transducers are used to create an area of high acoustic pressure.

3.1.1 Transducer Pressure

The amount of sound pressure a transducer produces is normally given as a Sound Pressure Level in decibels (dB SPL) on their datasheet for convenience. This dB SPL value is determined experimentally by the manufacturers for a given distance from source to receiver. This distance is typically 30cm. The equation for radiation pressure (3.1) requires the sound pressure to be in the units of Pascals (Pa), therefore it is necessary to convert dB SPL to Pa if one desires to use equation (3.1). The following is a standard equation used to determine the dB SPL using 20μPa as the zero reference point as this is the value for the threshold of perception of sound.

$$dB = 20\log\left(\frac{p}{20\mu}\right) \tag{3.2}$$

Rearranging (3.2) for p will give the sound pressure in Pa:

$$\begin{aligned} p &= 10^{\frac{dB+20\log(20\mu)}{20}} \\ &= 10^{0.05(dB+\log 20\mu)} \end{aligned} \tag{3.3}$$

The total sound pressure would then be a multiplication of the number of transducers (x) with the sound pressure (p). It is still more convenient to present total sound pressure (dB_T) in dB SPL, therefore the dB_T from x number of transducers is a summation of the individual logarithms:

$$\begin{aligned} dB_T &= 20\log\left(\frac{xp}{20\mu}\right) \\ &= 20\log x + 20\log\left(\frac{p}{20\mu}\right) \end{aligned} \tag{3.4}$$

In regards to sound pressure in Pascals, if the value of p is considered constant for all transducers, the above equation where x multiplies a constant value of p suggests that the relationship between the number of transducers and the total sound pressure is linear, however, this is under the assumption that all the transducers contribute equally towards the total. In practice this is not the case due to attenuation from the ultrasonic beam's directivity which will be discussed in subsection 3.1.2 Focussing Ultrasound.

3.1.2 Focussing Ultrasound

The sound pressure from one ultrasonic transducer is not enough to provide any tangible perception of the radiation force. In order to generate tactile feedback, multiple sources of ultrasound i.e. multiple ultrasonic transducers, must be combined together. In order to achieve this, the shape of the emitted ultrasonic beam needs consideration. Fig 3.3 shows a typical simplified 2D shape of emission for a transducer.

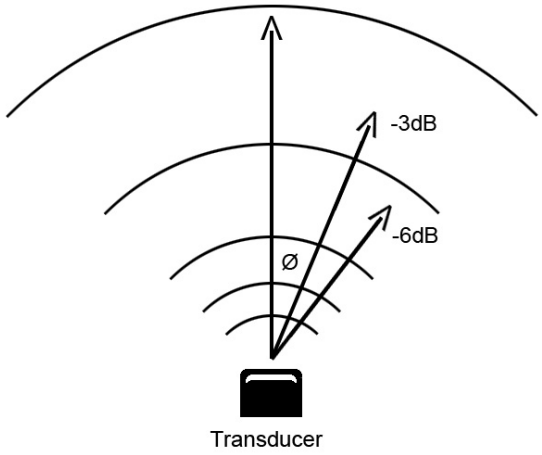

Figure 3.3: Shape of emission and beam divergence

The area of emission spreads out of the transducer in the shape of a cone. Because of this shape, all ultrasonic transducers will exhibit a physical phenomenon called the beam of divergence. This means a beam will get weaker as the beam strays away from the transducer's normal (the line which is perpendicular to the surface of the transducer). The angle ϕ determines the amount of divergence needed for the beam to suffer a loss of -3dB i.e. 50% loss. This information can be found in the manufacturer's datasheet for their product.

There are three general methods to focus ultrasound:

1. Electronically using a phased array. This means introducing a phase difference into each driving signal for the transducers. This phase difference is determined by evaluating the difference in distance a beam has to travel to reach the point of focus.

2. Mechanically by physically aligning the transducers towards the focal point so the centre line-of-sight are all facing the focal point. All the beams would then be equidistant to the focal point so requires no phase control to compensate for a difference in distance.

3. Using an acoustic lens to focus the emitted ultrasound towards a particular direction. This is generally a disadvantage as the focussed pressure will not be point-based but rather a pressure beam therefore it is not possible to localize a single point of tactile feedback in a three-dimensional workspace.

Method 1) has mainly been used in literature as the focus can be achieved with a control system consisting of software and electronics. Method 2) presents a less complex control system but places much demand on mechanical engineering as the precision of alignment will determine the effectiveness of the device. Both methods have been investigated in this thesis and are explained in greater detail in chapter 4.

3.1.3 Reflection Coefficient

For airborne ultrasound to exert a force on the surface of skin, the acoustic wave must be reflected rather than absorbed by the skin. This reflection occurs at the boundaries of the two different mediums, air and skin. The reflection is caused by a difference in the acoustic impedance of the two mediums. Therefore the percentage of reflection is determined by the impedance mismatch R which is calculated by the following equation:

$$R = \left| \frac{Z_s - Z_a}{Z_s + Z_a} \right| \tag{3.5}$$

Where the symbols:

Z_s = the acoustic impedance of skin [Ns/m^3]

Z_a = the acoustic impedance of air [Ns/m^3]

This in turn defines the reflection coefficient α:

$$\alpha \equiv 1 + R \qquad where \ \ (1 \geq \alpha \geq 2) \tag{3.6}$$

If the coefficient is equal to 1, then ultrasound is absorbed by the surface. A coefficient of 2 will completely reflect all of the acoustic energy. The impedance mismatch for air and skin is calculated by using equation (3.5) with acoustic impedance values of $1.52 \times 10^6 Ns/m^3$ and $0.0004 \times 10^6 Ns/m^3$ for air and skin respectively.

$$\begin{aligned} R &= \left| \frac{1.52 - 0.0004}{1.52 + 0.0004} \right| \times 100 \\ R &= 99.95\% \end{aligned} \tag{3.7}$$

This calculation suggests that almost all of the acoustic waves will be reflected off the surface and will not penetrate the skin and thus it is possible for the user to feel the force with their palm.

3.1.4 Acoustic Energy Attenuation

As an acoustic wave propagates away from its source, some energy is lost due to absorption. The rate of energy loss is dependent on several factors including temperature of the room and the frequency of the ultrasonic wave. A general equation to calculate the energy at a particular distance away from its source is as follows:

$$E = E_0 e^{-2\beta z} \tag{3.8}$$

Where the symbols:

E = Energy density at the distance z [J/m^3]

E_0 = Energy density at the surface of the transducer [J/m^3]

β = Attenuation Coefficient of ultrasound [Np/m]

z = the distance from transducer [m]

The chosen frequency for airborne tactile feedback is 40KHz. This is due to two main reasons as stated by Hoshi [78]: 40KHz transducers are commercially available and are easy to procure; the energy loss at 40KHz is significantly lower compared to higher frequencies. A high energy loss would reduce the total acoustic radiation pressure which means the sensation would become too weak to be felt. This particular frequency allows a reasonable range to be achieved when remotely positioning the sensation in the workspace.

3.2 Characteristics and Advantages

There are several reasons why ultrasound is an attractive medium for tactile feedback.

3.2.1 Spatial Resolution

The spatial resolution of ultrasound can be finely controlled. Depending on the frequency used, the diameter of the focal point can be as small as 1mm. The width of the focal point is estimated by:

$$w = 2\lambda\frac{R}{D} \tag{3.9}$$

Where the symbols:

w = width of the focal point

λ = wavelength of the ultrasound

R = distance from array to focal point

D = width of the transducer array

If $\frac{R}{D}$ = 1, then the width is determined solely by twice the wavelength of ultrasound. Choosing a higher frequency would achieve a finer focal point but consequently increases the energy loss so the range that the sensation can be remotely positioned at will be greatly reduced.

3.2.2 Bandwidth

Ultrasound exceeds the boundary of human tactile perception of 1KHz. Therefore it is easy to provide a constant pressure field or if desired, generate vibrotactile feedback by using frequencies lower than 1KHz. Nerve endings can also be stimulated with frequencies in the megahertz range but there are no recent literature describing its usage for such purpose.

3.2.3 Remote Sensation

The user normally maintains constant contact with a haptic device which can give rise to unwanted sensations. These devices may also suffer from inconsistent delivery of sensations due to difficulty in ensuring contact conditions are the same throughout the device's usage. Acoustic radiation pressure does not rely on direct contact with the device and thus is contact-free i.e. the sensation can be remotely presented anywhere in a workspace. In virtual environments and simulation, wearing peripherals detract from the overall immersive experience which makes acoustic radiation pressure an ideal medium for such purpose.

3.3 Summary

Acoustic Radiation Pressure is a physical phenomenon which can be utilized to generate a focalized force field. The phenomenon can be compared to momentum of air particles hitting against a surface and thus inducing a force. Airborne ultrasound has been used as tactile feedback in previous applications such as hologram interaction, musical instrument and digital manipulation from other researchers, however, ultrasound is not limited to this area. Other medical applications have employed ultrasound in the form of high intensity focussed ultrasound to ablate tumours and ultrasound imaging is used to obtain images of a patient's inner body structure.

To fully harvest this force, ultrasound must be fully reflected off the surface. This reflection condition can be achieved by considering the acoustic impedance mismatch of the two mediums. A significant difference in impedance will ensure almost 100% reflection. The energy loss is also considered. The loss is directly influenced by the frequency used for ultrasound. Hoshi et al has investigated and concluded that 40KHz is most suitable as the energy loss is almost insignificant compared to higher frequencies.

The force field can be created from ultrasonic transducers. The acoustic sound pressure emitted from a single transducer is not significant to create a tangible tactile sensation. Hence multiple ultrasonic transducers must be used to generate the focalized force field. The focalized force field can be generated by three methods; electronically with a phased array, mechanically by aligning the transducers towards a point and using an acoustic lens for focussing. Current applications favour the electronic method to create the force field as mechanical aligning the transducers can be more complex and requires precise construction.

This technology is an attractive medium for tactile feedback due to several characteristics. The spatial resolution of the focal point can be as small as 1mm. The bandwidth overlaps and exceeds the human tactile perception of 1KHz suggesting the technology's ability to stimulate a constant force and vibrotactile feedback if desired. It is also considered a contact-free technology as the user does not directly interact with the system itself.

Chapter 4

Building UltraSendo

This chapter will outline the construction of UltraSendo, a completely custom built tactile device and its predecessing prototypes. The device has three main functions which must be implemented to give it the ability to generate airborne ultrasonic force output (Fig 4.1).

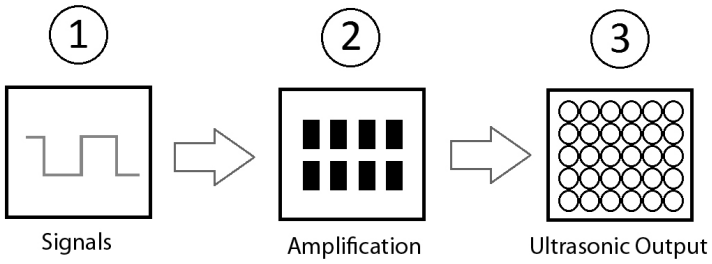

Figure 4.1: The three core functions which make up the tactile device, UltraSendo.

The first function is the generation of rectangular signals used to drive the ultrasonic transducers. These signals however are too weak to directly drive the ultrasonic transducers and hence the second function would be to amplify these signals. The third function is the force output created by an array of ultrasonic transducers. This output however can be influenced by changing the arrangements of the transducers in the array e.g. a planar or a hemispherical arrangement as discussed in Chapter 3.

Two prototypes, an Arduino board and FPGA board were built. The Arduino was used to first confirm that it was possible for us to affect the pressure at a particular point in mid-air by controlling the phase difference between each control signal. The Arduino, however, could not generate ultrasonic frequencies and was used to drive audible 1.8KHz emitters instead and thus an FPGA was used as a more sophisticated piece of hardware for generating higher frequencies to drive ultrasonic transducers. An FPGA also features more input and output channels so it is possible to drive more transducers with one component.

In this prototype a working amplifier was also developed as the signals from this component was too weak to drive ultrasonic transducers directly.

4.1 Arduino Prototype

A planar array of transducers emitting ultrasonic beams will generate an unsynchronized field of acoustic waves. The acoustic waves emitted from each transducer is capable of reaching the spot marked by a red X in Fig 4.2b due to their shape of emission as described in chapter 3. When the wave reaches this spot however, each wave is in a different position of its waveform (see section 4.1.1). In order to achieve a larger pressure amplitude, each wave must reach this spot marked by X at the same position of their waveform for superimposition i.e. constructive interference.

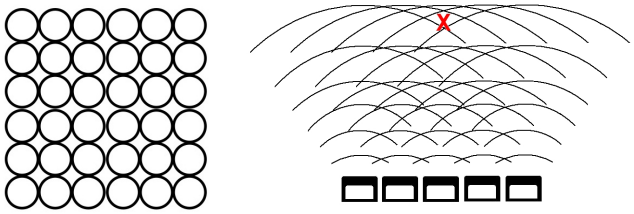

(a) Top down view (b) Side view beam patterns

Figure 4.2: Planar array of ultrasonic transducers

Focussing ultrasound for a planar array of transducers is achieved through software and electronics. The chosen development platform was an Arduino board (Fig 4.3a). The Arduino is a board mounted with a microcontroller and input/output ports with a programmable software environment in a language similar to Java. For this prototype, a single row of 1.8KHz audible transducers (Fig 4.3b) were used as this required little hardware set up. Even though this prototype will use audible transducers, the technique for focussing 40KHz transducers is similiar and will be discussed in greater depth later.

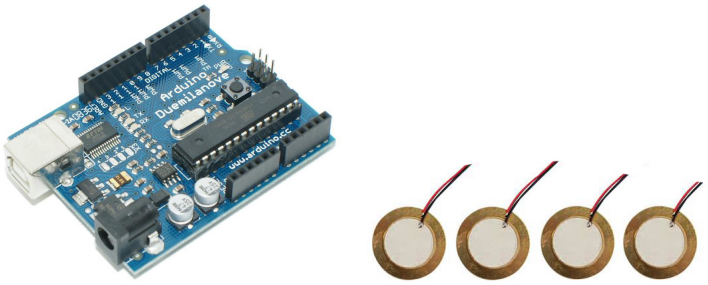

(a) Arduino Platform (b) Single row of 1.8KHz audible transducers

Figure 4.3: Arduino Prototype

4.1.1 Phase Shift

The phase is quantified as either a unit of time (given in seconds) or angle (given in degrees/radians). A phase difference determines the amount of shift between two waveforms. Naturally there is a phase difference in the waveforms at the chosen focal point marked by X in Fig 4.2 as the waves need to travel different distances to reach that spot. Referring to Fig 4.4, if transducer A's beam only needs to travel x distance then it will reach the focal point at the marked position in its waveform. Transducer B's beam, which is farther away by an extra d distance would reach that spot at a later position of its waveform.

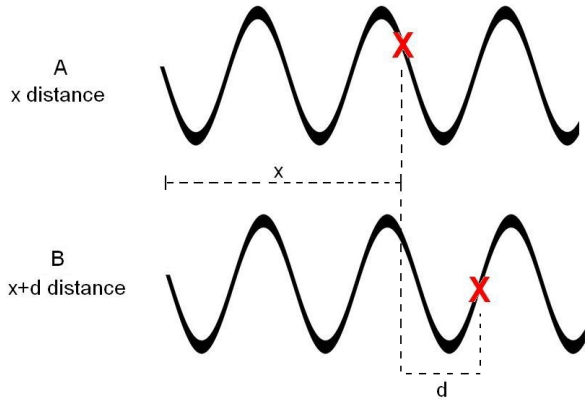

Figure 4.4: Position of waveform is different due to difference in distance travelled.

4.1.2 Synchronization

In order to synchronise the beams to superimpose at the same positions, a time delay in the driving signal is applied to compensate for the difference in distance and to re-align the waveforms so the beam reaches the destination with the same position of its waveform. The time delay required for a specific transducer is calculated by considering the euclidean distance of that transducer against a reference transducer. The transducer which is perpendicular to the focal point is chosen to be the reference as each length will then form a right-angled triangle shape which allows the use of Pythagoras Theorem to calculate the distances. Pythagoras Theorem for calculating the lengths of a right-angled triangle is stated as:

$$c = \sqrt{a^2 + b^2} \tag{4.1}$$

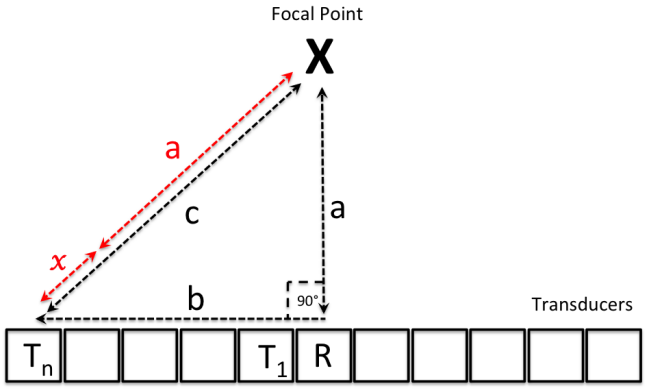

Figure 4.5: Side view: right-angled triangle for Pythagoras Theorem

Fig 4.5 shows a side view of the array of transducers. The lengths used to first calculate the distances that two waves have to travel to reach the focal point marked by an X are denoted a, b and c. Essentially a and c are the distances the waves from R and T_n respectively has to travel to reach the focal point. The lengths a and b are known variables because:

- The height of the focal point from the array of transducers is determined by the user so the length a is a known variable.
- Length b is the distance between the centre of transducers R and T_n. The width of a transducer is given by their manufacturer in the product datasheet.

The length c is unknown and must be determined. It is impractical and time consuming to physically measure the length c when determining the distances for all the transducers in the array. Therefore this length can be calculated using Pythagoras Theorem (4.1) when a and b are known. Once the length c is calculated, the difference in length between a and c is then the amount of phase shift required to re-align the waves to superimpose (denoted as $x = c - a$)

This phase difference is given in units of distance. It would be more useful if the phase difference was given in units of time for hardware to implement. This conversion is done by determining the ratio of difference according to the wavelength of the ultrasonic wave in the following equation:

$$J = \mathrm{mod}\left(\frac{x}{\lambda}\right) \tag{4.2}$$

Where the symbols:

J = ratio of difference

λ = wavelength of the ultrasonic wave

x = phase difference given in units of distance

When x is bigger than the wavelength λ, J would become greater than the value of 1.0. Since the waveform is a repeated pattern, any ratio value greater than 1.0 means the ratio will include the repeated sections. Therefore the modulus (remainder) is used to keep the ratio between values of 0.0 and 1.0.

The period of a wave is the time taken for one complete oscillation. The ratio of difference J is directly applied to the period of ultrasonic wave to find the time delay required to re-align the waves to superimpose at the focal point:

$$S = J\tau \tag{4.3}$$

Where the symbols:

S = time delay given in unit of time.

τ = the period of the ultrasonic wave

J = ratio of difference

Since J is already in decimal form it can be applied directly in (4.3). S is the time difference between the waves from transducers R and T_n to reach the focal point. This time delay can then be programmed into the electronics. Combining all three equations through substitution yields one convenient equation that can be used to auto-compute the time delays for each n^{th} transducer in the array against a reference transducer.

$$S_n = \frac{\sqrt{a^2 + b_n^2} - a}{\lambda} \times \tau \tag{4.4}$$

To further illustrate how these calculations are carried out, two worked examples are provided.

4.1.2.1 Worked Example 1

This example will avoid using equation (4.4) in order to show the logic behind the calculations. Consider the setup in the previous Fig 4.5, the time delay between transducers R and T_1 will be calculated. The focal point is set to be 150mm above the array and the distance between the centre of the two transducers is essentially the width of one transducer, given by its datasheet as 10mm. Using equation (4.1) the calculation becomes:

$$
\begin{aligned}
c &= \sqrt{a^2 + b^2} \\
c &= \sqrt{150^2 + 10^2} \\
c &= 150.33
\end{aligned}
$$

The difference in length (x) between a and c is $150.33 - 150 = 0.33$ mm (3.32×10^{-4} m). This number for x is then used in equation (4.2) where the wavelength (λ) of the 40KHz ultrasonic wave is 8.50×10^{-3} m

$$
\begin{aligned}
J &= \mathrm{mod}\left(\frac{x}{\lambda}\right) \\
J &= \mathrm{mod}\left(\frac{3.32 \times 10^{-4}}{8.50 \times 10^{-3}}\right) \\
J &= 3.91
\end{aligned}
$$

Taking this ratio and applying this to the period (τ) of ultrasonic which is 25μs in equation (4.3) yields:

$$
\begin{aligned}
S &= J\tau \\
S &= 3.91 \times 10^{-2} \times 25\mu \\
S &= 0.97\mu
\end{aligned}
$$

To conclude, the time delay required to re-align the two waves from transducers R and T_n to superimpose is 0.97 microseconds.

4.1.2.2 *Worked Example 2*

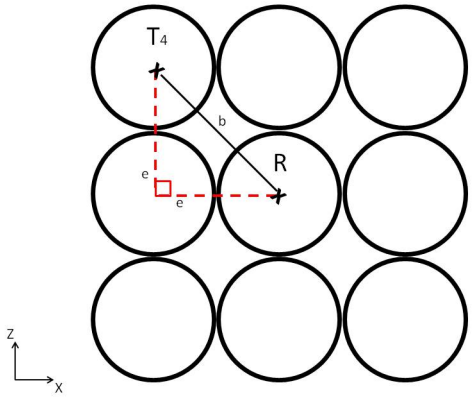

Figure 4.6: Top-down view: diagonal distance between transducers R and T_4

In order to calculate the difference between two ultrasonic waves, two lengths of the right-angled triangle must be known to use Pythagoras Theorem. Now consider the case in Fig 4.6 showing a top down view in the X-Z plane where the transducer T_4 is diagonally adjacent to the reference transducer R. In this case, the length b is unknown as it is not simply the width of the transducers as seen in the previous example. Hence it is not possible to use equation (4.4) until the length b is determined. To determine the length b, the widths of the transducers (10mm denoted as e) is used to form a secondary right-angled triangle along the X-Z plane to calculate the length b by using Pythagoras as follows:

$$b = \sqrt{e^2 + e^2}$$
$$b = 14.14mm$$

Now that b is determined to be 1.41×10^{-2}m, equation (4.4) can be used to calculate the time delay:

$$S = \frac{\sqrt{a^2 + b^2} - a}{\lambda} \times \tau$$
$$S = \frac{\sqrt{0.15^2 + (1.41 \times 10^{-2})^2} - 0.15}{8.50 \times 10^{-3}} \times 25\mu$$
$$S = 1.95\mu s$$

Therefore the time delay required to synchronize the ultrasonic waves from transducers R and T_4 is 1.95μs.

4.1.3 Control Signals

Although the physical output of the transducer is a sinusoidal waveform (as seen in Fig 4.4), the input control signal for driving the transducer is a voltage rectangular waveform (Fig 4.7). This voltage signal is amplified and fed into the transducer. The transducer acts like a low pass filter (allows low frequencies such as 40KHz to pass but attenuates higher frequency components i.e. the harmonics of the square wave) and converts the square wave into a sinusoidal ultrasonic wave.

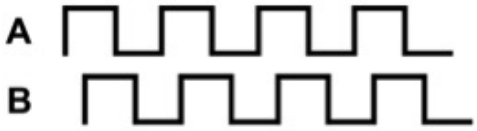

Figure 4.7: Input control signals in rectangular waveform

Since there will be a large number of control signals for a planar transducer array, software is used for the generation and management of these signals. The software should be programmed onto a programmable device that is capable of supporting the number of signals needed. Having all control signals managed by a single clock on one hardware avoids synchronization errors between multiple running clocks.

4.1.3.1 Binary Representation

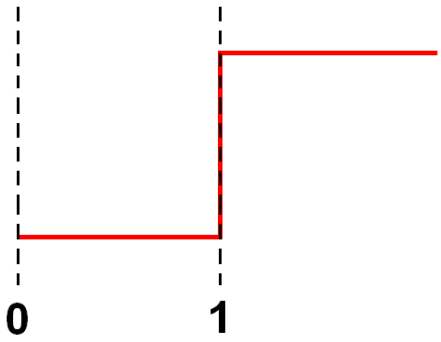

Figure 4.8: 2 bit binary representation of waveform

The easiest way to represent the square wave in software is a binary string. Since a square wave only has two states, the 1's and 0's in the string can indicate when the signal should be high or low voltage level respectively (Fig 4.8). Changing between these two states is called Signal Switching. A two bit binary string is sufficient to represent a whole waveform.

If a time delay is to be introduced into the signals however, then a single '01' will not be sufficient. The binary string must be split further. For instance, an eight bit string of '00001111' (Fig 4.9) would allow the system to introduce a time delay that is an eighth of the period of the ultrasonic wave.

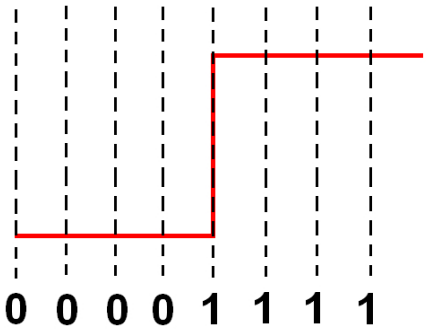

Figure 4.9: 8 bit binary representation of waveform

Using an eight bit binary string also means the clock must run eight times faster to produce the same frequency. For this system, a minimum time delay of sixteen divisions is required. The binary form would then be a sixteen bit string (Fig 4.10).

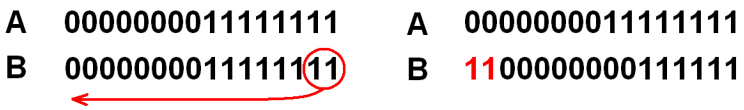

Figure 4.10: 16 bit binary string with circular shift to create a time delay

At 40KHz, the period time of the waveform is 25μs. Therefore each bit in the sixteen bit string represent a time interval of 1.56μs (25μs divided by 16). A circular shift is a bitwise operation, by shifting the bits to the left a time delay is introduced between the two signals (Fig 4.10). The number of bits shifted determines the time delay introduced. Therefore shifting by two bits gives a time delay of $2 \times 1.56\mu\text{s} = 3.12\mu\text{s}$.

4.1.4 Preliminary Experiment

A preliminary experiment was set up to verify the focussing technique. 1.8KHz audible transducers were used due to several reasons:

- Ultrasound is invisible and cannot be heard. Detecting its presence for evaluation would require extra equipment. Audible transducers eliminated this issue.
- The 1.8KHz transducers required no amplification to deliver an audible output.

The experiment was set up according to the diagram in Fig 4.11 with the audible transducers fixed onto the worktop.

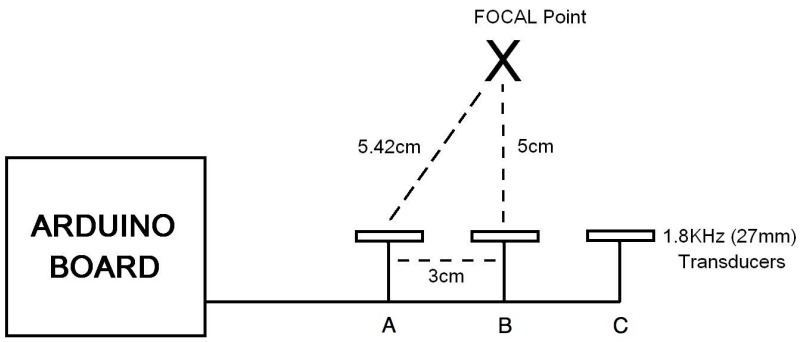

(a) Experiment schematic

(b) Sound Meter

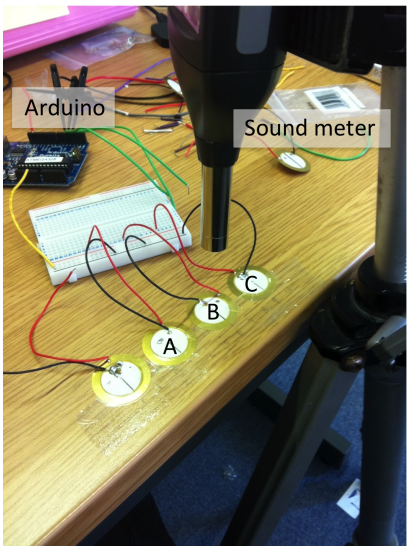

(c) Audible Transducers

Figure 4.11: Arduino hardware and experiment

The total sound pressure was measured using a sound meter positioned at the focal point marked in the diagram, directly above the central transducer labelled B.

4.1.4.1 Procedure

The experiment was divided into two parts. The first part consisted of only transducers A and B. The second part consisted of all three transducers A, B and C. A fourth transducer was included in the hardware as a spare.

A reference control signal which remained constant was used to drive transducer B and a second control signal that contained the time delay was used to drive transducers A and C. Since the algorithm split the binary representation into 16 segments (16 bits) it is possible to introduce a 1-bit, 2-bit, 3-bit... 15-bit delay into the signal. To see the effects of altering the phase difference on the total sound pressure, each bit delay was tested and the total sound pressure was recorded. The steps for the experiment were as follows:

1. Set control signals for transducers A and B to have no delays (unsynchronized).
2. Record sound pressure for this setting.
3. Add a single bit of delay between the A and B control signals i.e. delay by 1 bit.
4. Record sound pressure for this setting.
5. Add another bit to time delay e.g. delay by 2 bits.
6. Record sound pressure for this setting.
7. Repeat steps 5 -6 until the time delay has cycled through all 15 bits.

This procedure is repeated for the second part of the experiment to record the total sound pressure for all three transducers. Since transducers A and C are the same distance away from the focal point, the same control signal can be fed to both A and C.

4.1.4.2 Result

The results of measuring the decibel level (dB) at the marked focal point is shown in Fig 4.12. This graph shows that as there are changes in the phase, the sound pressure also increase showing constructive interference. When the control signals are 180° out of phase, the peak of one wave meets the trough of the other and thus creates destructive interference. This is good indication that by modifying the phase, we can control the pressure at that point. The blue line is for two transducers in operation. The red line is for three transducers in operation and shows that the peaks and troughs are in the same positions as the blue line but the change in amplitude is bigger with an extra transducer, confirming that more transducers can create a larger total pressure. Due to the difference in wavelength between 1.8KHz and 40KHz, these results are particular to 1.8KHz.

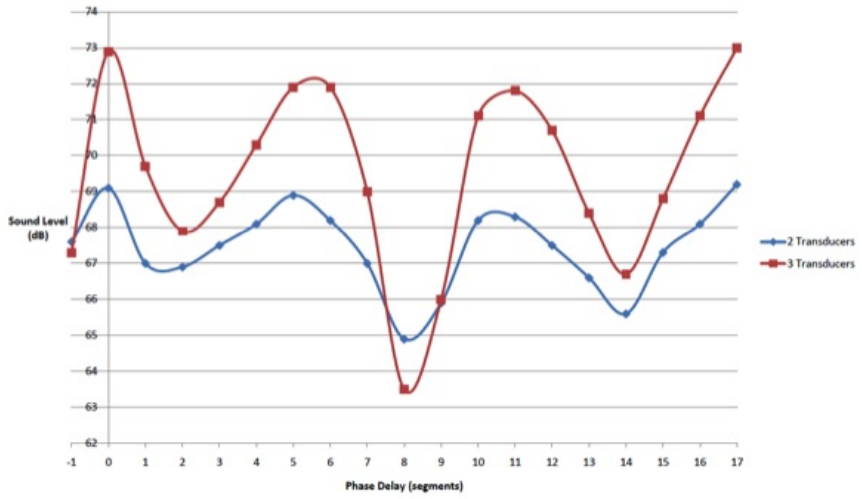

Figure 4.12: Sound pressure level as the phase of the driving signal is varied.

4.1.5 Prototype Conclusion

In this prototype, the focussing technique to manipulate the phase difference between each of the control signals is confirmed. Our initial investigation into an appropriate component to use as the controller for the tactile device which is intended to be used in a palpation simulator were published in [79]. It was found that running at maximum speed, the Arduino board was unable to generate signals at 40KHz. Another shortcoming of this platform was the limited number of input/output pins available for use. Based on existing airborne ultrasound devices by other researchers, the final tactile device would likely need more than two hundred signals to create significant amount of pressure that can be felt. Hence it was necessary to find another suitable component to act as the controller.

4.2 FPGA Prototype

Since the Arduino platform was unable to generate 40KHz signals, a more sophisticated digital electronic component called a Field Programmable Gate Array (FPGA) was used. The main objective of this prototype was to develop a working amplifier so the signals from the FPGA can be used to drive the ultrasonic transducers. The output voltage from the FPGA component is 5V, however, the ultrasonic transducer will require a voltage of 15V so the FPGA signal cannot directly drive the transducers without amplification.

There are several factors which needed consideration. Amplification is commonly achieved using a discrete component such as an operational amplifier or integrated circuit chip (op amp or IC chip) and there are several circuitry configurations that can be used with this component. The choice of circuitry is influenced by the nature of amplification required. In order to make an informed decision, one must appreciate what features of an op amp is relevant to the design before making any procurement.

The amplifier design was then tested against a mini array of ultrasonic transducers to validate its operation. The detection of ultrasonic output in air was carried out by setting up a transducer as a receiver. Also paper strips were used to verify the existence of the focal point.

4.2.1 Field Programmable Gate Array

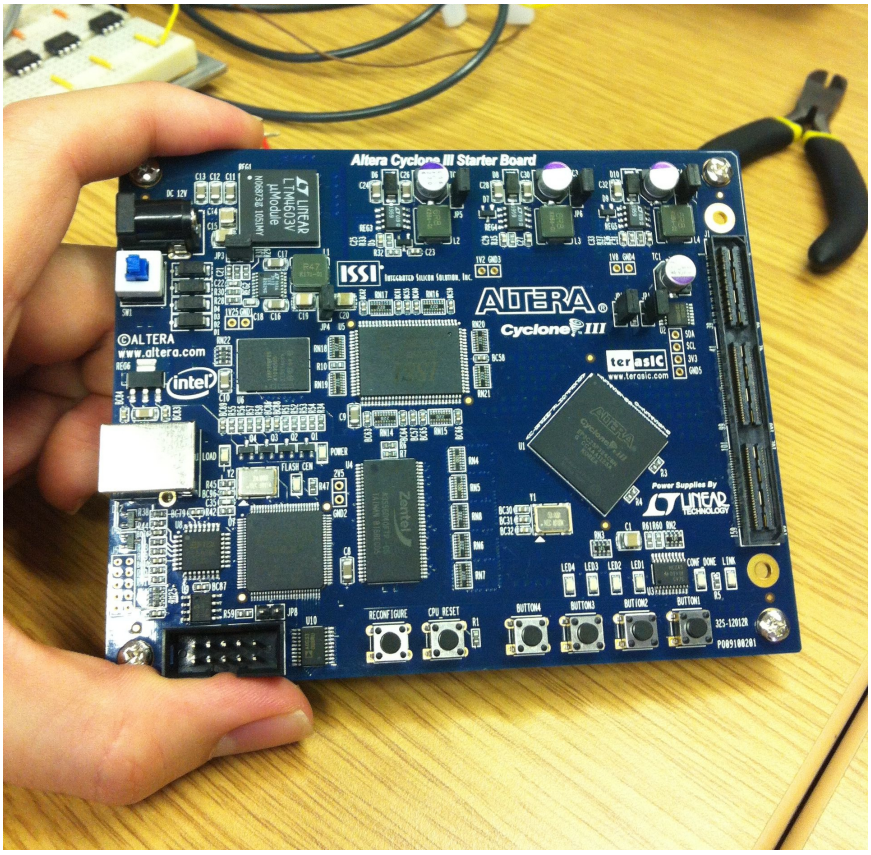

Figure 4.13: Field Programmable Gate Array (FPGA) Platform

Previously an Arduino platform was used to generate the control signals to drive a set of 1.8KHz transducers. The platform was found to be unable to reach the speed of 40KHz required to drive the ultrasonic transducer when no CPU cycles were wasted i.e. the board was executing at its maximum speed. A Field Programmable Gate Array platform shown in Fig 4.13 was chosen to replace the Arduino mainly because the FPGA had ten times more Input/Output pins, one signal for each transducer in the planar array. There are of course other possible components such as a Complex Programmable Logic Device (CPLD) but an FPGA was chosen because the original developer, Takayuki Hoshi had used an FPGA. Choosing the same family of component meant the original developer of ultrasonic tactile feedback could provide technical support.

4.2.1.1 Verilog Programming

The FPGA platform contains a built-in USB connector with the relevant firmware to allow the uploading of programs to the logic device. In order to create a program, an Integrated Development Environment desktop software called Quartus II was used. A hardware description language called Verilog was used to create the function of outputing a square wave.

4.2.1.2 Acessing the Input/Output Pins

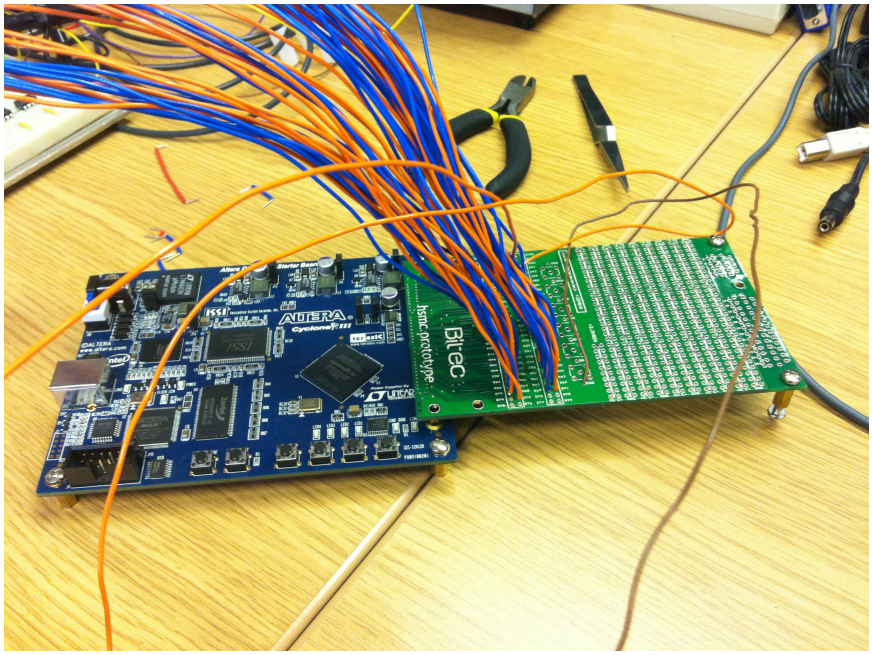

Figure 4.14: I/O pin fanout access board with wires soldered to the required ports

The input/output pins of the the FPGA platform is accessed by the High Speed Mezzanine Card interface integrated onto the platform for expansion cards to be connected (Fig 4.14). An input/output pin access fanout expansion board was used to connect each of the input/output pin of the FPGA to the op amp chip input terminals.

4.2.2 The Amplifier Design

There exists many operational amplifiers in the market with a large range of features, characteristics and capabilities. Choosing a suitable op amp is not an arbitrary but an informed choice. Therefore it is important to understand what is an op amp, by describing what an ideal op amp should be. This enables us to understand and select the most important key features of an op amp relevant to the needs of the amplification. The specification of an op amp chip is provided by its manufacturer in the form of a datasheet.

4.2.2.1 The Ideal Op Amp

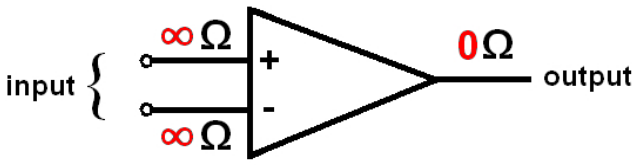

Figure 4.15: Ideal Op Amp pinout

An operational amplifier is a voltage-driven component and thus would ideally have an infinite input impedance and zero output impedance (Fig 4.15). In practice, this is equivalent to a resistance value in the megohm range for high impedance and values close to, but not, zero for low impedance. A high impedance input would prevent the amplifier drawing a large amount of current (power) from the original source.

4.2.2.2 Slew Rate and Maximum Voltage Supply

The Slew Rate is a measurement of how fast an op amp's output value can change i.e. the op amp chips responsiveness given in volts per microsecond. For example, $1V/\mu$s means that the edge can rise from 0V to 1V in 1 microsecond. An ideal infinite slew rate would give a perfect rectangular waveform as the edge would rise instantaneously. Practically, the slew rate is never infinite. If this slew rate is slower than the rising speed of the edge, it would be skewed (Fig 4.16).

A real world slew rate will always add extra time to the waveform's period. The significance of its effect can be considered neglible if the slew rate is sufficient. To calculate a minimum slew rate required for this system, the amount of extra time that can be tolerated in the waveform's period is considered.

A 40KHz waveform has a period time of 25μs. If the system can tolerate an increase of 5% in this period time (an extra $1,28\mu S$) then the maximum period can be 26.28μs which results in a 38KHz waveform. The chip must swing from -15V to +15V, so the

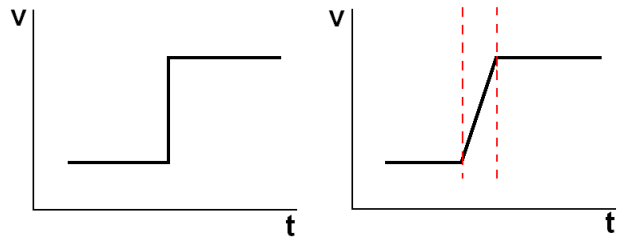

Figure 4.16: Ideal slew rate vs slower slew rate

voltage swing is 30V. $1,28\mu$s is the total added time from both the rising and falling edge of a square wave signal. Hence it is necessary to divide this value by two to give 0.64μs if we are to calculate the slew rate of one edge instead of two edges. 30V divided by 0.64μs gives a slew rate of $46.875V/\mu$s.

A Chip ideally has infinite gain i.e. it should amplify to an infinite value by an infinite factor. But in practice the maximum output value is restricted by the chips maximum supply voltage and power unit used. Since the desired output is +/-15 volts, this is the minimum that is required of the supply voltage.

4.2.2.3 Comparator Circuit

The polarity of the voltage in the control signal determines which direction the diaphragm of a transducer will move towards. The digital hardware used to generate the control signals does not contain a negative voltage value. If a circuit that only amplified the original signal was used, there would never be any negative polarity in the output. A negative voltage is necessary to pull the diaphragm of the transducer in the negative axis to generate maximum displacement of the diaphragm to produce maximum acoustic pressure (Fig 4.17).

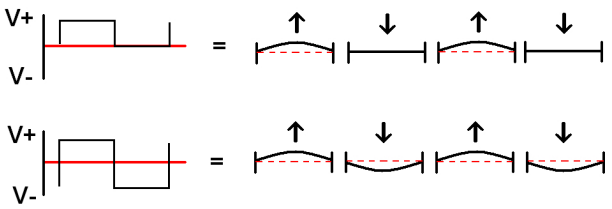

Figure 4.17: Transducer diaphragm movement according to the input voltage

Since the aim is to generate maximum displacement of the diaphragm, only the maximum voltage values -15V and +15V are required at the output. Thus a comparator circuit was chosen. The output voltage of a comparator circuit is typically the maximum value of

the voltage supply connected to the op amp. Rather than amplify, the main functionality of this circuit is to switch the polarity of the output voltage to either be a positive or negative value. A comparator circuit is configured with a LM301 op amp as shown in the circuit diagram (Fig 4.18).

The chip has two input pins; the inverting pin and non-inverting pin labelled as (2) and (3) respectively. Deciding which pin is the reference input is arbitrary as long as it is consistent across all the chips used. The input to (2) is a square wave from the Controller System and the input to (3) is a constant voltage value set by a potential divider.

4.2.2.4 The Reference Voltage Threshold

Referring to Fig 4.19, the threshold needs to be set so that it is cradled in between the input waveform as shown in (c). When (2)'s input is greater than the reference voltage the output swings to be the negative value of the power rail. When (2) is lower than this threshold, the output swings to the positive rail. If the threshold is set as in (a) then the output will always be negative, if set as (b), always positive. This is not the desired effect as switching the polarities is what drives the transducer.

4.2.2.5 Setting the Reference Voltage with Resistors

A Potential Divider is a basic circuit configuration shown in Fig 4.20 using two resistors to achieve a lower output voltage from a power supply with a higher voltage output. The output from the potential divider is connected to pin (3) on the LM301 op amp chip to set the reference threshold voltage. The output value is determined by the following equation:

$$V_o = V_s \times \frac{R_2}{R_1 + R_2} \tag{4.5}$$

Where the symbols:

V_o = the voltage at the output terminal

V_s = the voltage of the supply

R_n = the respective resistor labelled in Fig 4.20

Essentially, a portion of the power supply (V_S) is taken and applied to Pin 3 (V_O). Setting the threshold to 1.5V is adequate and this is a tenth of the power supply. Therefore R_1 must be 10 times bigger than R_2 to give a 10:1 ratio. Thus the resistors used in the amplifier could be 100KΩ and 10KΩ.

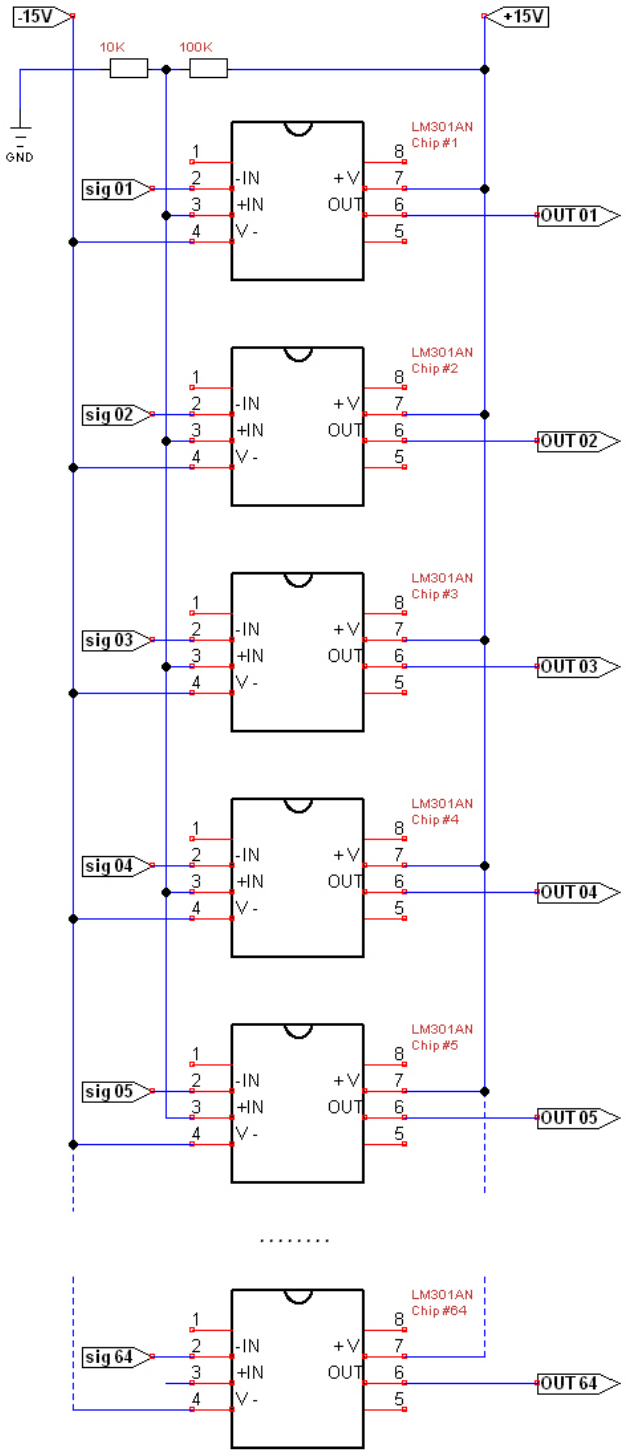

Figure 4.18: LM301 op amp comparator circuit.

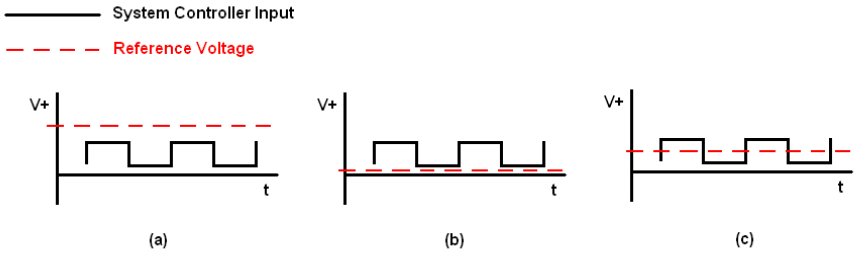

Figure 4.19: Reference Voltage Levels

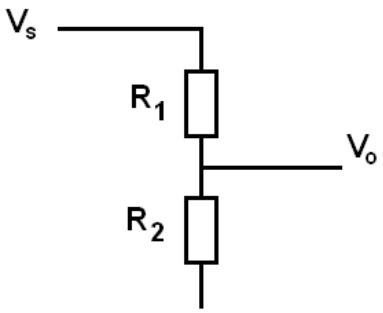

Figure 4.20: Potential Divider

4.2.2.6 Problem with Low Impedance Input

The initial op amp considered was an AD813 video amplifier which has an input impedance of 65Ω. It was chosen specifically for its high slew rate and 3 op amps in one IC packaging which will save space later when committing the design to a printed circuit board. It was later discovered that it was not possible to use this chip as it overheated to the point where it melted the prototype board it was mounted on (Fig 4.21).

Inspecting the datasheet further, the input pin for the chip was discovered to be of low impedance and the amount of current it can sink was extremely small.

The AD813 datasheet states the negative input pin has a resistance value of 65Ω and can only take several μA of current. It was later understood the chip was designed to be of low power consumption hence the extremely small current limit. This however meant the chip was drawing too much current from the comparator circuit configuration causing it to overheat internally.

As a rule of thumb, the input impedance of the op amp should generally be ten times bigger than the resistor values in the potential divider circuit to limit the amount of current entering the op amp. Each op amp will have a maximum amount of current that it can

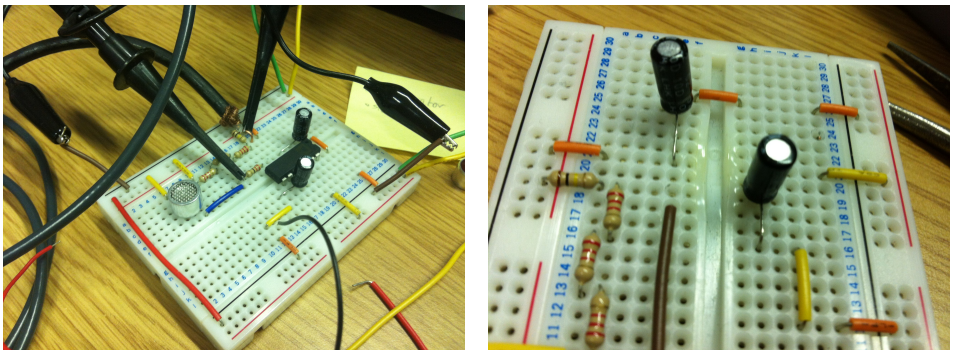

(a) AD813 mounted on a testing prototype board

(b) overheating melted the board underneath the IC

Figure 4.21: AD813 Overheating

accept. A low input impedance implies the reference voltage can only be set with resistors of very low values. Using such low value resistors mean a large amount of current will be sinked into the op amp. To illustrate this scenario further, the internal input resistance of the op amp is redrawn in Fig 4.22 to emphasize the internal resistance (R_i) is in fact parallel to one of the potential divider's resistor (R_2). This allows us to make calculations using the Parallel Resistance equation.

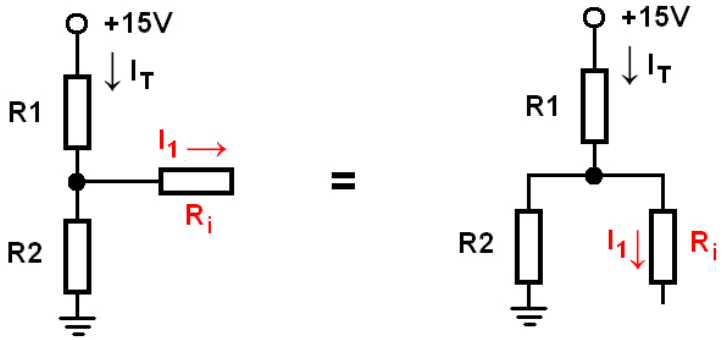

Figure 4.22: Internal resistance is parallel to external resistor

To calculate just how much voltage is dropped across (R_i), which determines what voltage the IC chip is receiving, the current running through the (R_i) branch must be determined. This is achieved through several steps of calculations as illustrated in the following steps with resistor values assigned in Fig 4.23.

1) Determine the total resistance of the whole circuit (R_T):

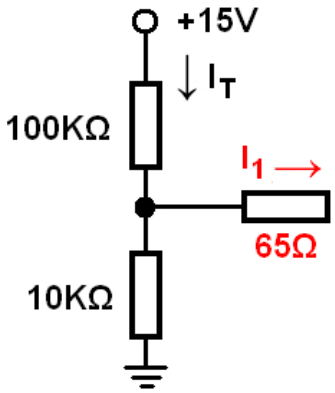

Figure 4.23: Potential Divider for AD813

$$
\begin{aligned}
R_T &= R_1 + \frac{R_2 R_i}{R_2 + R_i} \\
R_T &= 100K\Omega + \frac{10K\Omega \times 65\Omega}{10K\Omega + 65\Omega} \\
R_T &= 100,064.58\Omega
\end{aligned} \tag{4.6}
$$

2) Determine the total current in the circuit (I_T):

$$
\begin{aligned}
I_T &= \frac{V_S}{R_T} \\
I_T &= \frac{15V}{100,064.58\Omega} \\
I_T &= 0.1499mA
\end{aligned} \tag{4.7}
$$

3) Determine the branch current (I_i) of the internal resistance:

$$
\begin{aligned}
I_i &= I_T \times \frac{R_2}{R_2 + R_i} \\
I_i &= 0.1499mA \times \frac{10K\Omega}{10K\Omega + 65\Omega} \\
I_i &= 0.1489mA
\end{aligned} \tag{4.8}
$$

4) Determine voltage drop (V_i) across the internal resistance:

$$
\begin{aligned}
V_i &= I_i \times R_i \\
V_i &= 0.1489mA \times 65\Omega \\
V_i &= 0.97mV
\end{aligned} \tag{4.9}
$$

This voltage is significantly less than the 1.5Volts reference voltage that is required and almost all of the circuits current is entering the chip. The current is a hundredfold bigger than the μA rating the chip can accept. These are the reasons why the chip overheats and is not suitable for the comparator circuit.

4.2.2.7 Adding a Series Resistor

One may suggest adding a series resistor to the internal resistance branch to mimic the high impedance configuration (Fig 4.24). This will enable the potential divider to function properly but because the internal resistance is so small, there will virtually be little voltage dropped across it. This is verified by the following calculations assuming the ideal high impedance configuration.

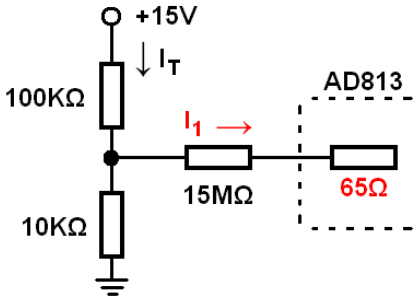

Figure 4.24: Adding extra resistor in series to internal resistance of chip

Following the same initial steps as the previous calculations, (R_3) is the additional 15MΩ resistor which is in series with the internal resistance (R_i) which resides inside the AD813 chip:

1) Determine the total resistance of the whole circuit (R_T):

$$
\begin{aligned}
R_T &= R_1 + \frac{R_2(R_3 + R_i)}{R_2 + R_3 + R_i} \\
R_T &= 100K\Omega + \frac{10K\Omega(15M\Omega + 65\Omega)}{10K\Omega + 15M\Omega + 65\Omega} \\
R_T &= 109,993.34\Omega
\end{aligned} \tag{4.10}
$$

2) Determine the total current in the circuit (I_T):

$$\begin{aligned} I_T &= \frac{V_s}{R_T} \\ I_T &= \frac{15V}{109,993.34\Omega} \\ I_T &= 0.1364mA \end{aligned} \tag{4.11}$$

3) Determine the branch current (I_i) of the internal resistance:

$$\begin{aligned} I_i &= I_T \times \frac{R_2}{R_2 + R_3 + R_i} \\ I_i &= 0.1364mA \times \frac{10K\Omega}{10K\Omega + 15M\Omega + 65\Omega} \\ I_i &= 90.87\mu A \end{aligned} \tag{4.12}$$

This current runs through both the 15MΩ and 65Ω resistors and is in the acceptable rating of μA. Although the current is significantly smaller, the following calculations will show that most of the voltage will be dropped on the 15MΩ resistor used as a potential divider rather than as internal resistance, meaning the chip does not receive the substantial amount of voltage that is required for the comparator circuit to function:

4) Determine voltage drop (V_3) across the 15MΩ Resistor (R_3):

$$\begin{aligned} V_3 &= I_i \times R_3 \\ V_3 &= 90.87\mu A \times 15M\Omega \\ V_3 &= 1.36V \end{aligned} \tag{4.13}$$

5) Determine voltage drop (V_i) across the 65Ω internal resistance (R_i):

$$\begin{aligned} V_i &= I_i \times R_i \\ V_i &= 90.87\mu A \times 65\Omega \\ V_i &= 5.90\mu V \end{aligned} \tag{4.14}$$

To conclude, this method will not provide a working solution. The amount of current has been corrected but the required voltage does not enter the chip itself and is dissipated on the 15M resistor.

4.2.2.8 *Amplifier Breadboard Version*

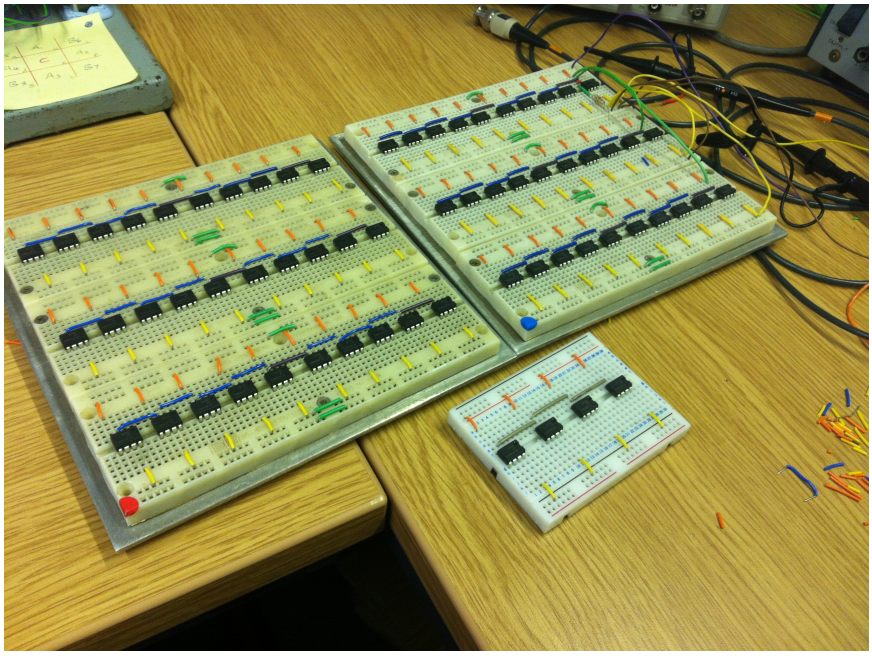

Figure 4.25: All 64 op amps configured to be Comparators

The comparator circuit was implemented with the LM301AN op amp chips. This amplifier supported sixty four individual channels allowing a total of sixty four ultrasonic transducers to be driven. The current solution is implemented on a temporary breadboard. After testing the amplifier does work, the design will later be committed to a Printed Circuit Board.

4.2.3 Mini Array of Ultrasonic Transducers

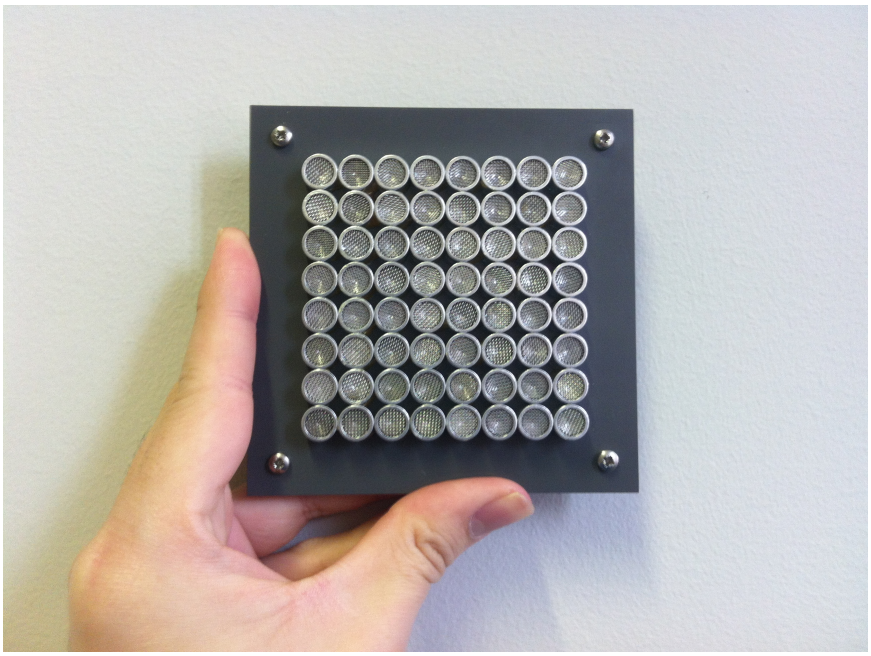

Figure 4.26: The Mini Array consisting of 8x8 (64 piece) ultrasonic transducers

To verify the operation of the amplifier a mini array of ultrasonic transducers was constructed. The array contained sixty four ultrasonic transducers arranged in an eight by eight square as shown in Fig 4.26

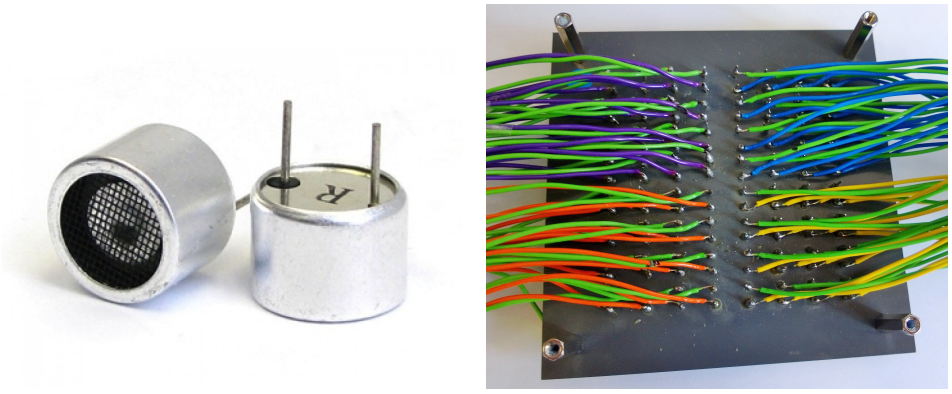

(a) The two metal leads on the bottom of the transducers.

(b) Array is divided into 4 quadrants marked with a unique colour wire.

Figure 4.27: Soldering wires to make connections from amplifier to array

At the bottom of each transducer, there are two metal leads for positive and negative input, one being physically shorter than the other to indicate which is positive and negative. The control signal could be connected to either lead as long it was consistent across all sixty

four transducers i.e. all the shorter leads on the transducer were soldered to a green wire to be connected to the ground connection on the amplifier.

It can be easy to confuse and connect the wrong transducer to the wrong port on the FPGA containing the control signal with the correct phase delay. Therefore the array was virtually divided into four quadrants, each with a different coloured wire to aid in making the correct connections to the right port on the FPGA board as shown in Fig 4.27.

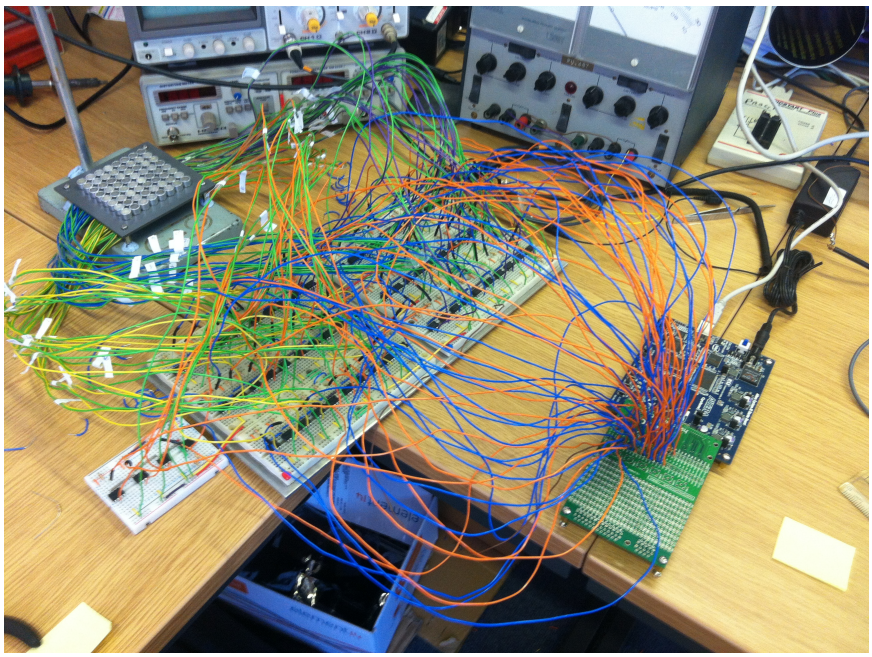

Figure 4.28: The completed FPGA Prototype

The completely assembled FPGA Prototype is shown in Fig 4.28. Each control signal from the FPGA is connected to each of the op amp chips on the amplifier. The amplified output signal from each op amp is then connected to its respective ultrasonic transducers.

4.2.3.1 *Detecting Ultrasonic Output*

To detect whether the mini array was successful in projecting a focal point, a sheet of paper with strips cut at the side was positioned above the array. If the focal point was present, it should push against the strips of paper. This observation was confirmed however, the force of the focal point was insufficient to stimulate any tangible sensation when the palm or fingers of a hand were used to feel for the focal point. To conclude, sixty four transducers were not enough to create a force sufficient for tactile sensation.

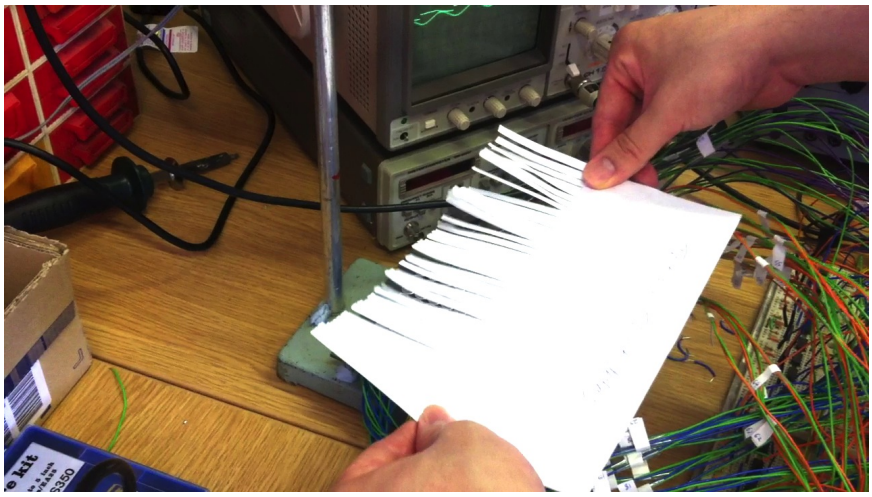

Figure 4.29: Ultrasonic focal point pushes against the paper strips

4.2.4 Prototype Conclusion

A working sixty four channel amplifier was built using a comparator circuit configuration for amplification. The comparator circuit allowed us to achieve a maximum voltage amplification up to the voltage of the power supply. The amplifier was used to drive a mini array of ultrasonic transducers to verify the operation of the amplifier. The mini array did produce a focal point but the force from all sixty four transducers were insufficient to stimulate a tactile sensation when a hand or finger was used to feel for the focal point.

This finding informed the next and final version of the tactile device named "Ultra-Sendo". The array of transducers needed further consideration to generate a bigger force for tactile sensation.

4.3 Final Version: UltraSendo

A mini array consisting of 64 ultrasonic transducers in a flat square arrangement was evaluated and found to be insufficient in providing a tactile sensation. This final version of the device will address this issue. In order to increase the force output two major changes were made to the array. The number of transducers were increased to a total of 271 due to using a new hemispherical arrangement for the array in comparison to the previous flat planar arrangement. The transducers will be arranged in hexagonal rings to fit as many transducers as possible into a given space. As there are ten hexagonal rings, it is possible to fit exactly 271 transducers onto the hemispherical array. The design of the hemispherical array will be discussed in this section.

The amplifier design will be converted to a printed circuit board for several reasons. The printed circuit board is permanent solution compared to a breadboard which is ideally used for quick prototyping. It also offers better electrical reliability as the connections are pernmanently soldered together rather than loosely connected via holes on the breadboard. The design of the printed circuit board will be discussed in this section.

In order to improve the textural sensation an interface was created so the user can make contact with a solid surface in comparison to feeling air particles. With the addition of an interface and modulating the control signal duty cycle, a fake human arterial pulse was simulated and displayed to the user. Finally an augmented reality visual representation of the virtual patient was created using software and chroma-key techniques allowing one to place their hand into the virtual environment to interact with the palpable surface. The development of the interface and computer software will be discussed in this section.

4.3.1 Hemispherical Natural Convergence

As described earlier in section 3.1.2 each transducer has a beam of divergence. As the focal point steers away from the centre line perpendicular (90°) to the transducer's surface, the power attenuates. A hemispherical arrangement would eliminate this issue as all the transducers will be directly facing the focal point ensuring all ultrasonic beam's power is maintained. This would result in an increased force output compared to a flat array with the same number of transducers.

4.3.1.1 Equidistance

Previously a flat planar array required phase shifts in the control signal to compensate for the difference in distance the ultrasonic beams from different transducers had to travel to reach the focal point. A hemispherical array will not suffer from this issue and thus the array can be driven with just one control signal that is copied and distributed to each transducer. Fig.4.30 illustrates this condition as a side view of the hemispherical array whose surface is spherical to guarantee equidistance for each transducer placed on this surface. All the ultrasonic beams will travel a distance of d to reach the focal point.

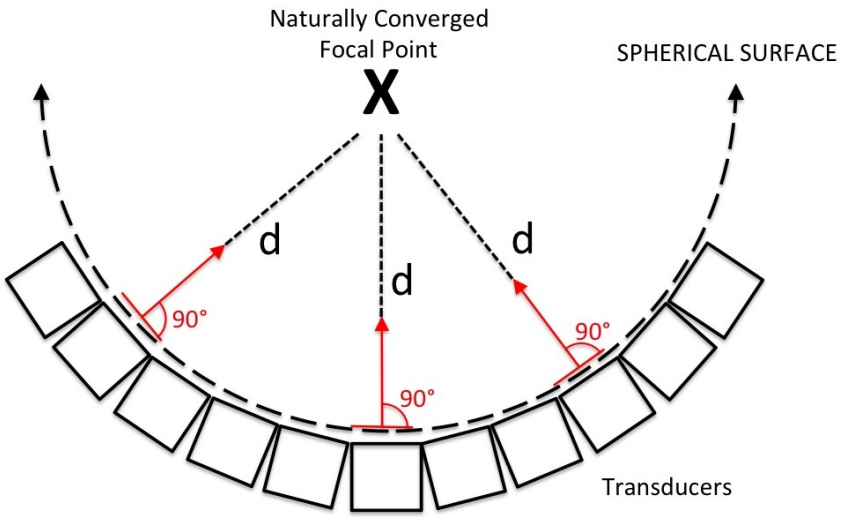

Figure 4.30: Distance from each transducer to focal point is the same.

It is still possible to re-locate the focal point but the distance would become different for each transducer and thus focussing must be compensated in the control signal. Hence in order to have the ability to re-locate the focal point, each transducer must have its own individual channel to feed different signals to the transducers. Fig.4.31 illustrates this scenario. The ultrasonic beam from the transducers will travel difference distances of a, b

and c which will require compensation by a phase shift in their respective control signal to re-synchronize the ultrasonic waveform. Moving the focal point away from the centre of the array will also reduce the force output as the focal point is no longer intersecting all 271 transducer's surface 90° Normal.

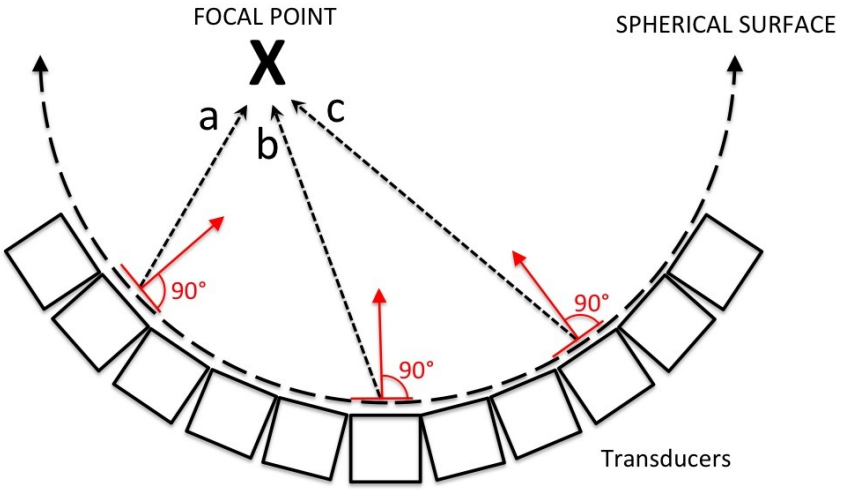

Figure 4.31: Distance from each transducer is different.

4.3.2 Modelling the Hemispherical Platform

To realize this hemispherical array, the hemispherical platform which the ultrasonic transducers will be mounted on must be designed to fit as many ultrasonic transducer as possible onto the spherical plane. Each transducer must be facing the naturally converged focal point at the centre of the array. This focal point was chosen to be 150mm above the array's surface resulting in a hemispherical plane of also 150mm. A model of the entire array including the transducers was created in a computer aided design software called Google Sketchup to assist in positioning the spacing between transducers. The software provided measuring tools, primitive shapes, shape rotation and translation tools to enable an accurate model to be produced. The modelled transducers were later removed before the model was sent to a 3D printer to be printed in thermoplastic to obtain just the hemispherical platform.

4.3.2.1 Hexagon Based Design

Tessellated hexagons is the most economical way of fitting as many transducers as possible into a given area. Each transducer was modelled with a hexagon base to facilitate the placement of the transducers as shown in Fig 4.32. The hexagon base is deliberately bigger

than the transducer to compensate for spacing when the transducers are rotated towards the focal point directly above the centre of the array. This is why the transducers were also modelled to detect any collisions that may occur within the placement.

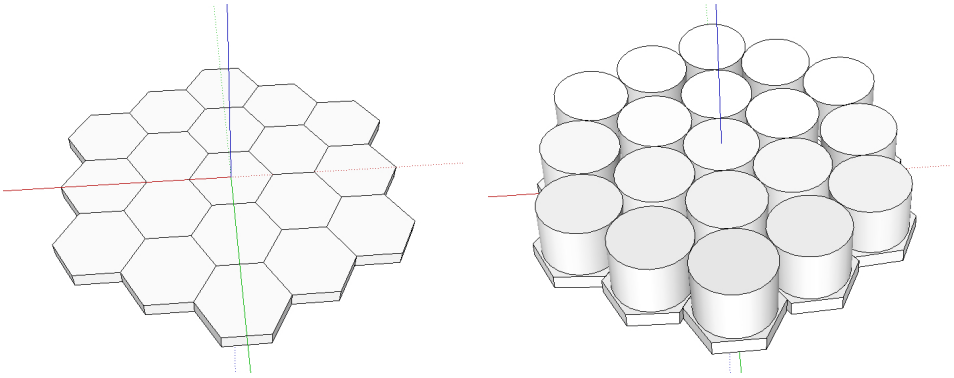

(a) Hexagon Base unit without modelled transducers

(b) Base unit with ultrasonic transducers modelled

Figure 4.32: Modelling of ultrasonic transducers with a hexagon based shape unit

4.3.2.2 Translation and Rotation of Hexagon Base

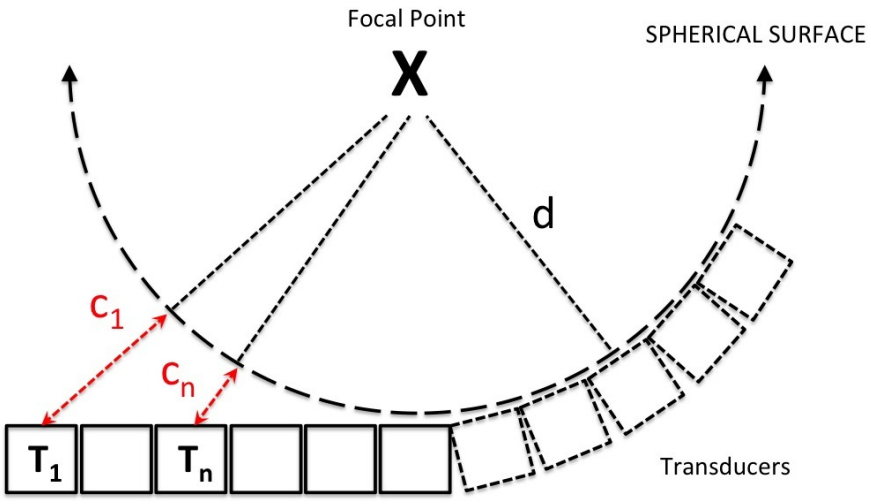

Figure 4.33: Translation distance from planar to the spherical surface

So far the transducers are all sitting on the same flat plane but if they are to be an equal distance away from the focal point, then all the transducers must be translated towards the focal point by a certain distance. Referring to Fig 4.34 the distances c_1, c_n etc, must be calculated to translate the respective transducers T_1,T_n etc to the spherical surface line.

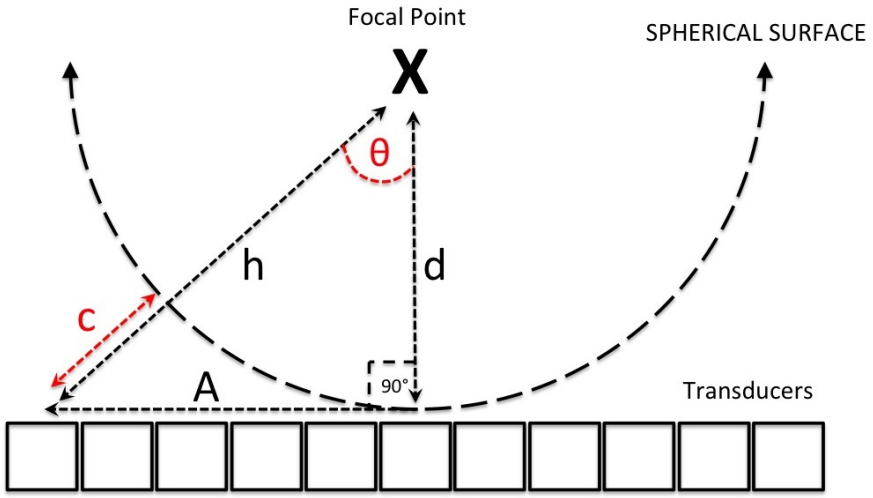

Figure 4.34: Trigonometry with a virtual right angled triangle

This calculation can be performed by visualizing a right angled triangle being formed between the focal point, the central transducer and the respective transducer illustrated in Fig 4.34. This method allows the following variables to be obtained to calculate translation and rotation values:

1. d is set to be 150mm as it is the radius from the transducer surface to the focal point.
2. A can be calculated as it is the distance between the centre of the respective transducer and the central transducer.
3. c is the translation distance required to move the transducer to the spherical surface line.
4. c can be calculated if the length h is known.
5. h is the hypothenuse of the right angle triangle which is essentially $h = c + d$.
6. Applying Pythagoras Theorem to the lengths d and A will obtain h.
7. The angle of rotation θ can be calculated using the trigonometric relationship $\tan\theta = A/d$

Calculating length A is more complex in comparison to the previous prototype's square arrangement. The hexagons has more sides than a square and thus involves more lengths than a single constant length compared with a square. This will be clearer with worked examples provided later.

There are 271 transducers. Calculating the translation and rotation for each transducer would be time consuming and in fact, redundant as some of the transducers will have the same translation and rotation values due to symmetry of the hexagon illustrated in Fig 4.35. There are six lines of symmetry for the hexagon. Therefore the array can be divided into 12 sections. Calculating the translation and rotation values for one of these sections is sufficient.

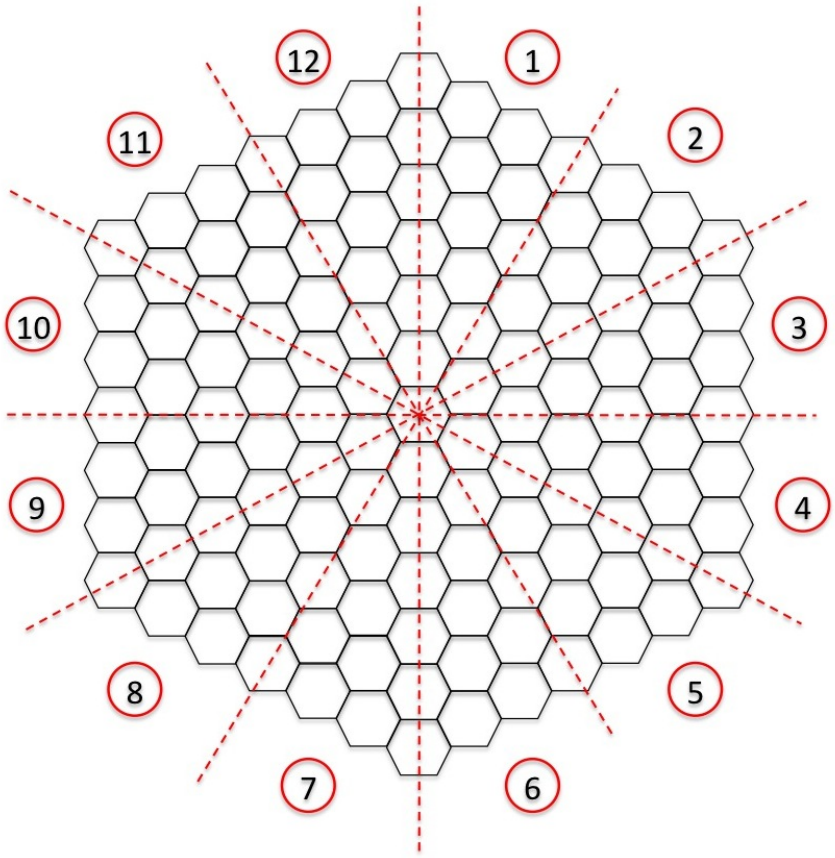

Figure 4.35: Symmetry lines for a hexagon array

4.3.2.3 Calculating the Translation Values

To calculate the translation value c, the length A (marked in Fig. 4.34) which is the distance between the central transducer and the respective transducer is required. The hexagon base has three lengths that can be used to make it easier to obtain A.

Fig 4.36 shows the three lengths of the hexagon. (1) is called the in-radius, (2) is called the side length and (3) is called the circum-radius. The side length marked in (2) of the hexagon was set to be 7mm. This choice was tested by modelling the transducer and estimating the minimum length the side of the hexagon should be. Since this is a regular

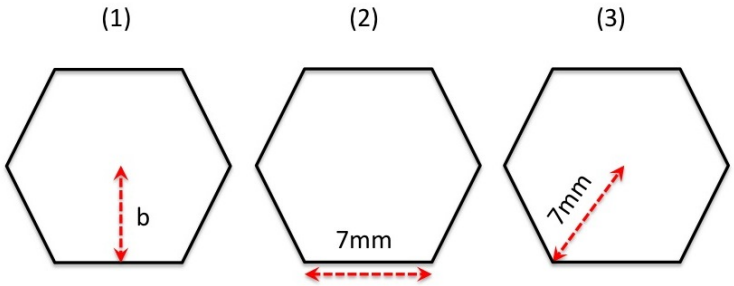

Figure 4.36: The three lengths of a hexagon used for calculating A

hexagon, setting the side length also meant the diagonal length marked in (3) is also 7mm. The in-radius b which is marked in (1) can be calculated by Pythagoras Theorem as shown in Fig.4.37. The result can later be verified by using the measuring tape tool in Google Sketchup as reassurance the calculation was correct.

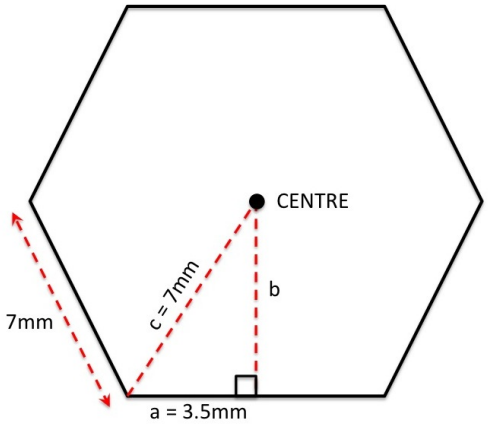

Figure 4.37: Calculating length b using pythagoras theorem

The length b was calculated using the following Pythagoras Theorem relationship for a right angled triangle:

$$\begin{aligned} b &= \sqrt{c^2 - a^2} \\ b &= \sqrt{7mm^2 - 3.5mm^2} \\ b &= 6.06mm \end{aligned} \tag{4.15}$$

Now that b is obtained, the three lengths of the hexagon are used in combination to calculate the length A between the central transducer and the desired transducer. To illustrate this calculation, a few worked examples are provided.

4.3.2.4 *Worked Example 1*

Fig.4.38 shows section (3) of the hexagon array with all the diagonal hexagons marked with a number. The hexagon base for the central transducer in the entire array is labelled as number (1). Let us calculate the translation value (c) and the rotation value (θ) for hexagon (4). As shown in the figure, the length A for any of these diagonal hexagons is just a mulitple of the length b which was previously determined to be 6.06mm. Therefore A for hexagon number (4) is the length b multiplied by 6 which results in a length of 36.13mm.

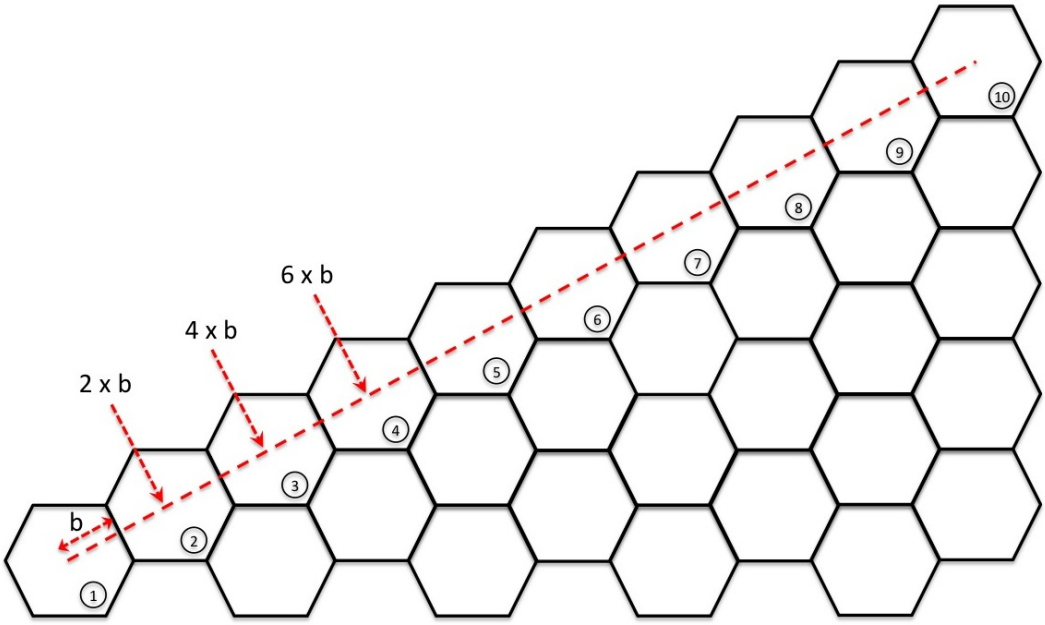

Figure 4.38: Using b to calculate the length of A along the diagonal

This value for A = 36.13mm is then used calculate h in Fig.4.39. It is important to note the spherical plane is formed from the surface of the transducer, however, A is derived from the hexagon base. This means d must also take into account the physical height of the transducer (7.1mm) as it is sitting on top of the hexagon base and thus the value of d is 157.1mm rather than 150mm in future calculations. The base also serves as a pivot point for the rotation operation. To calculate h, Pythagoras Theorem is applied to the lengths d and A.

$$\begin{aligned} h &= \sqrt{(d + 7.1mm)^2 + A^2} \\ h &= \sqrt{(150mm + 7.1mm)^{+}36.13mm^2} \\ h &= 161.20mm \end{aligned} \tag{4.16}$$

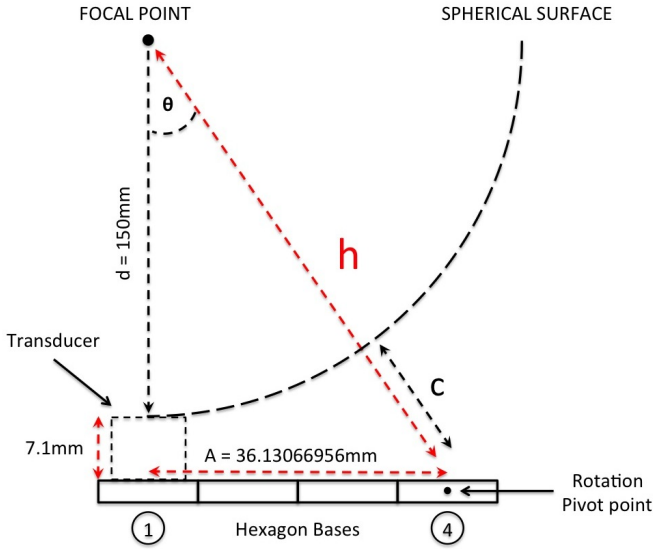

Figure 4.39: Height of ultrasonic transducer also needs to be included in the calculation

Now the translation value c can be calculated by deducting $(d + 7.1mm)$ from h (161.20mm - 157.1mm = 4.10mm). This is the distance the hexagon base needs to be translated towards the focal point in order to position the transducer's surface on the spherical plane.

Now the rotation angle θ needs to be determined to align the transducer's normal towards the focal point. This is determined by the following trigonometric relationship:

$$\begin{aligned} \theta &= \tan^{-1}\left(\frac{A}{d}\right) \\ \theta &= \tan^{-1}\left(\frac{36.13mm}{150mm + 7.1mm}\right) \\ \theta &= 12.95^{\circ} \end{aligned} \tag{4.17}$$

To summarize, the translation c and rotation θ values for hexagon (4) are determined to be 4.10mm and 12.95° which will be used in Google Sketchup to reposition the hexagon base.

4.3.2.5 *Worked Example 2*

Now consider calculating A for the horizontal hexagon bases shown in Fig.4.40. The length A for any of the horizontal bases can be obtained as they are a combination of hexagon's side length and circum-radius, both of which are 7mm and thus A is just a multiple of 7mm. Let us calculate A for hexagon base number (5). The distance from the central hexagon (1) to hexagon (5) involves traversing a combination of 12 side lengths and circum-radius and thus A is 12 x 7mm = 84mm.

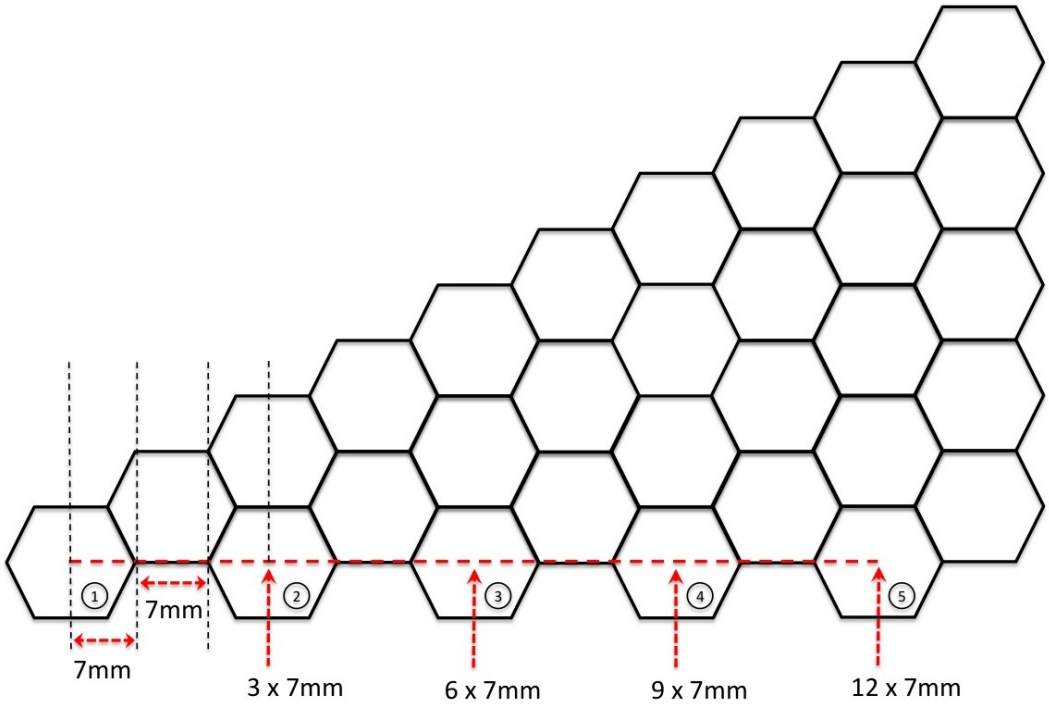

Figure 4.40: Using side length and circum-radius to calculate the length of A along the horizontal

As in the previous example, h can be calculated by applying Pythagoras Theorem to d and this newly calculated A:

$$h = \sqrt{(150mm + 7.1mm)^{+}84mm^2}$$
$$h = 178.14mm \tag{4.18}$$

The translation value c can be calculated by deducting (d+7.1mm) from h (178.14mm - 157.1mm = 21.04mm).

Now the rotation value θ is determined by the same trigonometric relationship in the previous example:

$$\theta = \tan^{-1}\left(\frac{84mm}{150mm + 7.1mm}\right)$$
$$\theta = 28.13^{\circ} \tag{4.19}$$

To summarize, the translation c and rotation θ values for horizontal hexagon (5) are determined to be 21.04mm and 28.13° which will be used in Google Sketchup to reposition the hexagon base.

4.3.2.6 *Worked Example 3*

Now consider the hexagon base (T) in the Fig. 4.41. This scenario is different to the previous two examples as the length A can be determined by applying Pythagoras to the two additional lengths (x) and (y). These lengths are a combination of side lengths, in-radius and circum-radius so the (x) is a mulitple of 7mm and (y) is a multiple of b previously determined to be 6.06mm. Therefore (x) is 9x7mm = 63mm and (y) is 4 x 6.06mm = 24.24mm. Applying Pythagoras to these lengths ($\sqrt{63mm^2 + 24.24mm^2}$) yields A = 67.50mm. Any A length for an arbitary hexagon can be obtained this way.

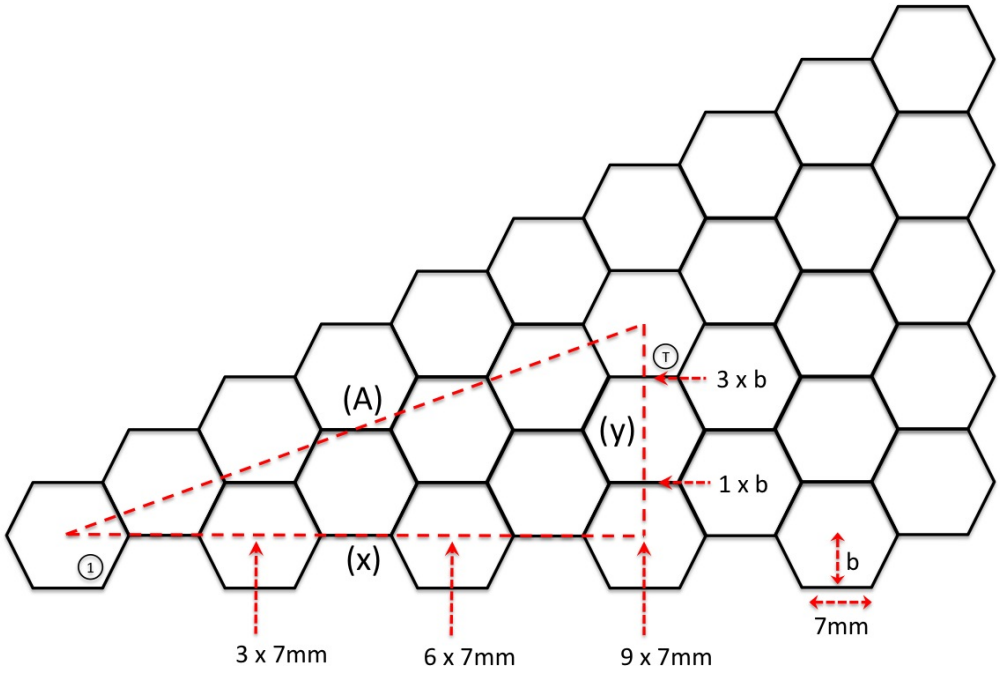

Figure 4.41: Using side length and circum-radius to calculate the length of A along the horizontal

As in the previous examples, h can be calculated by applying Pythagoras Theorem to d and this newly calculated A:

$$h = \sqrt{(150mm + 7.1mm)^{+}67.50mm^2}$$
$$h = 170.98mm \tag{4.20}$$

The translation value c can be calculated by deducting (d+7.1mm) from h (170.98mm - 157.1mm = 13.88mm).

Now the rotation value θ is determined by the same trigonometric relationship in the previous example:

$$\theta = \tan^{-1}\left(\frac{67.50mm}{150mm + 7.1mm}\right)$$
$$\theta = 23.25^{\circ} \tag{4.21}$$

To summarize, the translation c and rotation θ values for horizontal hexagon (T) are determined to be 13.88mm and 23.25° which will be used in Google Sketchup to reposition the hexagon base.

4.3.3 The Completed Hemispherical Model

Calculating the translation and rotation values for all the section (3) hexagons allows the array to be modelled accurately in Google Sketchup shown in Fig.4.42.

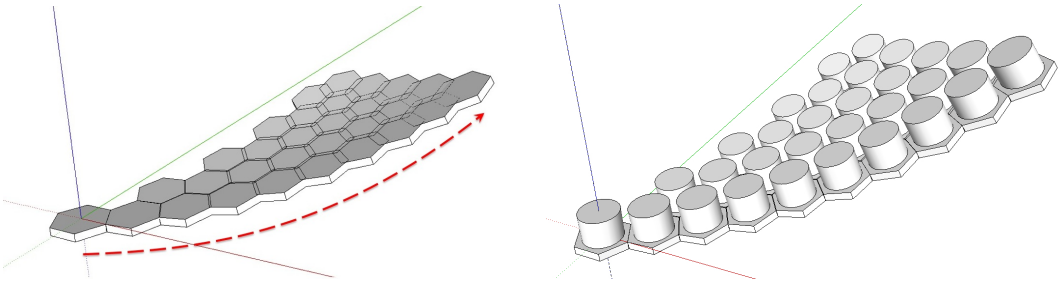

(a) Hexagon Base unit without modelled transducers

(b) Base unit with ultrasonic transducers modelled

Figure 4.42: Section (3) of the Hexagon Hemispherical Array

Initially the hexagon bases are translated to the correct position before the rotation operation is carried out to align the faces towards the focal point. Afterwards the transducers were modelled on top of the hexagon bases to visually detect any possible collisions between the transducers.

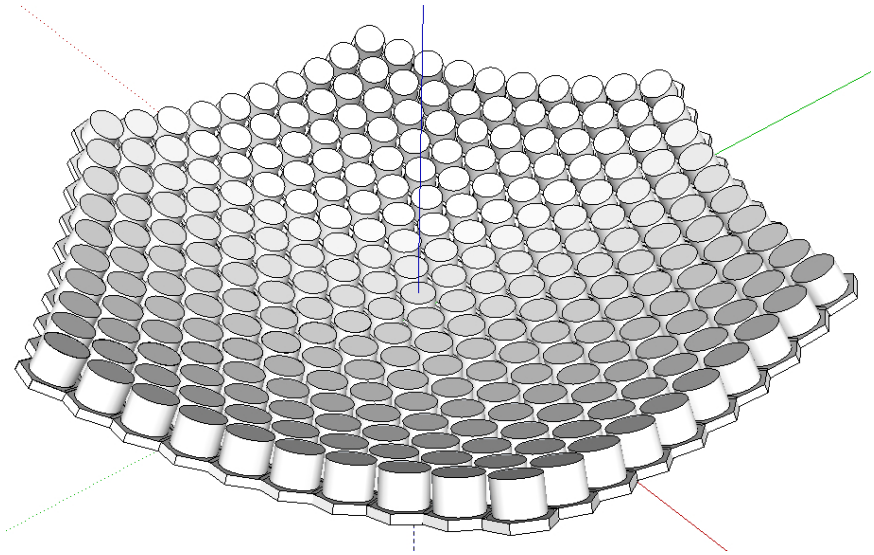

Figure 4.43: Using side length and circum-radius to calculate the length of A along the horizontal

Once this check was satisfactory, section (3) was duplicated to create the other eleven sections of the hemispherical array. The completed transducer modelling is shown in Fig.4.43.

The transducer models were then removed in order to place holes onto the hexagon base for the transducer leads to slot through. Six support legs were added to the underside of the hemispherical platform to suspend the platform facilitating the soldering of cables to the transducer leads later on. The final finished array with all 271 mounted to the platform and ribbon cables soldered to each transducer is shown in Fig.4.44.

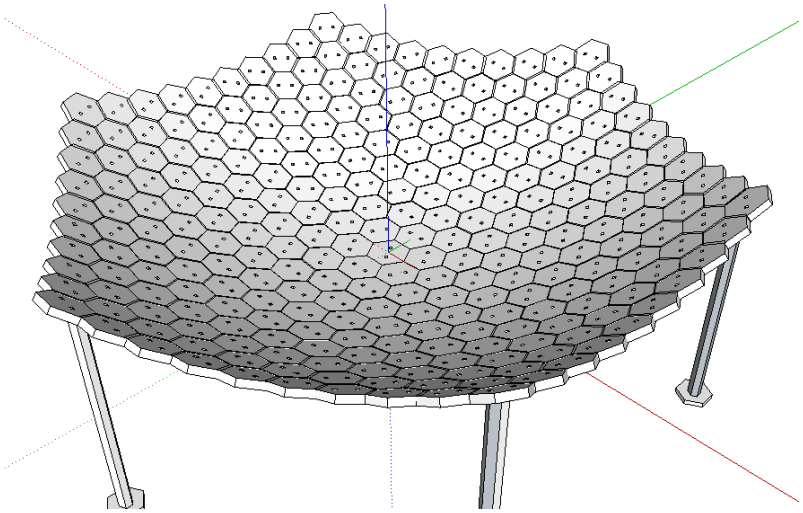

(a) The modelled platform with holes for mounting the transducer after being 3D printed.

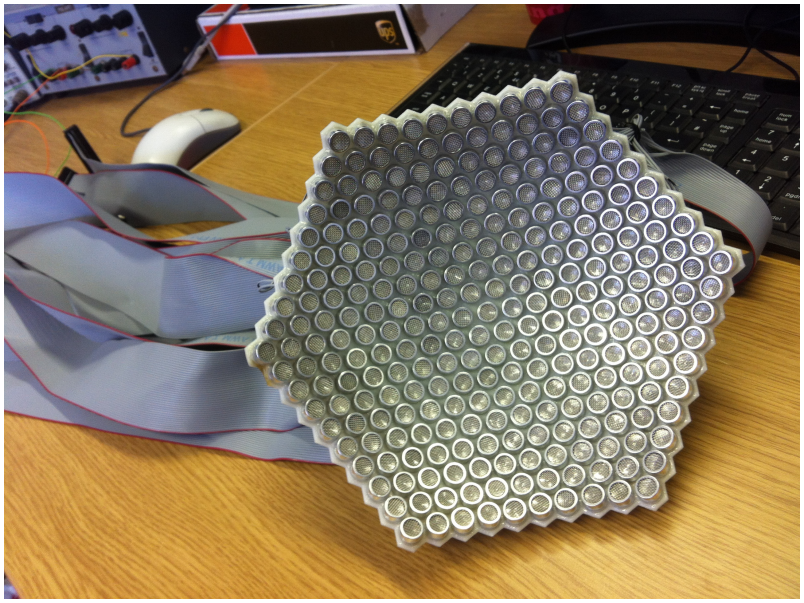

(b) The completed Hemispherical Array with all 271 ultrasonic transducers soldered to ribbon cables on the underside of the platform.

Figure 4.44: The completed hemispherical array

The completed hemispherical array is now ready to be connected to the amplifier boards which will be discussed in the next section.

4.3.4 Testing Transducers

To ensure that all the transducers were working, each individual transducer was tested before it was mounted onto the hemispherical platform. For the testing, a signal generator was used to create a 40KHz square wave signal. This signal was then amplified with a single op-amp chip. The amplified signal from the chip was then used to drive the ultrasonic transducer to emit ultrasonic waves. Another spare transducer was used as a receiver to detect the ultrasonic waves being emitted. It was soldered to a coaxial cable which connected to an oscilloscope. If ultrasonic waves were present, then the oscilloscope would show a sinusoidal wave in the form of a line. The amplitude of the line indicates the sound pressure of the ultrasonic wave.

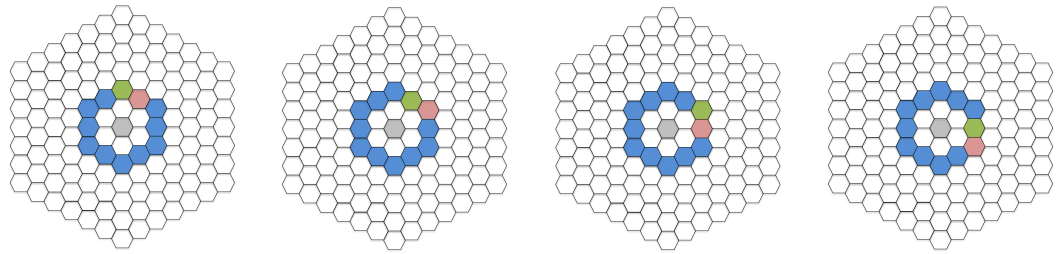

(a) (b) (c) (d)

Figure 4.45: Blue indicates hexagon ring in the test. Green and red is tested against each other. The red transducer becomes green in the next testing and is used as the reference and the untested adjacent transducer becomes the new red. Each pair of transducers are systematically tested across the hexagonal ring.

After mounting all the transducers onto the hemispherical array and the ribbon cables were soldered to the transducers, it was essential to confirm whether the wires were soldered to the correct lead on the bottom of each transducer. This test was done by using a pair of adjacent transducers on the array, with a spare transducer soldered to a coaxial cable to act as a receiver to detect and show the amplitude of the combined airborne wave from the pair of transducers. Since adjacent transducers are so close to each other, if one of the transducers were out of phase because of reversed wiring, then the waves would cancel each other creating destructive interference. This test was systematically carried out to test each transducer in each hexagonal ring by using a previously tested transducer as the second transducer in the pair testing as shown in Fig.4.45.

4.3.5 Printed Circuit Board

The printed circuit board for the amplifier was designed to host 20 op amp chips, one chip for each ultrasonic transducer resulting in a total of 14 amplifier boards being fabricated. The boards were designed to have the ability to be stacked upon each other to save desk space. This arrangement also allowed the device to be scaled up to support more than 280 transducers in incremenents of 20, if required in the future as further amplifier board could be created and stacked upon the existing boards. It can also be scaled down if need be by removing boards. Hence the design has been aimed to be re-usable and expandable for possible future modifications i.e. for driving a bigger or different array of transducers in future research.

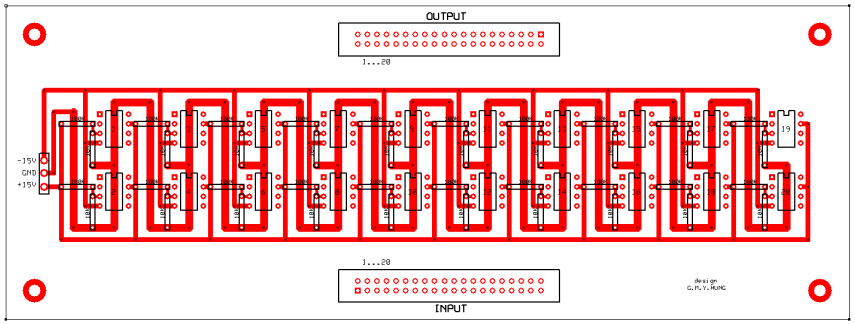

(a) The top layer of the PCB.

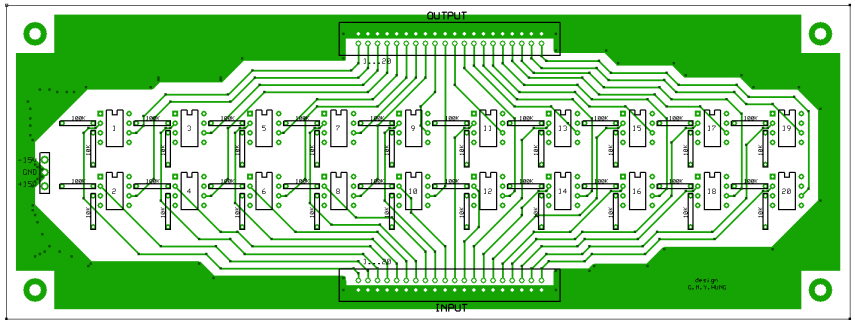

(b) The bottom "ground" layer of the PCB.

Figure 4.46: Top and bottom Printed Circuit Board design for the amplifier solution. Each board hosted 20 Op Amp chips.

As previously mentioned, a hemispherical array can be driven with one control signal. Another board (Fig.4.47) was designed to duplicate and distribute a copy of the control signal to all 271 transducers. The FPGA controller connects to this Distribution board which is connected to all 14 amplifier boards. The hemispherical array then connects to each amplifier board to receive the amplified signal to drive the ultrasonic transducers. Due to this arrangement, the current device cannot reposition the focal point. Adding this ability

in the future is to simply replace this Distribution board with another that contains enough individual channels connected to the FPGA controller. The existing amplifier boards and the hemispherical array are re-usable.

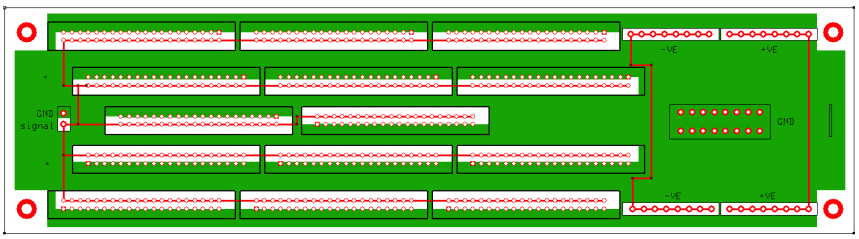

Figure 4.47: The Distribution Board designed to duplicate and distribute a single control signal to all connected amplifier boards.

4.3.6 UltraSendo

Fig.4.48 shows the completely assembled tactile device named "UltraSendo". The force output is a focal point, 150mm above the hemispherical array of ultrasonic transducers.

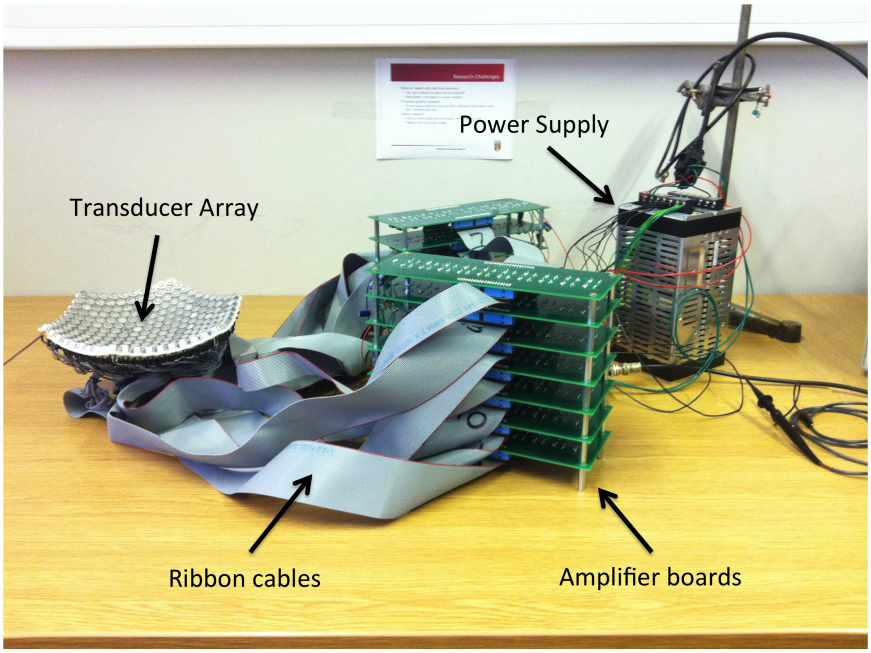

Figure 4.48: The completely assembled airborne tactile device, UltraSendo

The ultrasonic waves are constantly being emitted from the array resulting in a constant force, however, the force output has to be switched on and off rhythmically to replicate a human arterial pulse. This is achieved by modulating the control signal as shown in fig.4.49 where the original square wave control signal is modulated to include ON and

OFF intervals. The dashed lines indicates the OFF interval. Changing the length of the OFF interval will dictate the pulse rate of the virtual patient.

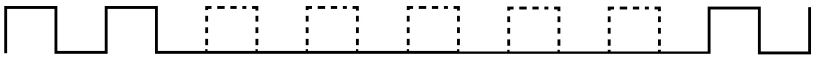

Figure 4.49: Modulating the control signal with ON/OFF intervals to make the force output pulsate.

The presented pulse rate is a Sinus (normal) rhythm but it is also possible to program an irregular beat pattern to simulate Arrhythmia (abnormal) conditions by using several different clocks that manage different periods of cycles of the waveform.

4.3.7 Membrane Interface

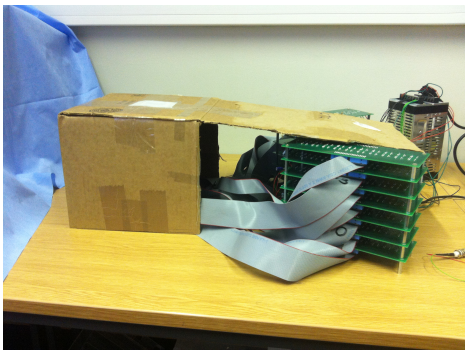

(a) A hollow box was placed above the array to provide a solid interface for users to interact with.

(b) The cutout on top of the box. The polythene material is actuated by the focal point emitted from the hemispherical array situated inside the hollow box.

Figure 4.50: Top and bottom Printed Circuit Board design for the amplifier solution. Each board hosted 20 Op Amp chips.

The completed tactile device still lacked the correct textural sensation as touching a patient's solid body is different to feeling air particles hitting the fingertips of the user's hand. In order to provide a solid surface for the user to make contact with, a hollow box with a small cutout on top was created and placed above the hemispherical array to provide this solid interface (Fig4.50). The surface of the box with the cutout was positioned to match the position of the focal point. The cutout was covered with a thin sheet of polythene, a thermoplastic polymer commonly used to make plastic carrier bags. It was light enough to be actuated upwards by the focal point when activated and sufficiently flexible to relax

when the focal point is turned off to return the material's position to rest. More importantly the material was non-porous as the air particles would bypass porous material and thus, would not actuate the surface up and down to mimic a human pulse.

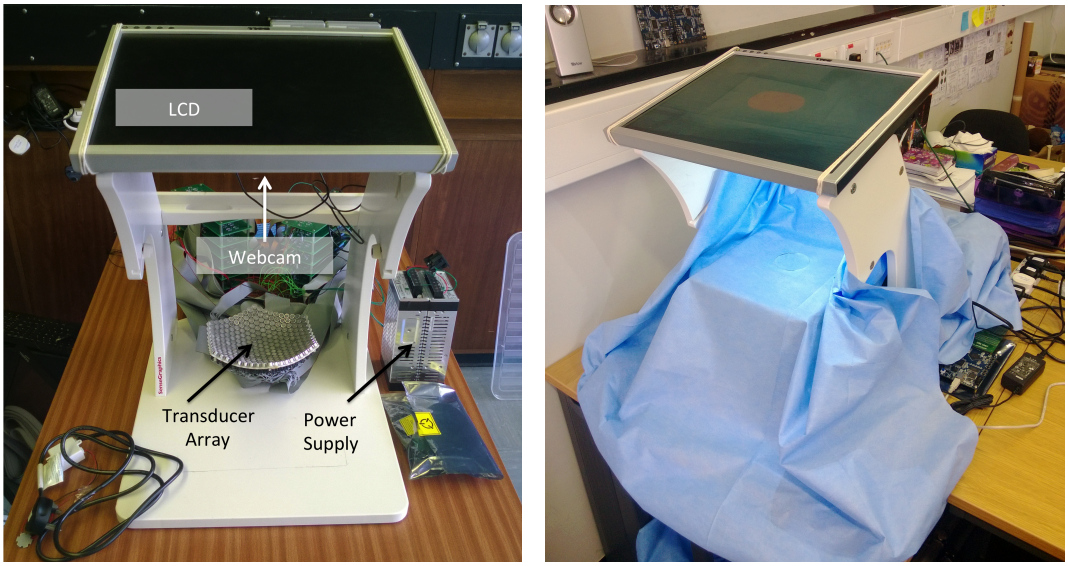

(a) Webcam is fixed on the underside and captures the space below the monitor.

(b) Blue cloth cloaks the underlying device and cardboard box interface.

Figure 4.51: The white structure made from wood holds up an LCD monitor which displays the virtual patient.

To demonstrate the simulated arterial pulse, UltraSendo was integrated into an Augmented Reality simulator. The idea of using augmented reality in simulation was previously achieved by Tim R Coles using a chroma-key technique commonly used in Hollywood movies where the actors are seen with a computer rendered scene. Most virtual simulators present only the virtual tool and the user's own pair of hands cannot be seen. Being able to see your own hands holding the virtual tool within the virtual environment enhances the realism of the simulation. To apply the chroma-key technique with UltraSendo, the entire device was covered in blue cloth. A monitor with a webcam installed on the underside was positioned above the UltraSendo interface as shown in Fig.4.51.

The software for an augmented reality palpation simulator already existed but the coding was deeply integrated with a Haptics Library for controlling force-feedback devices such as a Falcon. It was far more effective to re-create a similar software based on the earlier work than to directly modify a copy of the original. The software will be discussed in the next section onwards.

4.3.7.1 *Chroma-key Compositing*

Chroma-key works by analyzing the hue of the pixels in the video data. The pixel is set to be transparent depending on its hue. This hue can either be green or blue as they are the most distinctive from the colour of skin. For our augmented reality simulator, we have decided to use blue as this is the colour of the drapes used in surgery. A chromatic profile of the blue used in the chroma-key environment is first recorded to initiate the software. A video image of the chroma-key environment is captured by a webcam installed on the underside of a monitor positioned above the interface which is covered in blue cloth.

4.3.7.2 *Rendering Transparency*

The video data is analyzed by systematically checking each pixel's colour against a recorded chromatic profile. The original video image is in Red-Green-Blue (RGB) format. This is converted to Hue-Saturation-Value (HSV). This approach is more robust as the variation in colour intensity/brightness (V) is discarded so all shades of blue can be recognized by the software and replaced with transparency. Since there are now only two variables of interest (Hue and Saturation) it is possible to construct the chromatic profile as a 2D matrix or array to use as a reference lookup table. Hue and Saturation values range between 0 to 255. Therefore the chromatic profile can be represented as a 256 x 256 matrix, with each cell representing a possible combination of hue and saturation values.

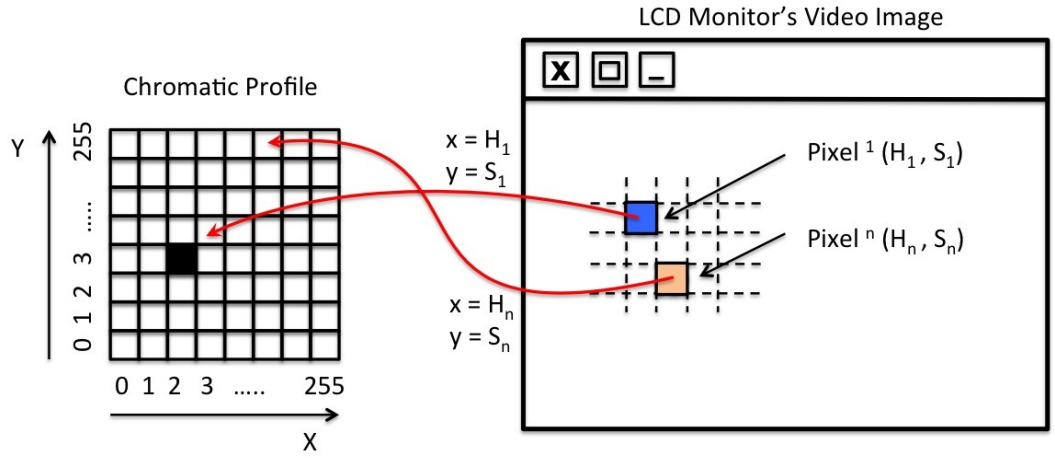

Figure 4.52: Evaluating whether the pixel should be transparent by looking up the Chromatic Profile

Every pixel in the video image is given an alpha value. A value of 0 means the pixel will be transparent whilst a value of 1 indicates the pixel should be visible. The chromatic profile is essentially a store of alpha values for each possible combination of

hue and saturation. To check whether a pixel in the video image should be transparent the pixel's hue and saturation is used as the (x) and (y) coordinates in the chromatic profile to lookup what value is stored at those coordinates. The stored value is retrieved and set as that pixel's alpha value. Only the hue and saturation values corresponding to blue will store alpha values of 0.

This process is illustrated in Fig.4.52. Pixel^1's hue (H^1) and saturation (S^1) value is used as the (x) and (y) coordinates to lookup what is stored in the chromatic profile. In the diagram an alpha value of 0 appears as black in the chromatic profile for illustration. Since the pixel is blue the stored alpha value will make Pixel^1 transparent. Systematically moving through all pixels, for example Pixel^n, the pixel's hue (H^n) and saturation (S^n) value is then used as (x) and (y) coordinates to lookup the stored alpha value. The stored value for this combination is visible so Pixel^n will be visible in the final video image.

4.3.7.3 Final Composition

A virtual environment of the drapes used in surgery is rendered with a patch of exposed skin to represent the virtual patient. The user then places their hand into this environment as shown in Fig.4.53 to palpate this patch of skin in an attempt to locate the artertial pulse indicating the presence of an underlying blood vessel. This concludes the creation of UltraSendo and the Palpation Simulator.

Figure 4.53: The user's hand is augmented into the virtual environment.

4.4 Summary

Two proceding prototypes were built prior to the completion of the final device. The purpose of the first prototype was to find a suitable component to serve as the controller. An Arduino was selected as an initial platform. The programming language for this platform was very similar to Java, a language that is considered to be easier to programme than hardware dependant languages such as Assembly or Verilog. The acoustic radiation pressure phenomenon and the technique for focussing acoustic waves at an arbitary point was also confirmed in this prototype. It was confirmed that manipulating the phase difference between the control signals was the key to focussing the acoustic waves. It was also concluded that an Arduino was unsuitable as it was unable to generate 40KHz control signals to drive ultrasonic transducers. To control each transducer individually, each transducer needed its own dedicated signal channel. The number of output ports on the Arduino was insufficient to support the number of channels required for a large array of transducers.

The second prototype featured a Field Programmable Gate Array (FPGA) as the controller. This component had hundreds of output ports and was able to generate 40KHz control signals. An amplifier solution to strengthen the control signals to drive ultrasonic transducers was also developed using a comparator circuit with LM301AN operational amplifier chips. Initial evaluation of a mini planar array of ultrasonic transducers concluded that 64 ultrasonic transducers were insufficient to provide a tangible sensation when felt by hand although the generated focal point was strong enough to push paper strips. The final design of UltraSendo was informed by these findings.

Subsequently UltraSendo, the final iteration of the design was built to achieve a larger force output. Increasing the number of transducers to 271 allowed this to be achieved but UltraSendo also featured a hemispherical array instead of a planar arrangement. Each ultrasonic transducer has a beam of divergence which is perpendicular to the surface of the transducer i.e. straight ahead of the transducer. Diverging away from this perpendicular line of sight reduces the power of the ultrasonic wave. A hemispherical arrangement aligned all the transducers to face the focal point 150mm above the array. A solid interface with a palpable membrane made from polythene was created to present a better textural sensation compared to feeling air pushing against the palm or fingertips. In order to use UltraSendo, the device need to be intergrated into the virtual reality simulation so the user does not see the device itself. To do this, blue cloth was used to mask the device and was integrated into an augmented reality simulator displaying a virtual patient for which the user can interact with and feel the sensation presented by UltraSendo. The construction details of UltraSendo, which was previously called UltraPulse has been published in [80].

The next step is to gather user feedback for UltraSendo in order to determine whether the sensation presented is considered to be realistic.

Chapter 5

End User Feedback

UltraSendo was designed to simulate a pulse and thrill sensation that are used to help diagnose an ailment (e.g. a thrill such as heart murmur) or to locate a target on a patient (e.g. an arterial pulse). To obtain user feedback on how realistic the sensation is, UltraSendo was brought to the Catheter Laboratory in Ysbyty Glan Clwyd in North Wales to collect expert user feedback. The Catheter Laboratory is a major facility in the region for the treatment of patients with heart and chest conditions. Treatments are carried out minimally invasively, often by inserting a guidewire and catheter into the patient's cardiovascular system. Eleven medical practitioners were asked to complete a short questionnaire regarding the sensation presented by UltraSendo. This user test session aimed to collect information regarding the realism of an arterial pulse and a thrill sensation to determine which is believed to be the most realistically displayed by UltraSendo.

5.1 User Test Procedure

Figure 5.1: Testing UltraSendo at Glan Clwyd Hospital

For this session, there were seven male and four female, making a total of eleven participants with the majority specialising in Cardiology. There was one medical physicists and two staff nurse who palpates for such sensations regularly. UltraSendo was setup up in a spare office room and staff were notified of this event upon arrival. It was a walk-in session allowing the participants to enter when they had a break from their schedules. The team was not particularly large so the session was closed after two hours when the majority of the team had already participated.

An introduction was given to arriving participants to explain the purpose of the evaluation and that UltraSendo aimed to realistically simulate a pulse and thrill that can be felt when palpating a real patient's body. They were asked to explore the palpable interface with their fingertips to search and feel for a pulse sensation. Then the user was asked to explore the same palpable interface with their palm to feel for a thrill sensation (Fig.5.1). After this interactive session, they were asked to rate how realistic they believed the sensation was as a pulse and thrill by completing a short questionnaire (Fig.5.2).

The questionnaire asked several questions which we felt were important to evaluate the quality of the presented sensation. Referring to Fig.5.2, question six asks whether the participant was able to detect the sensation at all regardless of whether the sensation was realistic. The purpose of this was to evaluate whether the sensation presented was strong enough to be felt. It would be meaningless for the sensation to be realistic but cannot be detected by the user. Question seven and eight separately asks the user to rate how realistic the sensation was in the perspective of a pulse and a thrill sensation and thus are mutually exclusive in this regard i.e. it is possible for a participant to give a high rating for pulse and yet a low rating for thrill. There is also a comment box for those participants who wish to provide more detailed feedback regarding the sensation presented.

UltraPulse Medical Tactile Sensation User Feedback Form

PRIFYSGOL BANGOR UNIVERSITY

Q1) Please indicate your gender:
☐ Male ☐ Female
Q2) Please indicate your handedness:
☐ Left-handed ☐ Right-handed
Q3) Please state your medical speciality:
Q4) Years of experience in your speciality:
☐ 1-5 ☐ 5-10 ☐ 10-15 ☐ +15
Q5) How many times do you perform palpation and/or check for heart murmur or a thrill, on a monthly basis?
☐ < 5 ☐ <10 ☐ <20 ☐ <30 ☐ +40
Q6) How easy was it to detect and locate the sensation?
1 2 3 4 5 6 7 8 Very difficult Very easy
Q7) When using your fingertips, how realistic would you rate the sensation as a Pulse?
1 2 3 4 5 6 7 8 Unrealistic Very realistic
Q8) When using the palm of your hand, how realistic would you rate the sensation as a Thrill?
1 2 3 4 5 6 7 8 Unrealistic Very Realistic
Q9) Comments
Here are some suggestions: • *any other procedures this sensation could simulate.* • *how the sensation can be improved.* • *additional comments*

Figure 5.2: Users were asked to complete this short questionnaire to rate the realism of the pulse and thrill sensation.

5.1.1 Results

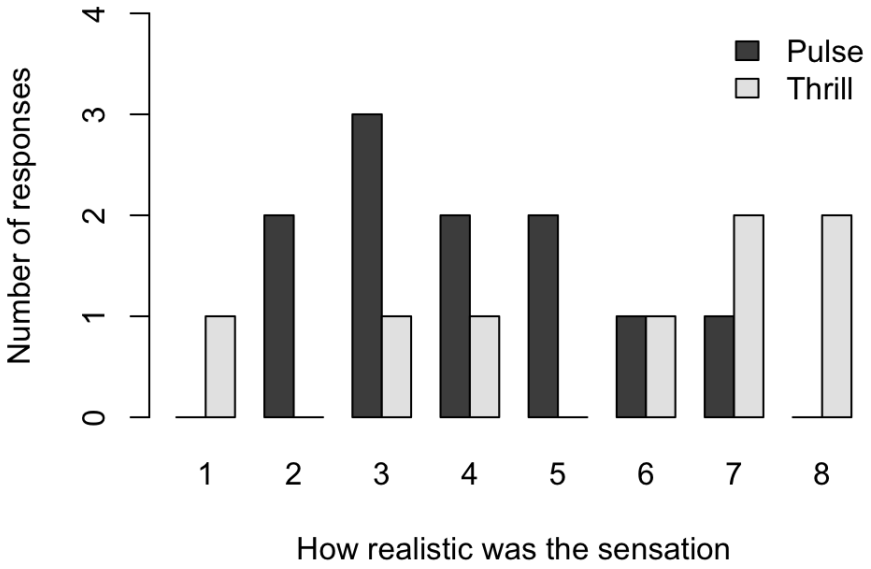

Figure 5.3: Thrill vs Pulse ratings

Referring to the graph (Fig.5.3) the distribution of responses for both the thrill and pulse sensation is shown. The x-axis is the range of ratings from ”unrealistic” to ”very realistic” and the y-axis shows how many responses each particular rating received.

The darker bars indicate the response distribution for the pulse sensation. The majority of the responses mostly reside on the left side towards the ”unrealistic” rating. The width of this distribution also spans across the whole range of ratings which indicates UltraSendo received a mixed review with some users believing it was very realistic. The majority of responses were in the middle of the range (rating realism as 2-5) suggesting the sensation was not realistic enough.

The lighter bars represents the distribution of responses for the thrill sensation. This distribution resides closer to the ”very realistic” rating but also exhibits the same width as the pulse sensation, indicating it too had a mixed review but the main part of the distribution resides on the ”realistic” side of the graph. The thrill sensation received more ”realistic” ratings compared to the arterial pulse.

5.1.1.1 Years of experience

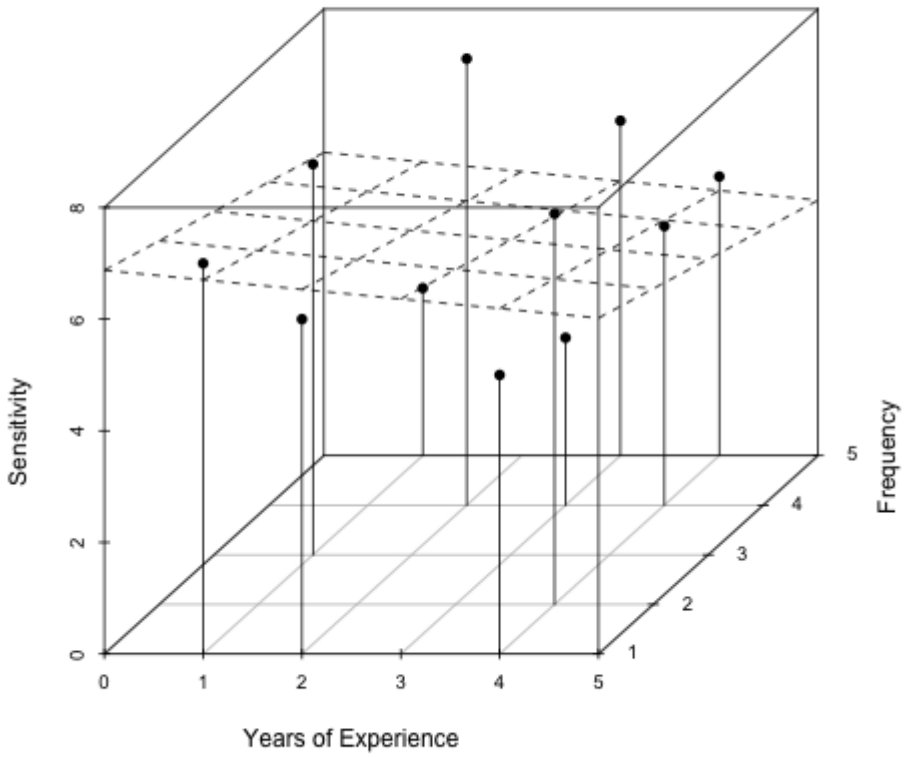

Figure 5.4: 3D plot to show the relationship between the ability to detect the sensation against the participants' experience in their field.

Users were asked to indicate their years of experience in their speciality from the following options: 1-5, 5-10, 10-15 and +15 years and how often they palpate patients on a monthly basis. These parameters are plotted as a 3D graph (Fig.5.4). Whereas the sample size is too small to make any definite conclusions, some potential trends can be observed. A regression plane, a type of best fit plane, is drawn for this plot to show the relationship between the parameters. The plane declines from left to right as years of experience and frequency of palpation increases. The junior clinicians are rating the fidelity of UltraSendo higher possibly because they have less experience of the sensation of a real palpation with which to compare against. The senior clinicians have been exposed to a wider range of forces and tactile sensations and thus could suggest the force generated by UltraSendo is apparently weaker than the real sensation.

5.1.1.2 Gender

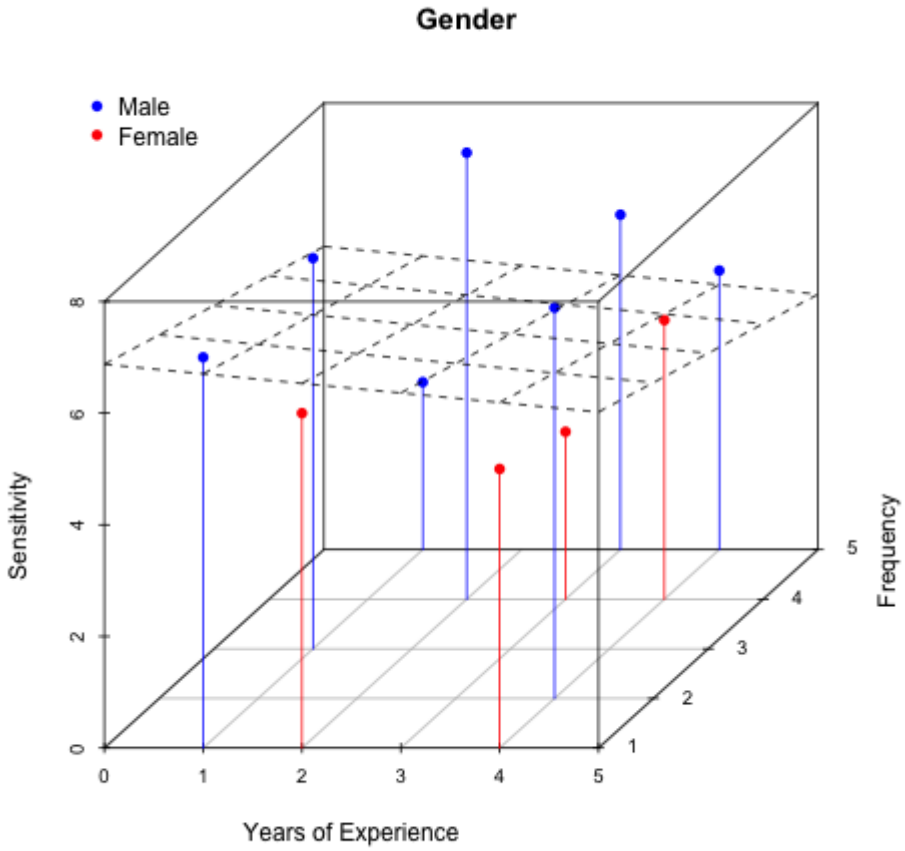

Figure 5.5: 3D plot with gender labels for each point.

Four female and seven male completed the session and their responses are colour coded in the above plot (Fig.5.5). The red points indicate the female responses and these points mainly lie towards the right side where the plane of regression shows a decline, however, most of these female participants were highly experienced so it is unclear at this stage whether the difference in sensitivity between male and female is due to gender alone or was their response influenced by their experience. There is insufficient data to statistically support any of these suggestions.

5.1.1.3 Handedness

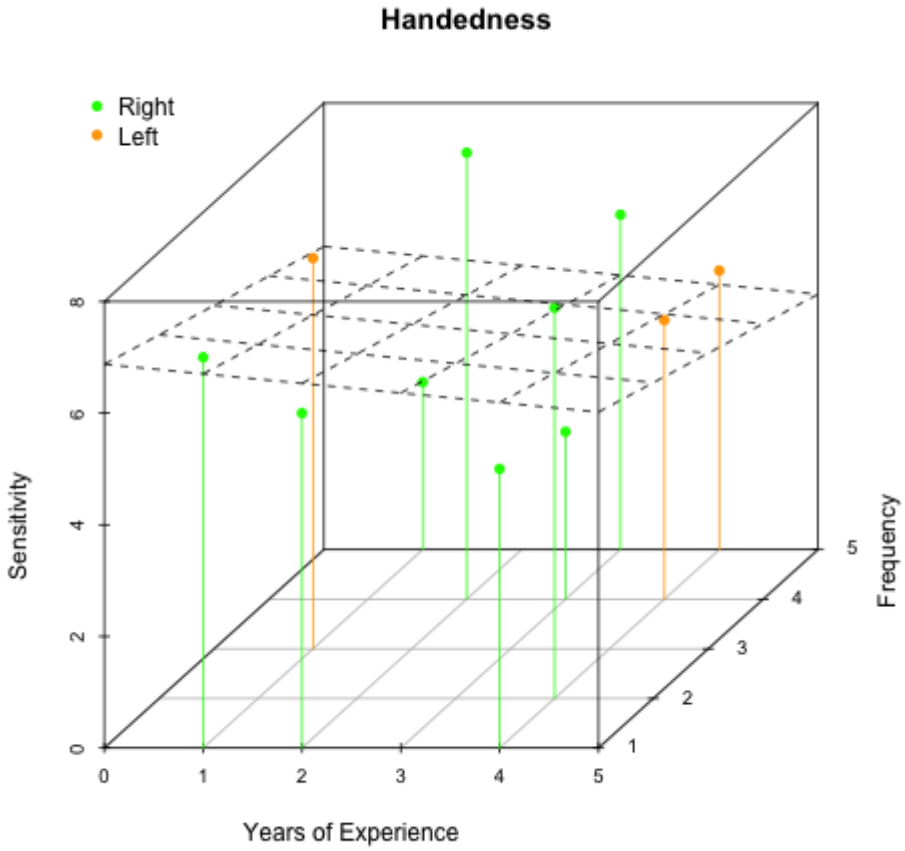

Figure 5.6: 3D plot with gender labels for each point.

The majority of the users were right-handed except for two participants and one participant claiming to be ambidexterous who's response is also colour coded to be orange to indicate his lefthandness in the above plot (Fig.5.6). The left handed participants all gave a less satisfied response to the sensation. These participants are either more experienced or palpate more regularly, however, due to the small sample here it is not sufficient to conclude that the difference in sensitivity is solely due to the left and right handedness of the participants rather than their experience or regularity in palpation.

5.1.1.4 *Observations and Comments*

	Comments
1	Only a light touch was required to feel a pulse, probably 5-10% of the usual required pressure. I couldn't feel heart murmur/thrill.
2	The sensation is closer to a thrill than a pulse.
3	It's very interesting and easy.
4	Improving the fabric (texture) of the interface could simulate the fat layer under the skin. The pulse should be blunt compared to sharp.
5	Feel that the pulse sensation should be felt a bit stronger.

Table 5.1: All the given comments from participants

Where comments were given by participants, these comments are listed in the table above (Table.5.1). Comment one and five from the table suggests that the force of the sensation needs further development to closer simulate the pulse sensation that the participant expects to find when palpating a real patient. An observation we made whilst watching the participants palpate UltraSendo was that almost all the participants initially depressed the interface with substantial amount of force that deformed the hollow cardboard box interface. This is probably the reason why the participants need not, and could not even if they wanted to, palpate with more strength otherwise the interface would break. Comment four suggested the palpable surface could be improved by presenting a surface that felt like human skin to increase the realism of the simulator. The palpable surface is currently covered by the blue drapes to integrate the device into the augmented reality simulator and thus may not feel like touching the skin of a human. The results we gathered, the comments given and the observation we made indicate there is still room for improvement for UltraSendo if a stronger output can be achieved and the interface is further developed to simulate the texture of human skin with a sturdier design to withstand heavier palpation.

5.2 Summary

UltraSendo was brought to Ysbyty Glan Clwyd in North Wales to find out whether medical practitioners believed the sensation presented by the device was realistic and also to determined whether this sensation was closer to a pulse or thrill sensation. Eleven medical practitioners with the majority having medical specialities in Cardiology provided user feedback. The results showed a mixture of responses but the pulse sensation was perceived to be less satisfactory compared to the thrill sensation which received higher ratings. Even though 3D plots for sensitivty i.e. whether the participant could feel the sensation or not, against gender and handedness were drawn, due to the small sample size it could not be concluded whether the difference in sensitivity is mainly due to years of experience and how frequently they palpate on a monthly basis or the participants gender and handedness. Constructive feedback from some participants show where there is room for improvement to enhance the realism. The force of the sensation needs to be increased and the interface needs further development to improve the textural sensation of touching the skin of a body. The hollow cardboard box will also need be replaced with another design which can withstand heavier palpation.

Chapter 6

Summary & Conclusion

This thesis has investigated the use of airborne ultrasound as tactile feedback in a medical context. The thesis aimed to answer this research question:

- Can acoustic radiation pressure from focussed airborne ultrasound deliver a realistical tactile sensation in a medical simulator?

We explored the simulation of two tactile sensations suggested by our clinical collaborators: a pulse and a thrill. Detection of a pulse and/or thrill are commonly carried out to aid diagnosis for a variety of illnesses, and is a skill that every clinician needs to learn. A custom airborne ultrasound tactile device which we called UltraSendo was built to investigate this hypothesis.

This technology offered several advantages over conventional technologies. Airborne ultrasound overlaps the maximum human tactile perception of 1KHz and thus is able to simulate the entire range of vibration feedback. A more flexible and configurable tactile feedback mechanism for medical simulators would allow a novice medical practitioner to train more effectively as a wider range of scenarios can be simulated for training. UltraSendo has the potential to be upgraded to be able to re-locate the position of the displayed sensation. In comparison to a previous palpation simulator built at Bangor University called PalpSim [81] which uses a hydraulically pressurized rubber tube to mimick an artery, it is not possible to re-locate the position where the tactile sensation is displayed due to the rubber tube being permanently fixed in place. UltraSendo is able to provide more controllability of the virtual patient parameters since the strength of the pulse sensation, pulse rate and pattern can all be changed. These parameters are not readily configurable in PalpSim.

In an attempt to answer the question presented in the hypothesis, a custom built airborne ultrasound called UltraSendo was constructed at Bangor University as ultrasound tactile displays were unavailable commercially at the time of this study. UltraSendo was

brought to the Catheter Laboratory in Ysbyty Glan Clwyd in North Wales to collect expert user feedback. The feedback was used to answer the question presented in the hypothesis.

6.0.1 Conclusion

To answer the hypothesis, UltraSendo was built and feedback was gathered from medical practitioners in Ysbyty Glan Glwyd. Although there was a mix of responses, the majority of responses for the sensation presented was unsatisfactory and constructive feedback from the participants pinpointed the areas that could be improved. According to some of the comments, the force from UltraSendo is weaker compared to palpating a real patient. This could be due to a small output force of the transducer array or the sturdiness of the interface which is made from a hollow cardboardbox. The interface is also covered in blue cloth and thus the participant is feeling the texture of the cloth instead of skin.

UltraSendo also has the ability to present abnormal pulse rates and beat patterns, however, this study has not collected user feedback for such because the feasibility of using airborne ultrasound had to be proved first. After gathering user feedback, the presented sensation is perceived to not be satisfactorily realistic by the majority of users. It is best to improve this aspect first so the user has passed the first barrier of questioning whether this sensation is realistic or not, before asking the user to try and diagnosis whether the virtual patient exhibits a normal pulse rhythm or an abnormal Arrhythmic condition.

6.0.2 Future Work

Currently UltraSendo displays the pulse/thrill sensation at a fixed focal point. This is because all 271 transducers are driven by the same control signal. In order to allow UltraSendo to have the ability to relocate the focal point of airborne ultrasound, each transducer must have its own control signal. By replacing the Distribution board with another printed circuit that makes unique connections from the amplifier to the FPGA component, each transducer can be driven individually. This could allow phase differences (delays in the signal) to be introduced similar to the previous planar array of transducers developed in an earlier prototype.

The current device for simulating palpation uses air as the transmission medium for ultrasound and a thin sheet of polythene as the palpable surface. This palpable surface is particularly fragile as the volume underneath this surface is hollow, thus the amount of force a user can apply to this surface is limited. This is reflected in the gathered user feedback as one user mentioned he was only required to use roughly 10% of the strength he would normally use to palpate for a pulse. Replacing the transmission medium of air with another

denser, solid medium would provide a stronger physical support for the palpable surface (Fig.6.1). Another observation is the deformation and damage to the interface as the user applies more force to palpate for the thrill sensation with their palm. Tolerating a higher amount of force applied to the device by the user could simulate deeper palpation where the sensation is further away from the surface of skin.

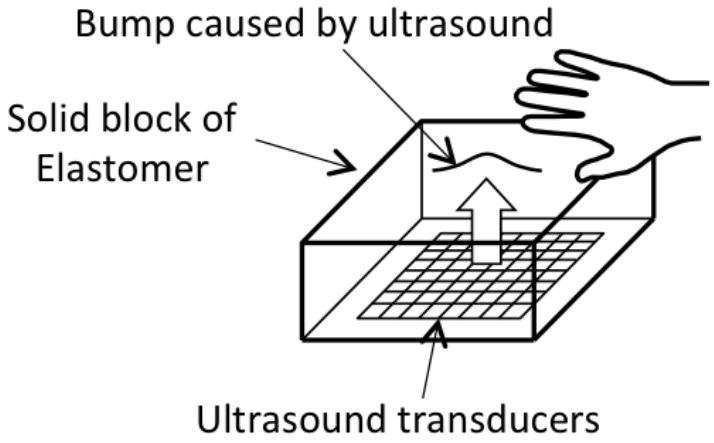

Figure 6.1: A block of gel with ultrasound transducers embedded

The textural sensation could also be improved by using material that feels closer to human skin. Elastomer is one such material, which can tolerate higher degrees of elastic deformation and thus is more resilient to damage compared to a thin sheet of polythene. Investigations can be carried out for denser mediums in order to further reduce the limitation in applicable force to the palpable surface and to improve the textural sensation. Possible mediums to initially investigate can be water and gel. Underwater transmission of ultrasound from a 2D (2-Dimensional) array of ultrasonic transducers would first be investigated to gain better understanding of how propagation occurs in a dense medium. The completion of this study would aid the investigation of ultrasonic propagation in gel.

In current literature, Iwamoto and Shinoda had explored focussing ultrasound in water for a 1D (1-Dimensional) array of transducers to create a high spatial resolution area for tactile sensation [82]. They have added a thin ultrasonic reflective film of polyurethane over the focal point of ultrasound for the user to interact with the focal point. To our knowledge there has yet to be investigations carried out for a 2D array of ultrasonic transducers. This research also differs to [82] as a pulsation effect is created onto a block of solid gel rather than a thin sheet of reflective film. A 2D array must be used to generate enough pressure for a tangible force to be felt for palpation. The new knowledge that would come

from investigating the underwater 2D ultrasonic transducer array would further advance and contribute to the field of underwater acoustics.

Completion of this study of ultrasonic propagation in gel could be adopted in adding tactile feedback to existing mannequin models which are also made from gel. Typical mannequins deliver tactile feedback in a fixed location, however, adapting acoustic radiation pressure for tactile feedback in a mannequin would allow the sensation to be re-positioned by adjusting the phase of each the signals which drive the ultrasonic transducers. Deeper palpation could also be achieved if a mannequin is used as the current prototype uses a hollow cardboard box which cannot withstand depression adequately. There are several issues that need consideration. The acoustic impedance of air and gel must be matched if ultrasound is to propagate from the medium of air to gel. A mismatch would increase the reflection coefficient meaning the ultrasound would be reflect at the boundary of the two mediums so ultrasound is unable to enter the gel for propagation to occur. For airborne ultrasound, 40KHz was chosen as the energy loss at this frequency is reasonable to achieve a large enough workspace, however, the medium of gel would have a different rate of loss due to its density. Therefore, a higher or lower frequency could be used if ultrasound propagates through gel. A higher frequency can achieve a small focal point as the width is determined by twice the wavelength of the acoustic wave.

6.1 Summary

This thesis has investigated the use of airborne ultrasound as tactile feedback in a medical context. A custom tactile device called UltraSendo was built at Bangor University featuring a hemispherical array of 271 ultrasonic transducers. A palpation simulator for an arterial pulse and thrill was created using UltraSendo. To the best of our knowledge, we are currently the first institution to apply airborne ultrasound as tactile feedback in the context of medical simulation for training purposes. A mixture of responses were gathered from medical practitioners in Ysbyty Glan Clwyd but the majority were unsatisfied, however, constructive feedback was given to highlight areas for improvement. A stronger force output needs to be developed and the hollow cardboard box interface will need a re-design to withstand heavier palpation. The textural sensation also needs improvement to simulate the sensation of touching skin. This investigation has been the first step in developing acoustic radiaton pressure to provide tactile feedback in medical training simulators.

References

[1] Timothy R. Coles, Dwight Meglan, and Nigel W. John. The Role of Haptics in Medical Training Simulators: A Survey of the State-of-the-art. *IEEE Transactions on Haptics*, 2010.

[2] V Luboz, Y Zhang, S Johnson, Y Song, C Kilkenny, C Hunt, H Woolnough, S Guediri, J Zhai, T Odetoyinbo, P Littler, A Fisher, C Hughes, N Chalmers, D Kessel, P J Clough, J Ward, R Phillips, T How, A Bulpitt, N W John, F Bello, and D Gould. ImaGiNe Seldinger: First Simulator for Seldinger Technique and Angiography Training. *Computer Methods and Programs in Biomedicine*, 111(2):419–34, August 2013.

[3] http://www.drugs.com/dict/seldinger-technique.html.

[4] http://www.thestar.com/life/2012/09/28/the_diy_atrial_fibrillation_test_that_could_save_your_brain.html.

[5] http://dc353.4shared.com/doc/1b3gmqsb/preview.html.

[6] http://www.osceskills.com/e-learning/subjects/cardiovascular-examination/.

[7] Christopher R Porta, James a Sebesta, Tommy a Brown, Scott R Steele, and Matthew J Martin. Training surgeons and the informed consent process: routine disclosure of trainee participation and its effect on patient willingness and consent rates. *Archives of surgery (Chicago, Ill. : 1960)*, 147(1):57–62, January 2012.

[8] http://www.caehealthcare.com/eng/patient-simulators/hps-human-patient-simulator.

[9] http://limbsandthings.com/uk/products/cardiology-patient-simulator-k.

[10] Akihiro Takeuchi. Arterial pulsation on a human patient simulator improved students' pulse assessment. *Journal of Biomedical Science and Engineering*, 05(05):285–289, 2012.

[11] T Takashina, T Masuzawa, and Y Fukui. A new cardiac auscultation simulator. *Clin Cardiol*, 1990.

[12] http://vpsim.pitt.edu/shell/caselist_assignments.aspx.

[13] http://www.laerdal.com/gb/doc/245/virtual-i-v-simulator.

[14] Sebastian Ullrich and Torsten Kuhlen. Haptic palpation for medical simulation in virtual environments. *IEEE transactions on visualization and computer graphics*, 18(4):617–25, April 2012.

[15] Timothy R Coles, Derek A Gould, Nigel W John, and Darwin G Caldwell. Virtual Femoral Palpation Simulation for Interventional Radiology Training. *Theory and Practice of Computer Graphics*, pages 1–4, 2010.

[16] A B Vallbo and R S Johansson. Properties of Cutaneous Mechanoreceptors in the Human Hand related to Touch Sensation. *Human Neurobiology*, 3(1):3–14, January 1984.

[17] Takayuki Iwamoto, Taro Maeda, and Hiroyuki Shinoda. Focused Ultrasound for Tactile Feeling Display. *The Eleventh International Conference on Artificial reality and Telexistence (ICAT'2001)*, 2001.

[18] http://www.mech.kuleuven.be/en/pma/research/ras/researchtopics/tactfb.html.

[19] R. S. Johansson and R. H. LaMotte. Tactile detection thresholds for a single asperity on an otherwise smooth surface. *Somatosensory Res*, 1(1):21–31, 1983.

[20] Dimitrios A Kontarinis, Robert D Howe, and Pierce Hall. Tactile Display of Vibratory Information in Teleoperation and Virtual Environments. *Presence*, 4(4):387–402, 1995.

[21] http://www.turbosquid.com/3d-models/ball-bearing-3d-ma/599006.

[22] http://science.howstuffworks.com/transport/engines-equipment/bearing3.htm.

[23] Shogo Okamoto, Masashi Konyo, and Satoshi Tadokoro. Vibrotactile Stimuli Applied to Finger Pads as Biases for Perceived Inertial and Viscous Loads. *IEEE Transactions on Haptics*, (99):1–10, 2011.

[24] Hsin-Yun Yao, Danny Grant, and Juan Manuel Cruz-Hernandez. Perceived Vibration Strength in Mobile Devices: The Effect of Weight and Frequency. *IEEE Transactions on Haptics*, 3(1):56–62, January 2010.

[25] http://www.neuroanatomy.wisc.edu/sclinic/weakness/weakness.htm.

[26] J L Mason and N a Mackay. Pain Sensations Associated with Electrocutaneous Stimulation. *IEEE Transactions on Bio-medical Engineering*, 23(5):405–9, October 1976.

[27] Hiroyuki Kajimoto. Electro-Tactile Display with Tactile Primary Color Approach. *Proceeedings of International Conference on Intelligent Robots and Systems*, 2004.

[28] Shinobu Kuroki, Hiroyuki Kajimoto, Hideaki Nii, Naoki Kawakami, and Susumu Tachi. Proposal for Tactile Sense Presentation that Combines Electrical and Mechanical Stimulus. *Second Joint EuroHaptics Conference and Symposium on Haptic Interfaces for Virtual Environment and Teleoperator Systems (WHC'07)*, pages 121–126, March 2007.

[29] Masahiro Furukawa, Naohisa Nagaya, Yuki Hashimoto, Hiroyuki Kajimoto, and Masahiko Inami. Measurement of the Detection Thresholds of Hair on Human Hairy Skin Using Direct Vibrotactile Stimulation. *World Haptics 2009 - Third Joint EuroHaptics conference and Symposium on Haptic Interfaces for Virtual Environment and Teleoperator Systems*, pages 127–132, March 2009.

[30] Mitchell E Tyler, Jacquelin G Braun, and Yuri P Danilov. Spatial Mapping of Electrotactile Sensation threshold and Intensity range on the Human Tongue: Initial Results. In *Annual International Conference of the IEEE Engineering in Medicine and Biology Society.*, volume 2009, pages 559–62, January 2009.

[31] R.D. Howe, D.A. Kontarinis, and W.J. Peine. Shape Memory Alloy Actuator Controller Design for Tactile Displays. *Proceedings of 1995 34th IEEE Conference on Decision and Control*, (December):3540–3544, 1995.

[32] D.a. Kontarinis, J.S. Son, W. Peine, and R.D. Howe. A Tactile Shape Sensing and Display System for Teleoperated Manipulation. *Proceedings of 1995 IEEE International Conference on Robotics and Automation*, pages 641–646, 1965.

[33] T Matsunaga. 2-D and 3-D Tactile Pin Display Using SMA Micro-coil Actuator and Magnetic Latch. In *The 13th International Conference on Solid-State Sensors, Actuators and Microsystems*, pages 325–328, 2005.

[34] Keishi Fukuyama, Naoki Takahashi, Feng Zhao, and Hideyuki Sawada. Tactile Display Using the Vibration of SMA Wires and the Evaluation of Perceived Sensations. *2009 2nd Conference on Human System Interactions*, pages 685–690, May 2009.

[35] Robert Scheibe, Mathias Moehring, and Bernd Froehlich. Tactile Feedback at the Finger Tips for Improved Direct Interaction in Immersive Environments. *2007 IEEE Virtual Reality Conference*, pages 293–294, 2007.

[36] C.R. Wagner, S.J. Lederman, and R.D. Howe. A Tactile Shape Display using RC Servomotors. *Proceedings 10th Symposium on Haptic Interfaces for Virtual Environment and Teleoperator Systems. HAPTICS 2002*, pages 354–355, 2002.

[37] Roopkanwal Samra, David Wang, and Mehrdad Hosseini Zadeh. Design and Evaluation of a Haptic Tactile Actuator to Simulate Rough Textures. *2010 IEEE Virtual Reality Conference (VR)*, pages 301–302, March 2010.

[38] L Santos-Carreras, K Leuenberger, P Retornaz, R Gassert, and H Bleuler. Design and Psychophysical Evaluation of a Tactile Pulse Display for Teleoperated Artery Palpation. In *International Conference on Intelligent Robots and Systems*, pages 5060–5066, Taiwan, 2010.

[39] Mario Cheng, Welber Marinovic, Marcus Watson, Sebastien Ourselin, Josh Passenger, Hans De Visser, Olivier Salvado, Stephan Riek, and Hans De. Abdominal Palpation Haptic Device for Colonoscopy Simulation using Pneumatic Control. *IEEE Transactions on Haptics*, 5(2):97–108, April 2012.

[40] Ian Oakley and Yeongmi Kim. Combining Point Force Haptic and Pneumatic Tactile Displays. *Proceedings of the EuroHaptics Conference (2006)*, pages 309–316, 2006.

[41] G. Moy, C. Wagner, and R.S. Fearing. A Compliant Tactile Display for Teletaction. *Proceedings 2000 ICRA. Millennium Conference. IEEE International Conference on Robotics and Automation. Symposia Proceedings (Cat. No.00CH37065)*, (April):3409–3415, 2000.

[42] http://team358.org/files/pneumatic/.

[43] Philip Moore and Sheng Pu. Pneumatic Servo Actuator Technology. *Actuator Technology: Current Practice and New Developments*, pages 3/1 – 3/6, 1996.

[44] Masahiro Takaiwa and Toshiro Noritsugu. Development of Breast Cancer Palpation Simulator using Pneumatic Parallel Manipulator. *SICE Annual Conference 2007*, pages 823–827, September 2007.

[45] http://www.societyofrobots.com/actuators_solenoids.shtml.

[46] Sang-moon Hwang, Hong-joo Lee, Shi-uk Chung, Gun-yong Hwang, and Beom-soo Kang. Development of Solenoid-Type Vibrators Used for Mobile Phones. *IEEE Transactions on Magnetics*, 39(5):3262–3264, 2003.

[47] S F Frisken-Gibson, P Bach-y Rita, W J Tompkins, and J G Webster. A 64-Solenoid, Four-Level Fingertip Search Display for the Blind. *IEEE Transactions on Biomedical Engineering*, 34(12):963–5, December 1987.

[48] http://www.crutchfield.com/s-p9foldjuu0i/p_575rfp3212/rockford-fosgate-punch-he2-rfp3212.html.

[49] Katsunari Sato and Susumu Tachi. Design of Electrotactile Stimulation to Represent Distribution of Force Vectors. *2010 IEEE Haptics Symposium*, pages 121–128, March 2010.

[50] Hiroyuki Kajimoto, Naoki Kawakami, Susumu Tachi, and Masahiko Inami. Smart-Touch : Electric Skin to Touch the. (February):36–43, 2004.

[51] http://www.robotica-up.org/assistive3.html.

[52] Sung H Han. Vibrotactile Feedback for Information Delivery in the Vehicle. *IEEE Transactions on Haptics*, 3(2):138–149, April 2010.

[53] Maria Karam, Frank A. Russo, and Deborah I. Fels. Designing the Model Human Cochlea: An Ambient Crossmodal Audio-Tactile Display. *IEEE Transactions on Haptics*, 2(3):160–169, July 2009.

[54] Kazuhide Okada, Gwan Kim, and Pyong Sik Pak. Sound Information Notification System by Two-channel Electrotactile Stimulation for Hearing Impaired Persons. In *Proceedings of the 29th Annual International Conference of the IEEE EMBS*, volume 2007, pages 3826–9, January 2007.

[55] Hui Tang and David J Beebe. An Oral Tactile Interface for Blind Navigation. *IEEE Transactions on Neural Systems and Rehabilitation Engineering*, 14(1):116–23, March 2006.

[56] Daigo Ikeya and Junichi Takeno. Research and Development of a Hand-held Vision system for the Visually Impaired. In *IEEE International Workshop on Robot and Human Interaction*, number September, pages 13–17, 1999.

[57] S Supriya and A Senthilkumar. Electronic Braille Pad. *International Conference on Control, Automation, Communication and Energy Conservation*, pages 2–6, 2009.

[58] Jussi Rantala, Roope Raisamo, Jani Lylykangas, Veikko Surakka, Jukka Raisamo, and Katri Salminen. Methods for Presenting Braille Characters on a Mobile Device with a Touchscreen and Tactile Feedback. *IEEE Transactions on Haptics*, 2(1):28–39, 2009.

[59] Ramiro Velazquez, Hermes Hernandez, and Enrique Preza. A Portable eBook Reader for the Blind. In *32nd Annual International Conference of the IEEE EMBS*, volume 2010, pages 2107–10, January 2010.

[60] Yau Wei-yun. Fake Finger Detection Using An Electrotactile Display System. In *Control, Automation, Robotics and Vision*, number December, pages 17–20, 2008.

[61] Shafiq Ur-Rehman, Li Lie, and Haibo Li. Vibrational Soccer: Tactile Rendering of Football Game on Mobiles. In *International Conference on Next Generation Mobile Applications, Services and Technologies*, number Ngmast, pages 3–7, 2007.

[62] Tae-Heon Yang, Sang-youn Kim, and Dong-soo Kwon. Applications of A Miniature Pin-Array Tactile Module for a Mobile Device. In *International Conference on Control, Automation and Systems*, pages 1301–1304, 2008.

[63] N Vuillerme, O Chenu, A Fleury, J Demongeot, and Y Payan. Optimizing The Use of an Artificial Tongue-placed Tactile Biofeedback for Improving Ankle Joint Position Sense in Humans. In *28th IEEE EMBS Annual International Conference*, volume 1, pages 6029–32, January 2006.

[64] Y P Danilov, M E Tyler, K L Skinner, and P Bach-y Rita. Efficacy of Electrotactile Vestibular Substitution in Patients with Bilateral Vestibular and Central Balance Loss. In *Proceedings of the 28th EMBS Annual International Conference*, volume Suppl, pages 6605–9, January 2006.

[65] Steven W. Wu, Richard E. Fan, Christopher R. Wottawa, Eileen G. Fowler, James W. Bisley, Warren S. Grundfest, and Martin O. Culjat. Torso-based Tactile Feedback System for Patients with Balance Disorders. *2010 IEEE Haptics Symposium*, pages 359–362, March 2010.

[66] J.. Lieberman and C.. Breazeal. TIKL: Development of a Wearable Vibrotactile Feedback Suit for Improved Human Motor Learning. *IEEE Transactions on Robotics*, 23(5):919–926, October 2007.

[67] Monika Seps, Konstantinos Dermitzakis, and Alejandro Hernandez-arieta. Study on Lower Back Electrotactile Stimulation Characteristics for Prosthetic Sensory Feedback. In *International Conference on Robotics and Systems*, number Figure 1, pages 3454–3459, 2011.

[68] A. U. Alahakone and S. M. N. a. Senanayake. A Real Time Vibrotactile Biofeedback System for Improving Lower Extremity Kinematic Motion during Sports Training. *2009 International Conference of Soft Computing and Pattern Recognition*, pages 610–615, 2009.

[69] B Jaffray. Minimally Invasive Surgery. *Archives of Disease in Childhood*, 90(5):537–42, May 2005.

[70] Brian T Bethea, Allison M Okamura, Masaya Kitagawa, Torin P Fitton, Stephen M Cattaneo, Vincent L Gott, William a Baumgartner, and David D Yuh. Application of Haptic Feedback to Robotic Surgery. *Journal of laparoendoscopic & advanced surgical techniques. Part A*, 14(3):191–5, June 2004.

[71] Christopher Wottawa, Richard E. Fan, Catherine E. Lewis, Brett Jordan, Martin O. Culjat, Warren S. Grundfest, and Erik P. Dutson. Laparoscopic Grasper with an Integrated Tactile Feedback System. *2009 ICME International Conference on Complex Medical Engineering*, pages 1–5, April 2009.

[72] William Mcmahan, Jamie Gewirtz, Dorsey Standish, Paul Martin, Jacquelyn A Kunkel, Magalie Lilavois, Alexei Wedmid, David I Lee, and Katherine J Kuchenbecker. Tool Contact Acceleration Feedback for Telerobotic Surgery. *IEEE Transactions on Haptics*, 4(3):210–220, 2011.

[73] Chih-Hung King, Martin O Culjat, Miguel L Franco, Catherine E Lewis, Erik P Dutson, Warren S Grundfest, and James W Bisley. Tactile Feedback Induces Reduced Grasping Force in Robot-Assisted Surgery. *IEEE Transactions on Haptics*, 2(2):103–110, 2009.

[74] Takayuki Hoshi, Daisu Abe, and Hiroyuki Shinoda. Adding Tactile Reaction to Hologram. *18th IEEE International Symposium on Robot and Human Interactive Communication*, pages 7–11, 2009.

[75] Miha Ciglar. An Ultrasound Based Instrument Generating Audible and Tactile Sound. In *New Interfaces for Musical Expression*, number Nime, pages 19–22, 2010.

[76] Mark Marshall, Tom Carter, Jason Alexander, and Sriram Subramanian. Ultra-Tangibles: Creating Movable Tangible Objects on Interactive Tables. *Proceedings of the 30th International Conference on Human Factors in Computing Systems*, 2012.

[77] Jens U. Quistgaard, Charles Desilets, and Pat Martin. High intensity focused ultrasound. *The European Aesthetics Guide*, 2010.

[78] Takayuki Hoshi, Masafumi Takahashi, Takayuki Iwamoto, and Hiroyuki Shinoda. Noncontact Tactile Display Based on Radiation Pressure of Airborne Ultrasound. *IEEE Transactions on Haptics*, 3(3):155–165, July 2010.

[79] Gary M Y Hung and Nigel W John. Airborne Ultrasound Pulse Force Device for Palpation Simulation. In *Theory and Practice of Computer Graphics 2011*, pages 61–62, Warwick University, 2011.

[80] Gary M Y Hung, Nigel W John, Chris Hancock, Derek A Gould, and Takayuki Hoshi. UltraPulse – Simulating a Human Arterial Pulse with Focussed Airborne Ultrasound. In *35th Annual International Conference of the IEEE EMBS Osaka, Japan*, volume 550, pages 2511–2514, 2013.

[81] Timothy R Coles, Nigel W John, and Darwin G Caldwell. The Case for Augmented Reality when Training in a Virtual Medical Environment. 2010.

[82] T. Iwamoto and H. Shinoda. Two-dimensional Scanning Tactile Display using Ultrasound Radiation Pressure. *2006 14th Symposium on Haptic Interfaces for Virtual Environment and Teleoperator Systems*, pages 57–61, 2006.

List of Figures